Effect of hydrodynamics on light utilization in large scale cultures of microalgae

Philipp Hartmann

UNIVERSITE DE NICE-SOPHIA ANTIPOLIS

ECOLE DOCTORALE STIC

SCIENCES ET TECHNOLOGIES DE L'INFORMATION ET DE LA COMMUNICATION

T H E S E

pour l'obtention du grade de

Docteur en Sciences

de l'Université de Nice-Sophia Antipolis

Mention : Automatique, traitement du signal et des images

présentée et soutenue par

Philipp HARTMANN

Effect of hydrodynamics on light utilization in large scale cultures of microalgae

Thèse dirigée par *Olivier BERNARD*

soutenue le *14/5/2014*

Jury :

M. Olivier BERNARD,	Directeur de Recherche,	Directeur
M. Antoine SCIANDRA,	Directeur de Recherche,	Co-Directeur
M. Clemens POSTEN,	Professeur,	Rapporteur
M. Jérémy PRUVOST,	Professeur,	Rapporteur
M. Alain Wande WOUVER,	Professeur,	Examinateur
M. Jérome MORCHAIN,	Maître de Conférences,	Examinateur

To my family.

I may not have gone where I intended to go, but I think I have ended up where I intended to be.

Douglas Adams

ABSTRACT

Microalgae are often seen as a promising candidate to contribute to energy generation in the future. However, the link between the energy contained in the biomass and the required energy to grow the microalgae, especially to mix the culture, is complex. Mixing has a direct effect on photosynthesis since it affects the way cells are successively transported between light and dark zones. The hydrodynamics modulate the frequency at which light is perceived by the cells.

In this thesis the question of nonlinear response of the photosynthesis process to varying light signals at different time scales has been investigated.

First, the impact of light frequency and photoacclimation on photosynthesis have been experimentally studied using a self-developed LED device to expose the green algae *Dunaliella salina* to light-dark cycles at different frequencies. The results support the hypothesis that mid-term photoacclimation depends on the average light intensity. Then, models have been developed according to our experimental observations. The effect of light-dark cycle frequency on the response of a mechanistic model for photosynthesis and growth has been studied and our results have confirmed that increasing the light supply frequency enhances photosynthetic efficiency. A model for photoacclimation has also been developed assuming both a change in the number and the cross section of the photosystems. Finally, a 3D hydrodynamic model for a raceway type culturing device has been used to compute Lagrangian trajectories numerically. Based on the trajectories, time-dependent light signals for individual cells have been calculated. Using these light signals, a photosynthesis model was integrated in order to investigate the dependency of photosynthetic efficiency on hydrodynamic regime.

RESUMÉ

Les microalgues sont souvent considérées comme des candidats potentiels pour la production d'énergie. Cependant, le lien entre l'énergie contenue dans la biomasse et l'énergie nécessaire pour cultiver les microalgues, en particulier pour agiter la culture, est complexe. Le mélange turbulent a un effet direct sur la photosynthèse car il affecte la façon dont les cellules sont successivement transportées entre la lumière et les zones sombres. En particulier, l'hydrodynamique module la fréquence à laquelle la lumière est perçue par les cellules.

Dans cette thèse nous avons étudié la réponse de la photosynthèse à divers régimes lumineux. Tout d'abord, l'impact de la fréquence d'éclairement et de la photoacclimatation a été étudié expérimentalement. Pour cela, un dispositif à base de LED a été développé et des cycles lumière-obscurité de fréquences variables ont été appliqués à la chlorophycée *Dunaliella salina*. Les expériences ont ainsi confirmé l'hypothèse selon laquelle la dynamique de photoacclimatation dépend de l'intensité lumineuse moyenne. Puis, des modèles ont été développés à partir de nos observations expérimentales. L'effet de cycles lumière-obscurité a été étudié à l'aide d'un modèle mécaniste de photosynthèse et de croissance et il a été montré que l'augmentation de la fréquence lumineuse augmente l'efficacité photosynthétique. Ensuite, nous avons développé un modèle de photoacclimatation, qui prend en compte une réponse du nombre et la taille des photosystèmes. Enfin, un modèle hydrodynamique 3D a été simulé pour un raceway. Cela a permis de reconstruire numériquement les trajectoires lagrangiennes de cellules, et donc d'évaluer le signal lumineux qu'elles perçoivent. Ces trajectoires réalistes, couplées à un modéle de photosynthèse ont permis de mieux comprendre l'effet du mélange sur l'efficacité photosynthétique.

ZUSAMMENFASSUNG

Mikroalgen werden häufig als vielversprechende Technologie zur Erzeugung erneuerbarer Energie bewertet. Das Verhältnis von Energie in der erzeugten Biomasse und benötigter Energie der Kultur hängt in komplexer Weise von den Kultivierungsbedingungen ab. Auf die kontinuierliche Mischung der Kultur wird ein wesentlicher Teil der benötigten Energie verwendet. Die Mischungsintensität bestimmt den Transport der Zellen zwischen hellen und dunklen Zonen im Medium und hat daher direkten Einfluss auf die Wachstumsraten der Algen. Die zeitabhängige Lichtintensität, welche einzelne Zellen absorbieren ist von der Hydrodynamik im System bestimmt.

In dieser Arbeit werden nichtlineare Effekte zeitveränderlicher Lichtsignale mit unterschiedlichen Zeitskalen untersucht. Im ersten Ansatz wird das Wachstumsverhalten von Mikroalgen unter dem Einfluss variabler Lichtsignale mit einem neuen Versuchsaufbau untesucht. Der Versuchsaufbau verfügt über eine frei programmierbare LED-Beleuchtung um die Grünalge *Dunaliella salina* unter dem Einfluss von hell-dunkel Zyklen zu studieren. Ein wichtiges Resultat dieser Studie ist, dass die physiologische Anpassung des Chlorophyll Gehalts unabhängig von der Alternationsfrequenz des Signals ist. In einem zweiten Ansatz, wird der Effekt von hell-dunkel Zyklen unterschiedlicher Wechselfrequenz auf ein mechanistisches Modell für Photosynthese studiert. Es wird gezeigt, dass eine höhere Frequenz höhere Reproduktionsraten stimuliert. Es wird ein Modell für Lichtakklimatisierung entwickelt, welches die physiologische Anpassung von Wirkungsquerschnitt und Anzahl der Photosysteme berücksichtigt. In der letzten Studie wird ein 3D Modell für die Hydrodynamik in der Kultur verwendet um Trajektorien der Zellen zu berechnen. Auf Basis dieser Trajektorien werden zeitabhängige Lichtprofile abgeleitet und ein Modell für Photosynthese numerisch integriert.

CONTENTS

ACRONYMS

CFD	Computational Fluid Dynamics
LD (-cycle)	Light Dark cycle
NPQ	Non-Photochemical Quenching
PBR	Photobioreactor
PI curve	Photosynthesis-Irradiance curve
PSU	Photosynthetic Unit
PSII	Photoreaction Center 2
PWM	Pulse width modulation

1

INTRODUCTION

The beginning is the most important part of the work.

Plato

One of the first publications claiming the hypothesis of global warming by increasing athmospheric CO_2 content was written by Manabe in 1980 [52]. Today, global warming as a consequence of anthropogenic CO_2 is a hot topic, which leads to extensive discourses in the scientific, ecologic, political and economical context. Current predictions of the development of the surface temperature give a very pessimistic outlook towards the end of the century, while politic measures for the decrease of emission of climate gases on global scale continuously fail. At the same time, certain countries invest billions of Euros directly by subsidies and indirectly by other regulative measures in reducing carbon emission on a national scale. At a closer look many of the political measures appear to be driven by specific national industry lobbies and the political will of future independence from import of fossil combustibles and uranium. There are numerous approaches for the production of energy with a reduced carbon emission such as: Hydraulic energy, Wind energy, Solar Energy, Combustion of regenerative wood stock, Carbon Capture and Storage Systems (CCS), Core fusion (ITER) and Biofuel. All of those approaches have their advantages and limitations. While the cost for utilization of fossil energy will increase due to scarcity of the resources and a possible implementation of a global Emission certificate market [1] , many of those technologies are likely to find a niche in the energy market of the future. The time line for this post-industrial evolution depends however strongly on the political will. Unfortunately, policy makers are in a position to trade off growth today against highly uncertain consequences of climate change in the future.

1. There exist Emission Certificate markets, but they are national and oftentimes their impact on emission is minor.

Microalgae play important roles in the global ecology, and are therefore an important factor to consider in the research framework of anthropogenic CO_2 emission. Microalgae are unicellular organisms living in salty or sweet water, and "have chlorophyll a as their primary photosynthetic pigment" [45]. While this definition includes a wide variety of organisms, it is sufficient for the context of this study to see microalgae as unicellular photosynthetic organisms. Without a doubt, production of organic carbon in the oceans from inorganic carbon (primary production) is the most important ecologic function of these photosynthetic microorganisms. Phytoplankton fixes about $45-50 Gty^{-1}$ of carbon, while terrestrial plants fix about $45-68 Gty^{-1}$ [49]. Most of this carbon processes through the marine food chain in order to be re-mineralized at the end, while a fraction of this carbon is fixed in calcium carbonates and non degrading organic carbon [17] and is therefore permanently removed from the carbon cycle. Another role of microalgae in carbon emission mitigation could be to contribute to CO_2 valorization: They can be cultivated in artificial ecosystems and consume CO_2 rich gaseous flue gas. Some species can store high amounts of lipids that can be turned into biofuel [72, 60], other species can be digested in an anaerobic process and lead to methane production [67]. They can thus potentially be a key actor for the future set up of the third biofuel generation and constitute a future source of green energy.

Micralgae growth conditions in natural environment and artificial culturing both imply turbulent hydrodynamics. This means, that each individual cell travels along a certain trajectory through the medium. According to this, the conditions regarding nutrient concentration, temperature and light exposure change with time also. Observations show, that a change in the hydrodynamics can

significantly change growth dynamics. When using dynamical models with estimated light signals from hydrodynamic simulation or measurement, these effects can be studied. Due to their different characteristics, natural (oceanic) environment has to be differentiated from artificial microalgae cultures.

In the Ocean, the hydrodynamics is very slow. A typical travel time from the surface to a very deep ocean layer and back is several hours [38]. The direct consequence of this slow hydrodynamics is a slow rate of change in the environmental parameters. Due to slow mixing and the large scale of the system, an indirect consequence is the heterogeneity of the medium in the parameters for nutrient availability. This is a vital factor since marine phytoplancton in the ocean mixed layer is generally nutrient limited. Light limitation plays also a role here, but the rate on which the perceived light of the cells change is very slow. This is also because of a weak light gradient due to the low distance-specific light attenuation of seawater.

In artificial cultures, such as open raceway ponds or closed photobioreactors (PBR) [60], the conditions differ. Although there is also a certain rate of mixing, the hydrodynamics is a lot faster *and* due to a high culture density the light gradient within the culture is a lot higher. For optimal growth, the growth medium is typically saturated in nutrients and CO_2. As a function of the intended culture density and design restrictions, the depth of the culture volume can vary between about 40 cm for open raceway ponds down to 1 cm for very high density closed PBR. In order to homogenize the medium and to avoid sedimentation, these cultures are mixed intensively. As a consequence of the small dimensions, fast mixing and high attenuation, the algae are exposed to a light signal which can vary on time scales down to 10^{-6} seconds [60]. It is generally assumed,

that increased mixing improves growth. In this context, approaches aiming at improve and rationalize the design of such culturing systems [60, 61] have been proposed, especially for photobioreactors. The less intensive raceway processes have not, as far as we know, been studied in this context.

1.1 APPLICATIONS OF BIOREACTORS

Cultivation of microalgae for Biofuel generation is one application of bioreactors but not the only one. Indeed, bioreactors can be found in various fields of biotechnology, such as wastewater treatment, food and pharmaceutical industry. They are used to grow several types of microorganisms, archae, bacteria, yeast, fungi, cyanobacteria, microalgae or even undifferentiated cells of higher organisms such as mammals. Their size ranges from systems of volume lower than one cubic meter for high added value production, to several thousand cubic meters for wastewater treatment. The possibilities of applications are only limited by the capabilities of the utilized organisms and the expense to cultivate them in self contained systems. Modern biotechnology can be expected to push the frontiers of this technology much further in the near future.

Industrial production of microalgae is a much younger technology, whose main objective is to produce biomass from which high added values compounds (colouring, antioxydant,...) are extracted. There are to date no industrial application for biofuel production, exploiting the potential of microalgae to store lipids. However, the existing microalgae production systems (mainly under the form of raceways) are among the largest industrial bioreactors. An industrial raceway occupies several thousands square meters, for a volume

Figure 1: Industry-Scale raceway culturing system (project salinalgue)

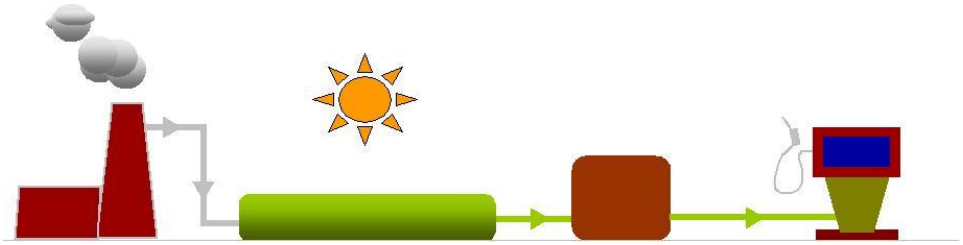

Figure 2: Full production cycle for biofuel production from microalgae

that can exceed thousand cubic meters. Example for a large scale algae bioreactor is shown in figure 1. Fig. 2 presents schematically the production chain for Biofuel generation from microalgae. The emitted flue gas from an industry site is a necessary CO_2 input for the microalgae culture. The microalgae are cultivated and in a final step the lipids are extracted and refined for the use as fuel.

The following paragraph explores the factors that affect productivity of these microalgal based production systems. Firstly the dependence of growth rate from light and nutrient availability will be discussed.

Photosynthesis on the scale of a single photoreactioncenter

There exist different pathways for the conversion of photon energy to chemical energy. Some basic principles are common in the mechanism for all autotrophic organisms: there is a membrane called *thylakoid*, which contains key proteins involved in the primary conversion of photon energy. The thylakoids are embedded in organelles called *chloroplasts* for eukaryotic organisms but not confined for prokaryote organisms. Thylakoids are encapsulating an aqueous phase which is called the thylakoid lumen. The thylakoid lumen integrates four major protein complexes:

- Photosystem I (PSI)
- Photosystem II (PSII)
- The Cytocrome b6f complex
- The ATP synthase

These Proteins and their interactions are illustrated in fig. 3. The basic principles can be understood based on the presented pathway, even if other pathways exist for photon conversion. The first step in the pathway is oxidation of a water molecule by means of the PSII. This reaction is a multi-step process: Firstly, photons are captured by the chlorophyll antennae, then the energy is transferred

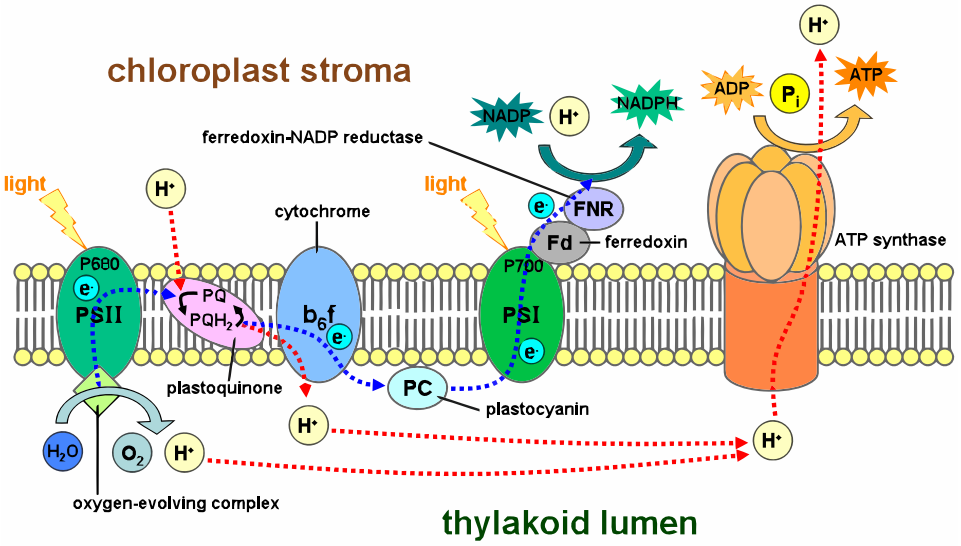

Figure 3: Schematic illustration of the thylakoid *source:Tameeria, Wikicommons*

by photochemical *quenching* [2] from one chlorophyll molecule to the other and finally to the PSII. The PSII in its excited state is highly oxidizing and splits a water molecule into molecular oxygen and two H^+ ions. The separated electrons trigger an electron transfer chain: by means of the plastoquinones and the cytochrome protein, an additional H^+ ion is transferred inside the thylakoid lumen and the electron is transferred to the PSI. The PSI uses the electron and the excitation energy of more photons for the reduction of $NADP^+$ to $NADPH + H^+$. Finally, the ATP synthease uses the proton chemical and electric potential between both sides of the membrane to synthesize ATP from ADP + and P_i.

The fluxes of electrons and molecules generated by these light reaction supplies energy for the dark phase of photosynthesis (Calvin

2. Photochemical quenching denominates energy transfer between molecules contributing to primary production. One important process of energy transfer is the Förster resonance energy transfer (FRET) [39]. It is a quantum mechanic process transferring the energy of an excited state from one molecule to another by means of a *virtual* photon. It is limited to distances which are smaller than the wavelength of the photon.

cycle), fixing CO_2 and transforming it into a small sugar (3-phosphoglycerate).

Photoinhibition

Extreme light conditions or very rapid changes in the light signal can lead to significant damage of the PSII reaction centers (c.f. Anderson et al. [1]). A damaged PSU has to be repaired by the synthesis of a new protein. Similar to the long term photoacclimation processes, this repair process is relatively slow and thus strong photoinhibition is followed by a regeneration period.

> Photoinhibition is " a light-dependent irreversible inactivation of the PSII reaction center activity, which can be restored only via the degradation (subsequent to photoinhibition) and synthesis of the D1 protein " (Tyystrjarvi and Aro, 1996 [70])

The inactivation of the protein occurs whenever the photoreaction centre gets hit by an excess number of photons in a short period. Statistically, this effect can also be observed for low light irradiances, but in this case the intracellular repair mechanisms are sufficient to prevent significant decreases in productivity.

Photoacclimation

Phytoplankton reacts physiologically to changes in light intensity, both at fast time scale by modulating its actual photosynthetic activity, but also by adapting at longer time scale its photosynthetic apparatus. Mid and long-term processes are called photoacclimation.

In a very simplified scope cells can enhance their light harvesting machinery to a low irradiance level in order to use the incident light most efficiently. They can reduce it at high light, in order to avoid damage of the photosynthetic apparatus due to overexcitation. Photoacclimation processes leads thus to modulations of their sensitivity to light. There exist different mechanisms for photoacclimation which differ in the timescale of response to the change of environmental light intensity.

Short term photoacclimation denominates all processes of the cell in order to adapt to the current light conditions without the synthesis of new proteins. This shifts the optimal light intensity closer to the actual irradiation and leads to a higher efficiency under constant conditions. Various physiological mechanisms may be affected. One class of mechanisms deactivates the excitons after the photon absorption. The energy can be re-emitted as fluorescence photons or dissipated thermally [18]. The latter processes are denominated by the term *Non-photochemical quenching (NPQ)*. There is evidence that NPQ is indirectly triggered by a pH gradient across the thylakoid membrane [40] involving the xanthophyll cycle.

To longer periods of unfavorable light conditions, the algae react by structural and physiological changes in order to avoid photoinhibition and optimize growth. This long term processes imply the synthesis of functional proteins, which is a very slow process and can be considered the limiting factor. By experiments, two dominant mechanisms could be identified: The alteration of the amount of chlorophyll per PSU and the alteration of the number of PSUs [27]. The cellular chlorophyll content is closely linked to these processes. Generally one could say, more chlorophyll means more photosynthesis for low irradiance . These acclimation processes can be quantified

by the carbon specific chlorophyll content of the cells. Typically, models for photoacclimation use this value as a state variable.

Growth and Nutrient Uptake

The general dynamics of microalgae in a batch culture is shown in fig. 4: In the first phase, the biomass grows exponentially, while substrate nitrogen is consumed. After nitrogen depletion, growth continues until a certain level where growth stops.

Assuming that the cells have an internal nutrient stock, this evolution can be explained as follows: In the first growth phase, the intracellular nutrient pool is filled up to a maximum concentration. After the depletion of the nutrients in the medium, the intracellular stock is decreased which leads to a gradually decreasing growth rate with progressive depletion of the internal quota. Droop [20] claimed, that this dynamics can be observed for nitrogen or phosphorus limited growth and not only for Vitamin B_{12} as it is reported in the first data supporting such a mechanism. There is plenty evidence proving that the assumptions of an intracellular pool of limiting element driving growth holds true for various conditions [68, 21]. This observation supported the Droop model, firstly published in 1966 [20], where the growth rate is not a function of external substrate (as assumed by Monod [54]) but of the internal elemental quota. There are numerous studies on the Droop model, this includes an approach to extend it for the use with multiple nutrients [11, 14] or to put it into a mechanistic framework [56]. Due to its scientific impact in the past decades, the Droop Model can be seen as an accepted gold standard for nutrient limited growth for unicellular organisms. In

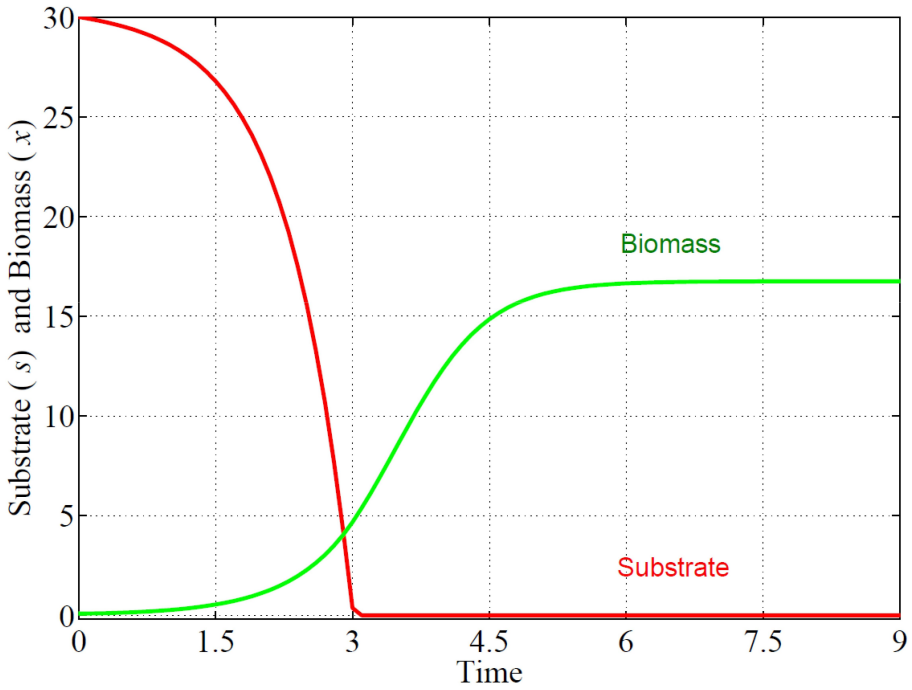

Figure 4: Dynamics of intracellular nitrogen and biomass for a batch photobioreactor growth experiment, assuming the Droop Model *source: [7]*

his model, Droop proposes the model variable q for the internal nitrogen quota of the cells with the growth rate dependency:

$$\mu(q) = \mu(\cdot)\left(1 - \frac{Q_0}{q}\right) \tag{1.1}$$

Whereas Q_0 is the minimum nitrogen quota that allows the cell to grow.

Photosynthesis Irradiance curve

Since the beginning of 20th century there have been efforts to measure and formalize the response photosynthetic organisms to different light irradiances. The firstly documented formulation for the limitation of Photosynthesis by light irradiance is proposed by Blackman in the year 1903 [8]. He describes the relation between Photosynthesis and irradiance as a linear increase for low irradiances and as constant after a certain saturation intensity. The response of photosynthesis to different light intensities – or Photosynthesis Irradiance curve (PI curve) – is today one of the most important characteristics to describe the photosynthetic response of phytoplankton population. It is defined as the dependency between the growth rate and the light intensity. In the following decade, many mathematical formulations for this characteristic property of plant growth dynamic were developed. In table 1 several formulations from the literature are listed. All of these static models for the dependence of photosynthesis from irradiance feature a saturation effect for irradiance exceeding a certain value. Furthermore, the formulations by Steele [69] and Peeters and Eilers [23] feature also the effect of photoinhibition. It is worth noting, that the formulation of Peeters and Eilers contains many parameters. This is due to the fact that it is a steady state solution of a dynamical model for photoinhibition. The parameters represent physiological properties and their model is capable of the description of the reponse to variable light signals also. Their model is presented in detail in paragraph 1.4.

P(I)	Reference	Inhibition
$\frac{I}{I+I_{1/2}}$	Monod[53]	no
$\frac{I}{\hat{I}} \cdot e^{1-\frac{I}{\hat{I}}}$	Steele [69]	yes
$\tanh(\frac{I}{I_k})$	Jassby and Platt [43]	no
$\frac{k\alpha\gamma\delta I}{\alpha\beta I^2+\alpha\delta I+\gamma\delta}$	Peeters and Eilers[23]	yes

Table 1: Empirical functions for light limited photoresponse using irradiance I and the parameters: Half saturation irradiance $I_{1/2}$, maximum productivity irradiance $\hat{I}$, and characteristic irradiance I_k (cmp. [3])

Today, the measurement of photosynthesis irradiance curves is part of the standard toolbox for photosynthesis research. It can be measured by monitoring cell numbers, CO_2 consumption or oxygen production in order to quantify the growth response of the algae to different irradiances. It should be highlighted that PI curves – by definition – imply a static interpretation of the growth response. This is sufficient for the characterisation of the ecological niche of a species but not for exact growth rate predictions in natural conditions.

Studies with dynamical light conditions

While PI curves are a static interpretation of the irradiance dependency of photosynthesis, there also exists a certain number of studies accounting variable light conditions. One of the most simple approaches is to observe physiological changes during a Ligh-Dark or Dark-Light transition, as it has been presented in a study of Neidhardt et al. [55]. In their study, pigment evolution and other charactersitics were tracked after High Light Low Light (HL-LL) transition. Furthermore, the PI curve was measured before and after

the transition. Before the development of LED lighting, the creation of precisely defined dynamical light signals for cultivation of microalgae has been a challenge. For the imitation of realistic illumination patterns very innovative technical approaches were developed, such as the experimental setup of Grobbelaar 1989 [33].

Recently, many studies have been carried out for the investigation of the impact of fast LD cycles with LED lighting, such as Vejrazka et al. [71] or Sforza et al. [66]. An important reason for this is that the biological response of such rapid cycles is considered to be the major factor for the potential increase in growth rate with mixing frequency for large scale cultures. In this spirit, there is a high number of studies focusing on an optimal design in order to maximize this gain in growth rate while keeping energy input to a minimum for specialized, high density Photobioreactors (PBR) experimentally: Qiang & Richmond focus on flat panel reactors [64], Doucha and Lívanský [19] on a special open design for biomass concentration, while Barbosa et al. and Bosma et. al. [4, 10] focus on bubble column reactors.

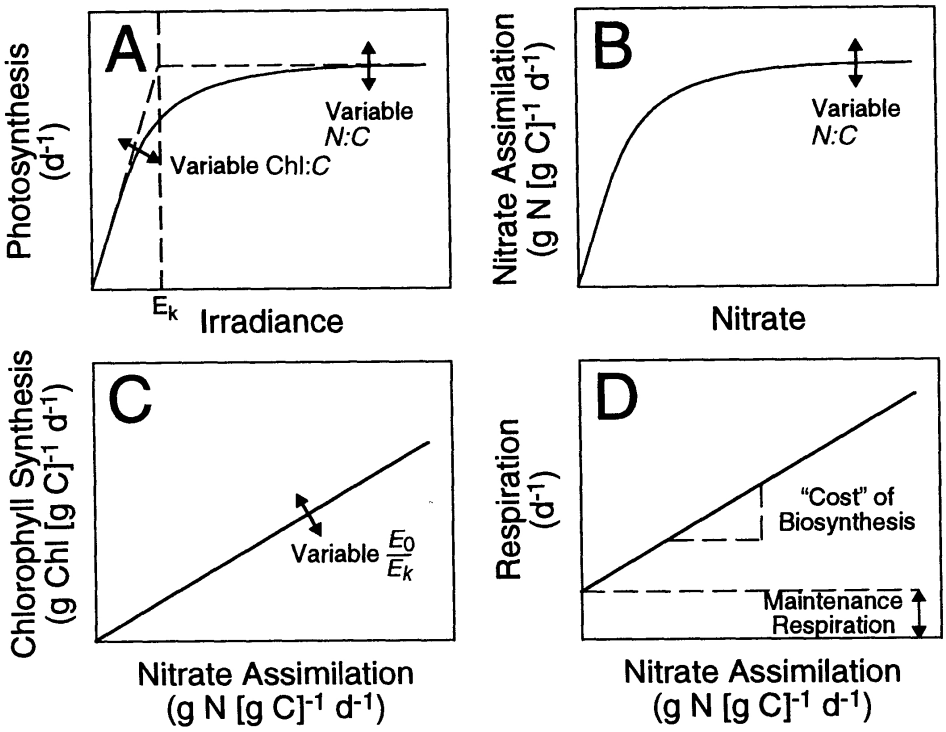

Figure 5: Important dependencies in the model of Geider et al. [30]. In particular: (A) Photosynthesis-Irradiance curve, (B) nitrate assimilation rate vs. intracellular nitrate, (C) chlorophyll synthesis vs. nitrate assimilation Rate, (D) respiration vs. nitrate assimilation *source: [30]*

1.4 DYNAMIC MODELS FOR PHOTOSYNTHESIS

The experimental findings from variable light conditions could not be explained by static models and motivate the development of dynamical models describing the growth of microalgae. In the following paragraphs, several dynamical microalgae growth models are presented. All of them target a specific time scale, either the fast time scale of the photosynthesis process [23] or the time scale of growth and acclimation [30].

Geider's Model for slow time scales

Geider et al. [32] developed a dynamic photosynthetic model for the understanding of oceanic growth phenomena such as bloom events. In the oceanic environment, the kinetics is slow while nutrient limitation and temperature variation play an important role. The proposed model includes mechanisms for nutrient uptake, chlorophyll synthesis and temperature dependent photosynthetic production and respiration. The model is built around some empirical properties which are widely accepted in the literature. Some of these properties are presented in fig 5:

- The slope of the chlorophyll specific Photosynthesis Irradiance curve is identical for different chlorophyll quota(see fig 5 A)
- Nitrate assimilation in the cells saturates at a certain level of intracellular nitrogen, as in the Droop model.(see fig 5 B)
- Chlorophyll Synthesis is positively linked to nitrogen assimilation and Irradiance.(see fig 5 C)
- Nitrogen uptake increases the respiration level in the cell due to its energy demand.(see fig 5 D)

The model is based on mass balances for carbon(C), nitrogen(N) and chlorophyll a(Chl). In the model, photosynthetic productivity follows a Poisson function of irradiance I:

$$P^C_{phot}(I) = P^C_{max}(T, Q)\left[1 - \exp\left(\frac{-\alpha^{Chl}\theta^C I}{P^C_{max}(T, Q)}\right)\right] \tag{1.2}$$

Whereas α^{Chl} is the Chl a-specific initial slope and θ^C is the Chl:C ratio. The maximum photosynthetic production P^C_{max} is a function of the intracellular Nitrogen quota Q and of the Temperature T:

$$P^C_{max} = P^C_{ref}\left[\frac{Q - Q_{min}}{Q_{max} - Q_{min}}\right]^n \chi(T) \tag{1.3}$$

In these equations, Q_{min} and Q_{max} represent the minimum and maximum N:C quota. n is a Shape-factor for the nitrogen dependency. $\chi(T)$ is a function of the temperature T.

Eq. 1.2 implies two important features of the model:

- Light *saturated* growth depends exclusively on the cellular nitrogen quota Q
- Light *limited* growth rate depends also on the Chl:C ratio θ^C

Alternative Formulations for Acclimation Dynamics

Bernard [7] presented a different formulation of the photoacclimation dynamics including nutrient dynamics. His model is based on the Droop model for nitrogen assimilation. For photoacclimation dynamics he introduced a variable $\dot{I}^*$, which is the current acclimated light intensity. At all instances, I^* approximates the received light intensity:

$$\dot{I}^* = \delta\mu(q, I)(I - I^*) \tag{1.4}$$

The chlorophyll content θ consequently appears as a derived value from the variables for intracellular nitrogen quota q and I^*.

$$\theta = \gamma_{max}\frac{k_{I*}}{I^* + k_{I*}}q \tag{1.5}$$

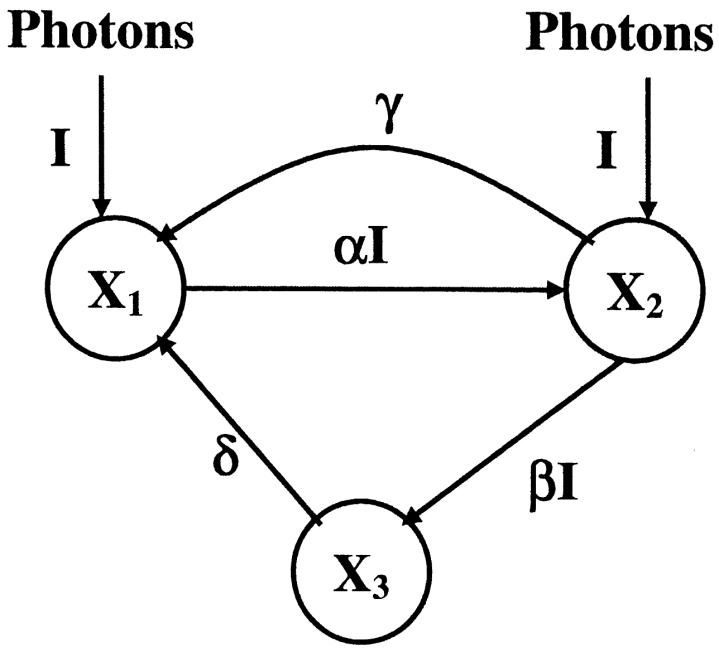

Figure 6: Schematic of the three states model of Eilers and Peeters. X_1 is the open state, X_2 the closed state and X_3 the inhibited state *(source: [74])*

Further, in his model the growth rate is defined as the following function

$$\mu(i, q, I^*) = \widetilde{\mu}\left(1 - \frac{Q_0}{q}\right) \frac{I}{I + \frac{K^*_{sI}}{\theta} + I^2/K_{il}} \tag{1.6}$$

Remark that this formulation follows a Haldane curve [35]. The coefficient K_{il} represents photoinhibition effects. Higher values of this coefficient impose a pronounced decrease in the productivity for high light irradiances. As the model of Geider, this formulation assures as well a constant initial slope of the chlorophyll specific PI curve for different acclimation states.

Eilers Peeters' model for fast and intermediate time scales

While Geider and Bernard among others provide models for the slow timescales of of nutrient uptake and pigment adaption. For rapid changes in the light conditions, there exists also approaches featuring a mechanistic formulation for fast physiological responses.

Eilers and Peeters [22] presented a dynamic model to account for the fast timescale of photosynthesis, and explain the photoinhibition mechanisms. The model simplifies photosynthesis to the function of "'photosynthetic factories"' which can be in three different states: open(X_1), closed(X_2) and inhibited(X_3). Transitions between these states represent photochemical and enzymatic processes. Fig. 6 shows the three states and the transitions between them. The excitation of the photosystems appears with the rate αI, while the deexciation – respectively photochemical quenching – happens at the rate γ. In addition to these transitions between open and closed state, there is also an inhibition process (at the rate βI) which turns photocenters from closed to inhibited due to overexcitation with excess amounts of photons, and a enzymatic repair process at the rate δ turning inhibited photocenters back to the open state. For the steady state solution of the model one obtains:

$$p(I) = \frac{k\alpha\gamma\delta I}{\alpha\beta I^2 + \alpha\delta I + \gamma\delta} \tag{1.7}$$

This is a classical Haldane shape [35] photosynthesis irradiance curve. Eilers and Peeters furthermore propose extensions for temperature dependence and oxygen consumption as a function of photoinhibition. However, a key result of their study is the following:

> "Our main finding is that static interpretations of production [irradiance] curves are incomplete and confusing. We feel that many of the controversies in the literature about the existence and importance of photoinhibition can be explained in this way. [...] [I]t is not appropriate to search for sophisticated theoretical production curves, except perhaps for steady state conditions. But steady state conditions are rare in nature." [22]

This statement is based only on the dynamic nature of inhibition processes. We will see in chapter 5, that adding acclimation processes supports this conclusion even more.

The dynamical model for photoinhibition proposed by Han [36] differs structurally only minimally from the model of Eilers and Peeters. In fig. 7, its structure is presented. When comparing it to the structure of Eilers and Peeters, it can be seen that it only differs in the repair process transition, which turns the inhibited photocenters back to closed state instead of open state as in Eilers and Peeters. The steady state solution for both models as in eq. 1.7 is structurally identical. Due to the seperability of the time scales in both models, all other solutions should be quantitatively similar as well. Nevertheless, analytical deductions might be different. The Han model and its properties will be discussed in depth in ch. 4. It can be said that the model of Eilers and Peeters [23, 22], respectively the model of Han [36] is the quasi gold standard for the dynamic modelisation of photoinhibition. To the author's best knowledge, most recent approaches are based on these. However, a recent study consider single photon transitions and intermediate states replacing the linear open/closed transition [76]. There exists a model by Esposito et al. [25], which directly couples the model of Geider with the Han Model.

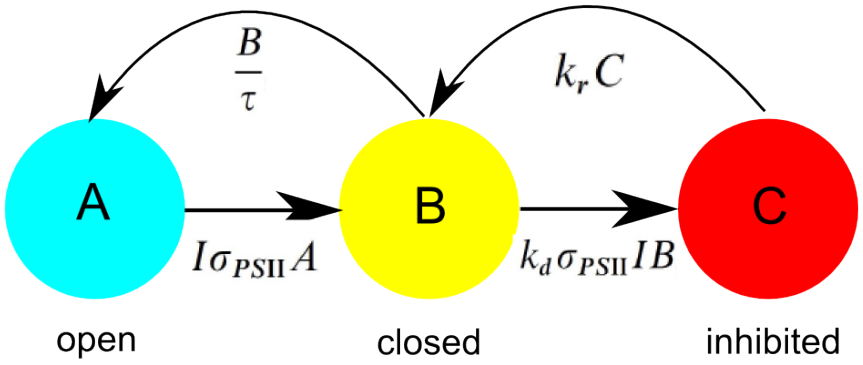

Figure 7: Structure of the Han Model [36] showing the three state variables open A, closed B and inhibited C and the respective transition terms.

In order to simplify the structure they removed the fast dynamics of the Han model. With their model the authors aim on the dynamics in the ocean and shallow water zones.

García-Camacho's dynamic model for photosynthetic productivity including photoacclimation and -inhibition

In a recent study, García-Camacho [29] present a mechanistic model including photoinhibition *and* acclimation. Their work adresses an important research gap: The inclusion of mid-term and short term processes in one physiological model. Fig. 8 shows a representation of photosynthesis, illustrating the important processes which are considered in their model. When comparing to fig. 6, it is obvious that the structure of the Eilers and Peeters model builds the basis for their approach.The constant transition rates for repair processes

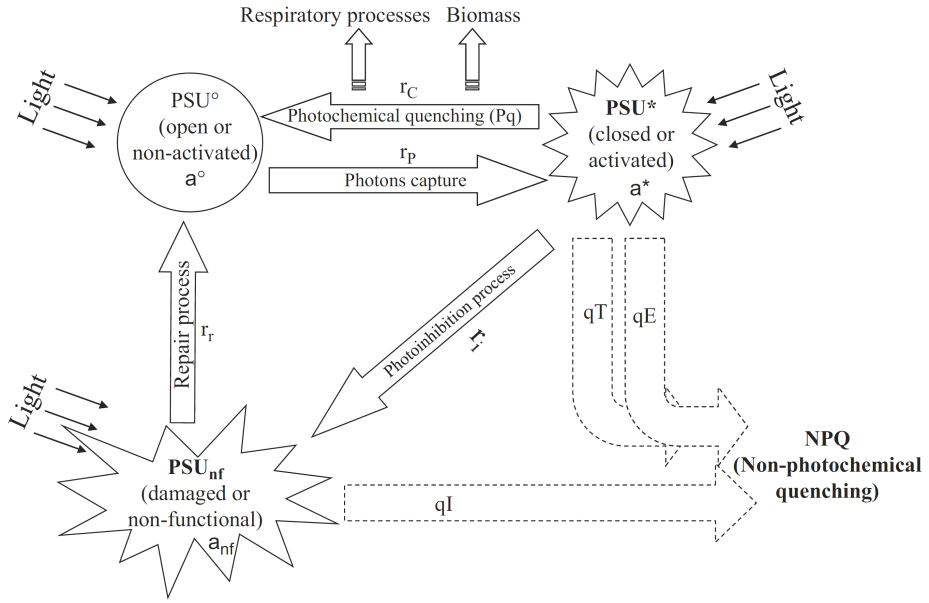

Figure 8: Schematic representation of Photosynthesis, as it is the basis for the model of García-Camacho et al. [29] (*source:[29]*)

and photosynthetic production are replaced by Monod functions in order to describe these processes more precisely. For acclimation processes, they choose a logistic approach, which allows for different acclimation kinetics for HL-LL transitions compared to LL-HL transitions. Due to the complexity and the vast amount of parameters of the model, however, it is hard to collect enough data to convincingly validate it.

1.5 THE EFFECT ON HYDRODYNAMICS ON PHOTOSYNTHETIC EFFICIENCY

Microalgae cultures typically have a very high particle density which consequently causes also a high optical density. Due to mixing, cells are continuously advected between dark area and bright regions. Due to the dynamic nature of photosynthesis, this drastic changes in

light intensity received by the cells can lead to significant effects on the growth rate.

This mechanism has led several authors to analyze flow patterns and mixing by hydrodynamic models. Hydrodynamic modeling results are typically represented by time dependent velocity fields for local water flows (Euler approach) or trajectories of single (virtual) particles (Lagrangian Approach). Both results are equivalent, given the formulations have a comparable resolution. Velocity fields primarily allow for a macroscopic analysis of i.e. local dispersion or energy dissipation. Pruvost et al. [63] proposed an innovative toric PBR design while presenting an in-depth analysis of its hydrodynamic properties. By validation with Particle Image Velocimetry (PIV), they ended up with a trust-able model which allows for the comparison of different impeller models for mixing and the prediction of dispersion dynamics. On a macroscopic scale, these characteristics imply how much energy must be invested for mixing in order to provide good growth conditions. In a more recent work, Pruvost et al. [62] presented an approach for coupling hydrodynamics with a biological model using lagrangian particle trajectories using the toric reactor design. Similarly to Luo and Al-Dahhan [50], they found that the average light intensity which is calculated based on the trajectories is different from the average light intensity for the volume. While Luo and Al-Dahhan propose that this could be a measure to improve efficiency of photobioreactors, Pruvost et al. show that this effect is energetically inconsistent and that it indirectly results from the non-equally distributed resistance time of the simulated particles in the volume. Pruvost et al. consequently applied different strategies to correct this factor and finally define consistent light profiles with a static photosynthetic model. As they say, such a model does not

account for flashing light effects. So finally they showed, that an influence on the growth rate by design of the hydrodynamic properties can only be estimated using models which account for cycling LD effects.

Sastre et al. [65] propose the application of a helical static mixer for tubular PBR. They claim to reach very high Reynolds numbers with this mixer. The objective of this extreme mixing is to provide highly variable light signals for individual cells with high frequencies. This high mixing frequency should stimulate dynamical effects of photosynthesis, such as the flashing light effect. In a more detailed CFD analysis by Perner-Nochta and Posten [59], it is shown that indeed frequencies up to 1 khz in the light signals could be reached. They document that with their approach near wall effects are not well represented. This is remarkable, since Pruvost interpreted accumulation at the walls as an indicator for nonhomogeneous particle density. In chapter 6, we observe a similar effect using a completely different model for hydrodynamics at the bottom of the raceway volume. Considering models for radiative transfer and the overall deduction of light signals, however, the distribution of the biomass in the reactor plays an important role.

Regarding raceway pond culturing systems, modeling effort is focused on the effect of macroscopic external parameters such as temperature and surface light irradiance [42, 16]. The effect of mixing has been empirically studied by CFD, and design improvements have been proposed [48, 15]. However, these Eulerian approaches rely on macroscopic consideration and do not take into account the variability of the light signal on single cell scale. Therefore they are not feasible in order to estimate which mechanisms play the

important roles and what is the effect of mixing, beyond nutrient homogenization.

The flashing Light effect

Short term fluctuations of light intensity can modify photosynthetic activity. This effect was firstly described by Phillips and Myers [44]. They found that growing cells illuminated with short light flashes have shown a more efficient growth (Quantum Yield) than under continuous illumination. The growth rate increase changes with flashing frequency and the duration of light and dark periods and can lead to a growth rate of up to 25 % [26].

Falkowski and Raven [26] present two possible physiological processes as possible mechanics behind the flashing light effect: (1) Enhanced post-illumination respiration and (2) the disequilibrium between photosynthetic electron transport and the Calvin(-Benson) cycle. The first hypothesis follows the logic that respiration increases with light intensity, but also with the length of illumination. Effectively, the respiration enhancement due to light exposure is claimed to be much smaller for flashing light signals with high flashing frequencies due to this reduced respiration rate. Indeed, Beardall et al.[5] show that there is an increase of post-illumination dark respiration which increases with the duration of the illumination phase. The second hypothesis is based on the argument, that the Calvin cycle is the bottle neck for the production in continuous illumination. For sufficiently short light flashes, the ATP which is generated by the electron which are produced during the light phase are sufficient to aliment the comparably slow Calvin cycle throughout the dark phase and allow for its continuous operation.

These two physiological mechanisms are not the only ones to be considered to contribute to the flashing light effect. Iluz et al. [41] proposes three other mechanisms to contribute as well: photoinhibition, thermal dissipation and the xanthophyll cycle. According to them, the amount of which each off these mechanisms contribute to the flashing light effect will strongly depend on the conditions. Even though all presented mechanisms are very different in nature, they are all expected to lead to increased growth rate with flash frequency. This is due to the fact that all of these effects create a negative feed back with extended exposure to high light irradiances. For photoinhibition this feedback effect is very plausible and simple: Long term high irradiation periods increase photodamage and therefore reduce the number of active photocenters. According to this, higher flashing frequencies will reduce the photodamage due to the shorter illumination period leading to a higher overall efficiency of the photosynthetic apparatus. Thermal dissipation, xantophyll cycle are protective mechanisms which can mitigate the amount of photodamage short term by dissipating excess energy non-photochemically. Especially photoinhibition and photoprotective mechanisms work on similar time scales while both being negative feed back effects. This makes it very difficult to identify the influence of one single process in flashing light experiments.

For the creation of models this creates a difficult situation: Different mechanisms which are inseparable in their time scale will lead to a similar behavior of the biological system. A model considering all possible mechanisms at once will consequently be highly over-parametrized to the collectible data. What can be observed is that many authors include only selected physiological mechanisms, while describing the flashing light effect well e.g. [75]. This approach

is acceptable for using the model as a predictive tool for growth rate. Nevertheless, it should always be considered, that the validation of the model is not a proof that the considered effect in the model is actually the experimentally observed one. In this Thesis we will exhaustively discuss and use the model of Han for photoinhibition. Depending on the specific application, what is called photoinhibition should be more appropriately interpreted as the sum of photoinhibition and all other effects reducing photosynthetic production at similar time scales.

1.6 OBJECTIVE OF THIS THESIS

This thesis investigates of the growth rate improvement effect from mixing of raceway cultures. In this context, the influence of specific hydrodynamic regimes on the response of dynamical biological models is regarded. To approach this task four major challenges have to be addressed: (1) Suitable dynamical biological models have to be formulated, (2) The influence of dynamical light signals has to be investigated, (3) Important macroscopic dependencies have to be validated experimentally and (4) Hydrodynamics has to be considered realistically as a basis for the estimation of realistic light signals.

Ch. 3 presents an experimental study on the growth rate and pigment evolution for LD cycles of different cycling frequencies. This experimental study shows that microalgae photoacclimate in the same way to signals with the same average light dose but different cycling frequencies. In ch. 4 we can show that the observed flashing light effect can be well described by the proposed model for photoinhibition and nutrient uptake. It appears, that this effect can

contribute to growth rate increase by mixing. The observed evolution of pigment content from ch. 3 has motivated the development of the acclimation model in ch. 5. While this model shares important properties with well known acclimation models, it includes photoinhibition processes. In order to assess the hydrodynamic conditions in raceway systems realistically, the final study proposes the coupling of a hydrodynamic model with a model for photoinhibition and the derivation of the growth rate of the entire system based on this. Apart from the signal cycling frequency, also the standard deviation of the light signal has been identified to have an influence on the overall growth rate.

2

MATERIAL AND METHODS

By three methods we may learn wisdom: First, by reflection, which is noblest; Second, by imitation, which is easiest; and third by experience, which is the bitterest.

Confucius

This chapter presents the material and the methods which have been used during this thesis. Firstly, the experimental setup that has been used to collect experimental data supporting then the model developments is presented. The computer driven Marine Environment simulator [51] has been modified for this study in order to generate the fast varying light pattern representing light fluctuations at a single cell scale. The specific developments which have been carried out are explained in paragraph *Light supply*. Secondly, the simulation tool used to simulate the raceway hydrodynamics is presented, providing estimations of the lagrangian trajectories of microalgae cells inside the water volume.

2.1 EXPERIMENTAL METHODS

In ch. 3, an experimental study on the growth of *Dunaliella salina* is presented. An innovative experimental setup has been developed and utilized for this. In the following paragraphs the methods applied for this experiments are presented. These paragraphs are an extended version of the Materials and Methods section of the article manuscript.

2.1.1 *Algae, growth medium and pre-cultivation conditions*

Laboratory experiments were conducted with the Chlorophyceae *Dunaliella salina* strain CCAP 18/19, from the Culture Collection of Algae and Protozoa (CCAP) in sterile filtered F/2 medium [34], prepared from aged, Mediterranean Sea surface water (38 g L^{-1}) collected at the permanent Point B SOMLIT station (43°41,10'N

and 7°18,94'E). The seawater was filtered through 1 μm Durapore filter mounted in an housing for single cartridge to eliminate the majority of particles and stored in the dark at room temperature for 2 months. Before use, the seawater was filtered through 0.1 μm Durapore filter, then autoclaved at 120°C for 30 min. After cooling and sterile addition of macro- and micronutrients [34], the medium was transferred to the photobioreactors through a 0.2 μm sterile filter.

The strain was maintained and propagated in the same medium in polycarbonate flasks. Pre-cultures were grown for at least 10 generations at 300 μE m^{-2} s^{-1} in the exponential phase in light-dark (12:12) incubator (SANYO MLR-351) at 27°C.

2.1.2 *Experimental design*

Growth experiments were performed in 8 aseptic, double-walled borosilicate glass photobioreactors (SCHOTT DURAN) with a capacity of 600 mL. The reactors were placed in two experimental chambers, each of them with two independent compartments. A closed water circuit with a cryastat inside the double walls maintained a constant temperature of 27°C in the reactors – a value which is reported to be optimal for the growth of this strain [28]. Magnetic stirrers were used to homogenize the cultures. Bubbling was provided with air filtered by a Whatman filter (0.2 μm). pH was regulated at 8.3 using CO_2 controller linked to pH sensors in each culture [6]. The same conditions were applied to both vessels in each compartment in order to duplicate the experiment.

Light supply

Photobioreactors were illuminated with LEDs (Led SmartArray, 12 x Nichia LEDs, 6W; Lumitronix). 6 LEDs were identically set up in each box on each side of the two cultures (fig. 9), connected to an open-source electronics prototyping platform Arduino to generate continuous light (CL) and flashed illumination (FL) at the desired intensities and frequencies.

The Arduino board supplies a pulse width modulation (PWM) signal as an output, which – using high power LED drivers which were available at this time – would consequently lead to flickering at frequencies between 100 Hz and 10 kHz. In the utilized setup we used the Arduino board with the 'LED shield' from a small retailer. The Arduino board allows for the free programming of any light signal using 255 discrete intensities levels. Each LED shield supplies 4 high power LED drivers in order to apply a current to the LEDs which is proportional to the input signal from Arduino. In order to minimize the flickering effects from the (PWM) signal, the input signal for the Drivers has been smoothed out by a RC Low pass filter which is a feature of the LED shield. Control measurements showed, that the light fluctuation amplitude from the PWM signal was below 15 %, which is a reasonable result compared to 100 % when not using the RC filter. The fact that the light signal is virtually limitless customizable is an important feature for a follow-up studies, in which more realistic light profiles can be.

For each experiment, the two duplicates in the right compartment were exposed to continuous light (CLA/CLB), named thereafter 400A-cont and 400B-cont. Other photobioreactors were exposed to flashing light in the three other compartments (FLA/FLB),

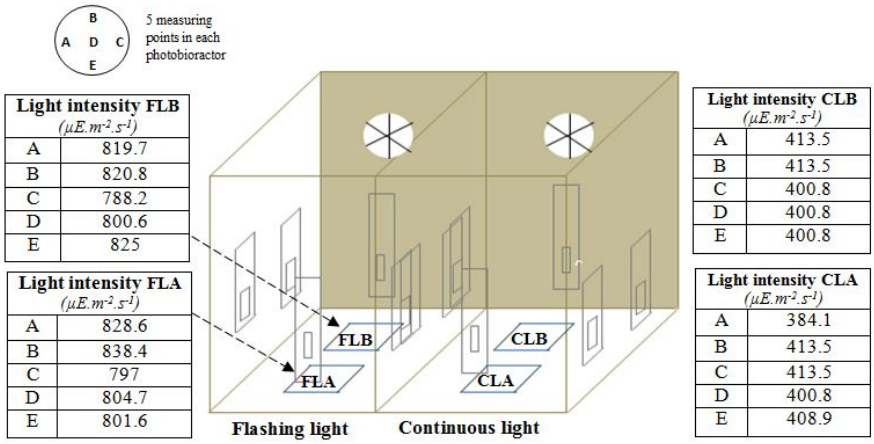

Figure 9: Schematic representation of experimental setup. In each box of this experimental chamber, grey rectangles indicate the position of the light sources. In the right part of the chamber, the two duplicates are exposed to continuous light (CLA/CLB).In the left part, the two duplicates are exposed to flashing light (FLA/FLB)

named $800A_{\Delta t_{light}-\Delta t_{dark}}$ and $800B_{\Delta t_{light}-\Delta t_{dark}}$ with pulsed light conditions resulted in precise duration of flashes (Δt_{light}) and dark (Δt_{dark}).

2.1.3 *Culture conditions*

Turbidostat experiments were performed using a computer driven culturing system [24]. In order to be able to supply the specific light profiles for this study, the light device has been replaced by a freely programmable LED system. This continuous culturing method implies daily adjustment of the dilution rate to ensure that nutrients are non limiting and to keep the cells at a constant density and in replete condition. Culture medium was renewed with a peristaltic pump to insure a constant culture volume, set at 500 mL. 8 peristaltic pumps have been used. These experiments were performed to determine the effects of different dynamic light signals on growth

rate and several physiological properties. Cultures were kept at a low optical density in order to reduce shelf-shading. All nutrients (such as N, P, S, macronutrients) were provided in excess, so that algae growth was limited only by light availability. To maintain a constantly homogeneous light distribution in each culture during the entire experiment, cultures were stabilized at 2 10^5 cells mL^{-1}. Measurements were conducted during two experiments for 17 days and 16 days. Different light regimes with an equal average total light dose were applied. The intermittent light regime consisted of equal light-on (I=800 µE m^{-2} s^{-1}) and dark intervals (L:D = 1:1), and was compared with continuous light of equal mean irradiance (I=400 µE m^{-2} s^{-1}), close to the optimal intensity for the growth of *Dunaliella salina* [28]. Flashed light signals (I= 800 µE m^{-2} s^{-1}), with a duration of lighting flash Δt of 30 s (f=0.017 Hz), 15 s (f=0.033 Hz), 2 s (f=0.25 Hz) and 0.1 s (f=5 Hz) were applied. In addition, signals with different LD ratios were applied: 2s of HL phase (I=1000 µE m^{-2} s^{-1}) with 3s of dark phase (L:D = 2:3) and 2s of HL phasee (I=600 µE m^{-2} s^{-1}) with 1s of dark phase (L:D = 2:1) are applied. Consistently to previous studies [28], these light intensities do not lead to inhibitory effect on *Dunaliella salina* growth. Irradiance was monitored in 5 positions in each photobioreactor using a light meter (Biospherical Instruments US-SQS/D) (fig.9).

All parameters listed thereafter were measured daily, starting on day 1 for cell size and abundance and on day 4 for all others. The tested light regimes are summarized in table 2.

Experiment	Condition code	Light intensity ($\mu E\ m^{-2}\ s^{-1}$)	f (Hz)	Flash time (Δt_{light}) (s)	Dark time (Δt_{dark}) (s)
1 (17 days)	800_{2-2}	800 ± 25.4	0.25	2	2
	800_{15-15}	800 ± 20.1	0.033	15	15
	800_{30-30}	800 ± 19.3	0.017	30	30
	400-cont$_1$	400 ± 21.5	-	∞	-
2 (16 days)	$800_{0.1-0.1}$	800 ± 25.4	5	0.1	0.1
	800_{2-3}	1000 ± 20.1	0.2	2	3
	800_{2-1}	600 ± 19.3	0.33	2	1
	400-cont$_2$	400 ± 21.5	-	∞	-

Table 2: Description of light regimes tested employed for *Dunaliella salina* growth in turbidostat culture. Alternating cycles of light and dark have same integrated light intensity corresponding to 400 $\mu E\ m^{-2}\ s^{-1}$ of continuous light. Pulsed light conditions resulted in precise duration of flashes (Δt_{light}) and dark (Δt_{dark}). Each experiment was done in a biological duplicate in two independent photobioreactors

2.1.4 *Cell size and abundance*

After inoculation, the changes in population density and mean diameter were monitored in triplicates, using a Coulter Counter Beckman (Multisizer 3) with a 50 µm aperture tube. In parallel, cell abundance was also determined using a monitored liquid particle counter (Hiac 9703+). Daily averages of the cells abundances of turbidostat cultivations remained stable for consecutive days, which indicates the equilibrium state of the cultures regarding growth rate and dilution. In this setup, turbidostat cultivations in steady state has been stabilized to 2 10^5 cells mL^{-1}.

Based on the dilution rate (d, day^{-1}) and the apparent growth rate (μa, day^{-1}), the specific growth rate (μ, day^{-1}) was calculated according to the following relation: $\mu = d + \mu a$.

2.1.5 *Pigment extraction and analysis*

Pigments were extracted and quantified from the algae starting with day 4 of the cultivation period. Samples of 3 mL cell suspension were taken from the reactors once per day and transferred to 10 mL tubes wrapped with aluminium paper to prevent photobleaching [47]. Extraction was done using 6 mL of 90% acetone per tube, thereafter stored during 1 hour at -20°C. Cells were precipitated by centrifugation at 2000 rpm for 5 minutes. Absorbance was measured at 470 nm, 644.80 nm, 661.60 nm and 700 nm, corresponding to absorption maxima of carotenoids, chlorophyll *a* and chlorophyll *b* respectively [47], with a UV/Vis spectrophotometer (Perkin Elmer, Lambda 2). Pigment composition is presented as the temporal average ± SD of two replicates (four replicates for continuous light).

Concentrations of chlorophyll *a* (C_a), chlorophyll *b* (C_b) and of total carotenoids (C_{x+c}) were calculated from the equations according to Lichtenthaler [47]: $[C_a] = 11.24A_{661.6} - 2.04A_{644.8}$ (µg mL^{-1} solution)

$[C_b] = 20.13A_{644.8} - 4.19A_{661.6}$ (µg mL^{-1})

$[C_{x+c}] = (1000A_{470} - 1.90C_a - 63.14C_b)/214$ (µg mL^{-1})

2.1.6 *Elemental stoichiometry*

Samples (6.8 mL) were first filtered onto pre-combusted (4h at 450°C) GF/C filters (Whatman) and then dried at 60°C before analysis with a CHN analyser (2400 Series II CHNS/O - Pekin Elmer). Nitrogen (pmol-N cell^{-1}) and carbon (pmol-C cell^{-1}) cells contents

were estimated using the cell abundance measured at the time of sampling.

2.1.7 *Lipid analysis*

Total lipid concentration was quantified according to the Bligh and Dyer's method [9]. Samples of 200 mL cell suspension were precipitated by centrifugation at 2000 rpm for 10 minutes. Then, cell pellets were frozen and stored at -80°C waiting for extraction. Two successive extractions with a monophasic mixture of chloroform:methanol: salt water (1:2:0.8 v/v) were done. Chloroform and water were then added for phase separation (2:2:1.8 v/v). The chloroform phase was evaporated and total lipids (TL) were stored at -80°C under nitrogen atmosphere to avoid oxidation, until analysis.

2.2 HYDRODYNAMIC SIMULATION OF RACEWAY SYSTEMS WITH FRESHKISS

In ch. 6, the implementation 'FRESHKISS' of a hydrodynamic model for raceway systems is used for modeling light profiles of single algae cells in raceway systems. The following paragraph presents the basis of this approach.

In general case of a hydrodynamic system, the Navier-Stokes equations have to be solved. For this task, there exists commercial software like FLUENT and COMSOL which can solve complex flow patterns using methods of finite difference, finite elements or finite volumes.

The raceway pond has an open water surface. Open surfaces complicate the problem considerably and demand for the solution of the parabolic free surface Navier-Stokes equations [13]. As a matter of fact, the treatment of these equations with classical methods lead to issues regarding computation and can hardly guarantee important physical properties such as the positivity of the water depth.

Bernard et. al. [12] therefore have suggested to use a modified Saint-Venant system. This approach is possible, since the flow in a raceway pond can be considered as a shallow water flow. They propose to use a 'multilayer Saint-Venant System', which is an approach which is proven to feasible [2].

The Saint-Venant approximation is applicable for shallow water volumes. In this approximation, the water velocity is averaged over the (shallow) depth column z: $u(x, z, t) = \bar{u}(x, t)$. The multilayer Saint-Venant system considers a stack of such shallow water systems and the water exchanges between these layers.

To further simplify the calculus, the hydrostatic assumption has been taken: no vertical acceleration exists apart from the direct surrounding of the paddlewheel. The paddlewheel itself is simplified as a volumetric force on the water, and can be decomposed in a component in x and z direction:

$$F_{wheel}(x,z,t) = F_x(x,z,t)\mathbf{e_x} + F_z(x,z,t)\mathbf{e_z} \tag{2.1}$$

With this force term, the 2D hydrostatic Navier-Stokes equations are the following:

$$\begin{cases} \frac{\partial \rho}{\partial t} + \frac{\partial \rho u}{\partial x} + \frac{\partial \rho w}{\partial z} = 0 \\ \frac{\partial \rho u}{\partial t} + \frac{\partial \rho u^2}{\partial x} + \frac{\partial \rho u w}{\partial z} + \frac{\partial p}{\partial x} = \frac{\partial \sum_{xx}}{\partial x} + \frac{\partial \sum_{xz}}{\partial z} + F_x(x,z,t) \\ \frac{\partial p}{\partial z} = -\rho g + \frac{\partial \sum_{zx}}{\partial x} + \frac{\partial \sum_{zz}}{\partial z} + F_z(x,z,t) \end{cases}$$

Where (u, w) represents the velocity vector, p(x,z,t) is the pressure, g the gravity acceleration and ρ the water density. Σ_{ij} represents the viscosity tensor. The first equation describes mass conservation, the second impulse conservation and the third one energy conservation. This system is then solved with the constraints: $t > T_0, x \in \mathbb{R}$ and $z_b(x) \leqslant z \leqslant \eta(x,t)$ with $\eta(x,t)$ being the position of the open water surface. For the calculus, the equations are resolved for each layer. However, the average value of all layers for the velocity is used in the consecutive steps $u(x,z,t) \approx \sum_{\alpha=1}^{N} u_\alpha(x,t)$.

These equations have been discretized according to Audusse et. al [2] and expanded to a 3D mesh representing the raceway. Fig. 10 shows a representation of the 2D mesh structure at the bottom of the raceway. For the 3D simulation, this mesh consisting of

3360 vertices has been extruded in 20 layers. The numerical solver was implemented in C++ and needed approximately 2 weeks of calculation for 60.000s of simulation time.

Fig. 11 shows the raceway volume superposed with information of the velocity magnitude and an exemplary trajectory. In general, the velocity field is calculated by the multi-layer Saint-Venant approach and trajectories are subsequently calculated by tracing virtual particles assuming that they follow the velocity-field of the water. Particles which – due to the time discretisation would exit the volume are reflected by the boarders of the volume.

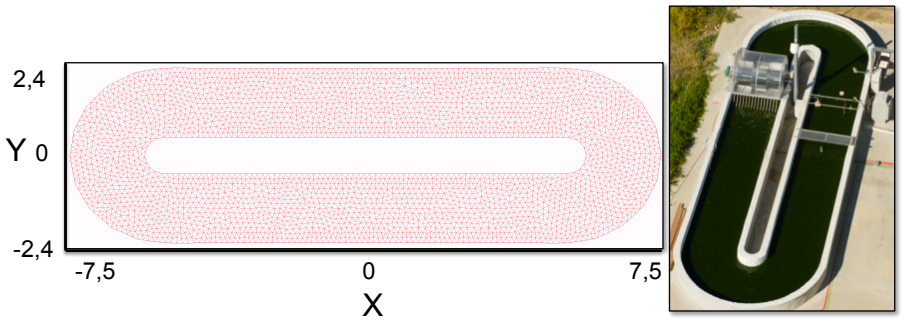

Figure 10: Picture and 2D mesh of the raceway system in INRA, Narbonne (length = 15 m, width = 4,80 m)

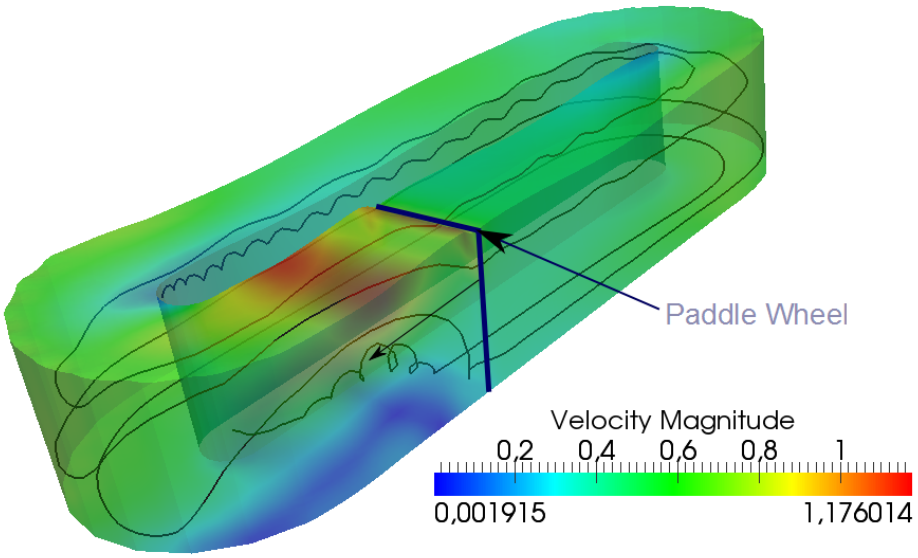

Figure 11: 3D representation of the water volume and its velocity field in the numerical simolations. A particular trajectory is also represented.

3

LONG-TERM ADAPTIVE RESPONSE TO HIGH-FREQUENCY LIGHT SIGNALS IN THE UNICELLULAR EUKARIOTE DUNALIELLA SALINA

Life is short, the art long, opportunity fleeting, experiment treacherous, judgement difficult.

Hippokrates of Kos

In this chapter, an experimental study on the long term reaction of *Dunaliella salina* to LD cycles is presented. The objective is to investigate reactions in the pigment content and the growth rate of the algae to dynamical light conditions. The experimental conditions are chosen adequately in order to quantify the increase in growth rate for increasing light flashing frequencies – the flashing light effect. The hypothesis that microalgae acclimate to the average light dose, is furthermore put to the test by the presented study. Other studies following the pigment evolution under controlled variable light conditions for an extended time period of comparable length do – to the authors best knowledge – not exist.

Experiments with flashing light stimulation of microalgae are carried out for over 60 years now [44]. The recent development of high power LED light sources however makes it a lot easier to provide a setup for such an experimental study; Some recent studies aim on the investigation of the response of microalgae growth to flashing light signals [71, 66]. Both studies measure an increase in growth rate with increased LD frequency; Due to lacking data about chlorophyll content [71] or the relatively short growth phase [66], these studies do not allow to distinguish acclimation from short term effects.

For the experiment, we have developed a novel setup which is presented in ch. 2. It uses a freely programmable microcontroller (Arduino) in conjunction with high power warm white LEDs. Continuous cultures were kept in duplicates for an extended time period and cell abundance, pigment evolution and other physiological parameters have been tracked for different LD cycle signals.

Long-term adaptive response to high-frequency light signals in the unicellular photosynthetic eukaryote *Dunaliella salina*

Charlotte Combe[b,c,*], Philipp Hartmann[a,b,c], Sophie Rabouille[b,c], Olivier Bernard[a,b,c], Antoine Sciandra[b,c]

[a] *BIOCORE-INRIA, BP93, 06902 Sophia-Antipolis Cedex, France*
[b] *Sorbonne Universités, UPMC Univ Paris 06, UMR 7093, LOV, Observatoire océanologique, F-06230, Villefranche/mer, France*
[c] *CNRS, UMR 7093, LOV, Observatoire océanologique, F-06230, Villefranche/mer, France*

[*] Corresponding author
Email addresses: philipp.hartmann@inria.fr (Philipp Hartmann), olivier.bernard@inria.fr (Olivier Bernard), sciandra@obs-vlfr.fr (Antoine Sciandra)

Abstract

Biofuels from microalgae are a promising solution in a society in which renewable energy development has become a major challenge. To compete with fossil fuels, it is necessary to get high productivity at a lower cost. Research efforts are thus necessary to optimize microalgal cultivation processes. Productivity is tightly related to photosynthetic efficiency, and therefore to light availability at cell scale. In a highly turbid medium, the light signal received by a single floating phytoplankton cell in a dense culture is a succession of flashes. The growth characteristics of microalgae under dynamic light conditions are thus fundamental information to understand nonlinear properties of the photosynthetic process and to improve photobioreactor design and operation. Studies of the long term consequences of dynamical light on photosynthesis require a very specific experimental set-up; hence, available literature data on this topic is scarce. In order to investigate the growth response of the unicellular photosynthetic eukaryote *Dunaliella salina* (Chlorophyceae) to intermittent light exposure, different light regimes using LEDs with the same average total light dose were applied in this study. Continuous illumination and flashing light with different durations of light flashes (Δt of 30 s, 15 s, 2 s and 0.1 s) were compared. Specific growth rate, photosynthetic pigment, lipid productivity and elemental composition were measured for two duplicates of each condition using continuous cultures. Under intermittent light specific growth of increasing frequency rate from 0.25 to 0.93 day^{-1} was measured. Photosynthesis efficiency has enhanced with light frequency, while no significant differences in carbon specific and chlorophyll content were observed. Pigment analysis shows that – within this range of LD frequency – cells photoacclimated to the average light intensity.

1. Introduction

The use of fossil fuels as a major form of energy is unsustainable since it is leading to resources depletion and the accumulation of greenhouse gas in the environment (Höök and Tang, 2012). Thus, the development of regenerative energy sources that can reduce fossil fuel consumption and particularly petroleum derived transport fuels is a crucial challenge (Chisti, 2008).

In the context of renewable energy, unicellular photosynthetic microorganisms (abusively called "microalgae") using photons as energy source to fix carbon dioxide (CO_2) have received specific attention. Because of their high biomass productivity and growth rate (doubling times may be as short as 3.5h (Gordon R., 2012)), compared with terrestrial plants, and the high lipid content of some species (up to 50% dry weight triacylglycerols (TAG) (Amaro et al, 2011)), microalgae are currently promoted as a key player in the third generation biofuel feedstock (Mata et al, 2010). Indeed, some species of algae which grow in a wide range of aquatic environments (Hannon et al, 2010), have the capacity to store high TAG quantities (Rodolfi et al, 2009) after nutrient starvation or exposure to excess light. Microalgae cultures can mitigate industrial CO_2 emissions while being independent from fertile soil and do therefore not compete with agricultural food production (Gouveia and Oliveira, 2009).

In industrial cultures phytoplankton growth is limited by light (Sarmiento and Gruber, 2006). The photosynthetic organisms are exposed to a variable and dynamic environment. Particularly, hydrodynamics induce vertical motion which mixes the water column and chaotically changes the position of individual microalgae cells and therefore the light they receive. In artificial culture systems, the effect of this coupling between hydrodynamics and biology is larger as changes in light perceived by cells can be very fast, with time constants ranging from milliseconds to tens of minutes.

Microalgae are generally cultivated in open pond raceway systems or closed photobioreactors (PBRs). Raceway ponds are shallow artificial culture systems (about 10-40 cm depth). Paddle wheels create a turbulent flow leading to a complex hydrodynamical mixing. In such dense cultures, the high optical density leads to strong light gradients. Due to intense turbulence and the strong light gradient, algal cells are exposed to time varying light intensities (Pulz, 2001). Hydrodynamics determines the cell trajectories in the medium and therefore, for given light conditions at the surface pond, the received

light signal: individual cells move back and forth from high light to total darkness. The light perceived by a single cell is thus a succession of rapid light/dark (L/D) changes (Litchman, 2000; Perner-Nochta and Posten, 2007; Vejrazka et al, 2011; Boulanger et al, 2013). In heavily mixed photobioreactors, light signals experienced by cells were characterized by fluctuation rates of up to 1 kHz (Perner-Nochta and Posten, 2007). Few studies have so far been carried out in open ponds, in which realistic trajectories of cells are still unknown.

To compete with fossil fuels, the use of microalgae has to reach high productivity at a low cost. Research efforts are thus necessary to reduce the energy required for mixing while improving productivity. The link between productivity and mixing, through its effect on light supply at the cell scale, must then be elucidated as the pattern of light delivery controls photosynthetic efficiency (Richmond, 2004; Posten, 2009). This effect is even more important when dealing with photoinhibition occurring for outdoor cultures inevitably exposed to high light intensities. Peak intensities from sunlight can be as high as 1500 μmol photons m^{-2} s^{-1} (Litchman, 2000). One of the known causes of photoinhibition induced by high light exposure is the production of highly reactive oxygenic species and byproducts that induce photo-oxydative damages (Murata et al, 2007; Li et al, 2009). Increasing light intensities saturate the photosystem so that the photosynthetic yield decreases. This inhibiting effect is counteracted by a repair process, which works more slowly (Murata et al, 2007; Nixon et al, 2010).

Microalgae photoacclimate in order to adapt their light harvesting efficiency to the available light. Photoacclimation operates through physical adjustment of the photosynthetic system at the time scale as the cell growth. Such adaptation involves changes in cell pigmentation or in structural characteristics such as adjustments in the number and/or the size of photosystems antennas (Falkowski and Owens, 1980; Falkowski and LaRoche, 1991; Herzig and Dubinsky, 1992). An increase in cellular photosynthetic pigment content (such as chlorophyll) is for instance commonly observed in strains grown under low irradiances. Accordingly, pigment content decreases in cells exposed to high irradiances in order to minimize photo-oxidation processes (Richardson et al, 1983; MacIntyre et al, 2002). While photoacclimation in continuous irradiance conditions has already been studied and documented (Herzig and Dubinsky, 1992; MacIntyre et al, 2002; Garcia-Camacho et al, 2012), acclimation mechanisms of the photosynthetic apparatus in fast and dynamic light

condition have not been investigated experimentally. One important research question is, whether algae exposed to flashing or fluctuating light acclimate to the peak intensity or to an intermediate value. In raceways, irradiance fluctuations experienced by cells are closely dependent upon the rotation speed of the paddle wheel. Hence, knowledge of the photosynthetic response to fluctuating lights will shed light on the relation between the energy input for the paddle wheels and the system productivity.

Data from the literature suggest that a rapid alternation between light and darkness is beneficial to photosynthetic efficiency (Gordon and Polle, 2007; Grobbelaar, 2010; Vejrazka et al, 2011; Sforza et al, 2012). In some cases of fast cycles, full light integration has been shown, meaning that cells use flashing light and continuous light with the same efficiency of equal average intensity (Phillips and Myers, 1954; Kok, 1956; Terry, 1986; Grobbelaar et al, 1996; Matthijs et al, 1996; Nedbal et al, 1996). Nevertheless, the threshold for this full light integration is not well defined as flash frequencies from 5 Hz to 1 kHz have been reported (Kok, 1956; Terry, 1986; Matthijs et al, 1996; Nedbal et al, 1996). The way algae respond to flashing light is still unclear and may well be species specific. These time scales are representative of photobioreactors conditions, and the effect of light fluctuation within a less intensely agitated raceway is less documented. So far, few data have been reported on the photoacclimation of algae growth under flashing light, only some studies evaluated flash effects only on short term based on photosynthetic oxygen evolution (Kok, 1956; Grobbelaar et al, 1996; Nedbal et al, 1996; Brindley et al, 2011) or without waiting acclimation (Vejrazka et al, 2011) or even in short-term batch (Sforza et al, 2012).

This work focuses on the effect of light modulation on growth for *Dunaliella salina*. Experiments were performed to understand if, for a given light dose, the pattern of light exposure impacts growth rate and several physiological properties (pigments, lipids, nitrogen quota). The response to continuous or intermittent light regimes with different frequencies has been studied in long-term turbidostat experiments. Photosynthetic response and photoacclimation processes have then been compared.

2. Materials and Methods

Materials and Methods can be found in ch. 2.1.

3. Results

3.1. Growth of Dunaliella salina *as a function of flash modulation frequency*

The experiment showed strongly consistent results between the two duplicate cultures of each light condition. Unless otherwise specified, results are provided as average values between the two duplicates cultures.

3.1.1. Specific growth rate

Growth rates measured for the different light regimes during turbidostat experiments can be found in table 1. The specific growth rate increased with the cycle frequency, with a highest value of 1.03 ± 0.048 day^{-1} (mean ± SD, n=4) observed under continuous illumination. Under intermittent light, when L/D frequency increased from 0.017 Hz to 5 Hz, *Dunaliella salina* presents specific growth rates ranging from 0.25 ± 0.029 to 0.93± 0.033 day^{-1} (mean ± SD, n=2), *i.e.* from 1.1 to 4 times lower than continuous light (Fig. 1). A Tuckey test shows that each condition leads to a growth rate value which is significantly different from each other condition with a 95% confidence level (α = 0.05; $F_{0.05,3.8}$=4.07, F=14.49, P=0.001, ANOVA and Tuckey HSD test).

Condition code	f (Hz)	μ (day^{-1}) (± SD)
800_{30-30}	0.017	0.25 ± 0.03
800_{15-15}	0.033	0.44 ± 0.01
1000_{2-3}	0.2	0.65 ± 0.04
800_{2-2}	0.25	0.73 ± 0.02
600_{2-1}	0.33	0.78 ± 0.03
$800_{0.1-0.1}$	5	0.93 ± 0.03
400-cont	-	1.03 ± 0.05

Table 1: Specific growth rate under continuous and flashing light conditions. Each experiment was done in a biological duplicate in two independent photobioreactors

3.2. Chlorophyll content

Chlorophyll *a* content and C:Chl *a* ratio are presented in figure 3. In all treatments, Chl *a* cell content increased for nine days before stabilizing at 4.21 ± 0.24 pg $cell^{-1}$ in average (Fig. 2). *Dunaliella salina* presents Chl *a* content ranging from 4.08 ± 0.24 (800_{2-1}) to 4.53 ± 0.29 pg $cell^{-1}$ in continuous light (mean ± SD) (Fig.3). An ANOVA test shows that there is no significant difference between each conditions (α=0.05; $F_{0.05,6,63}$=2.25,F=2.12,P=0.012). C:Chla ratio (μgC/μgChla) ranged from 26.2 ± 7.15 to 33.7 ± 6.1.

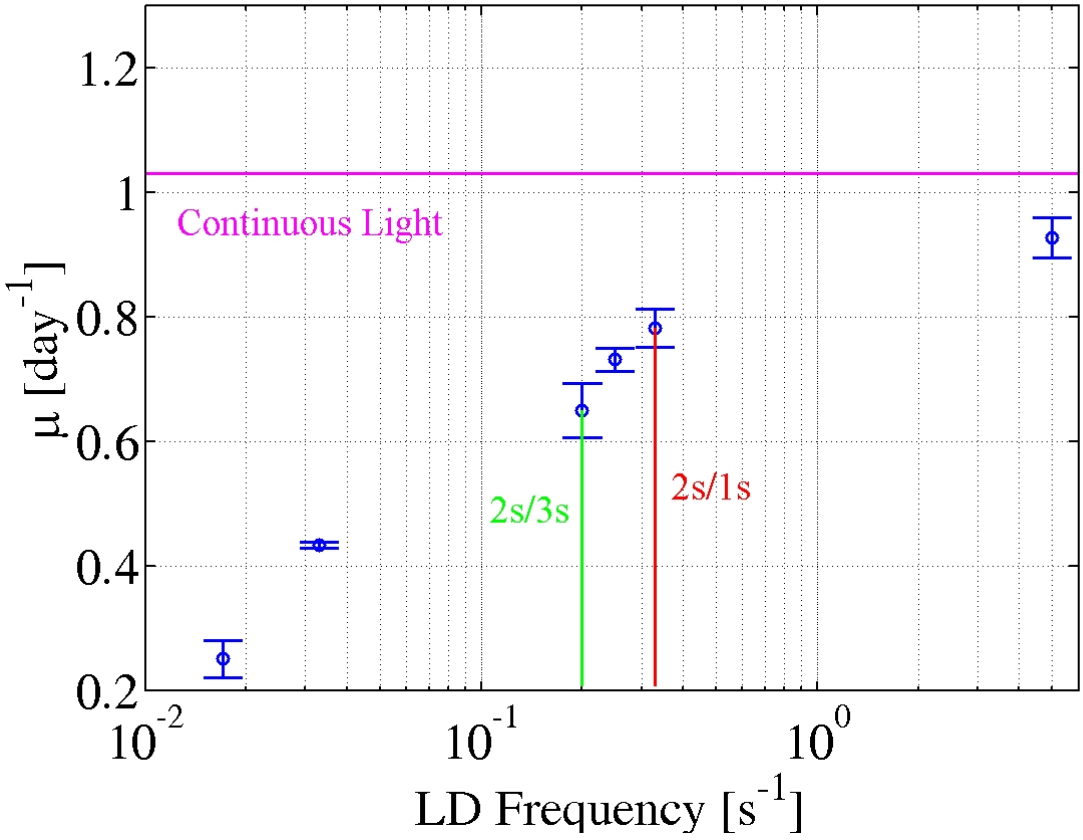

Figure 1: Evolution of specific growth rate μ for reference and flashing light experiments. Results are provided as average values between the two duplicate cultures of each light condition ($\pm$ SD)

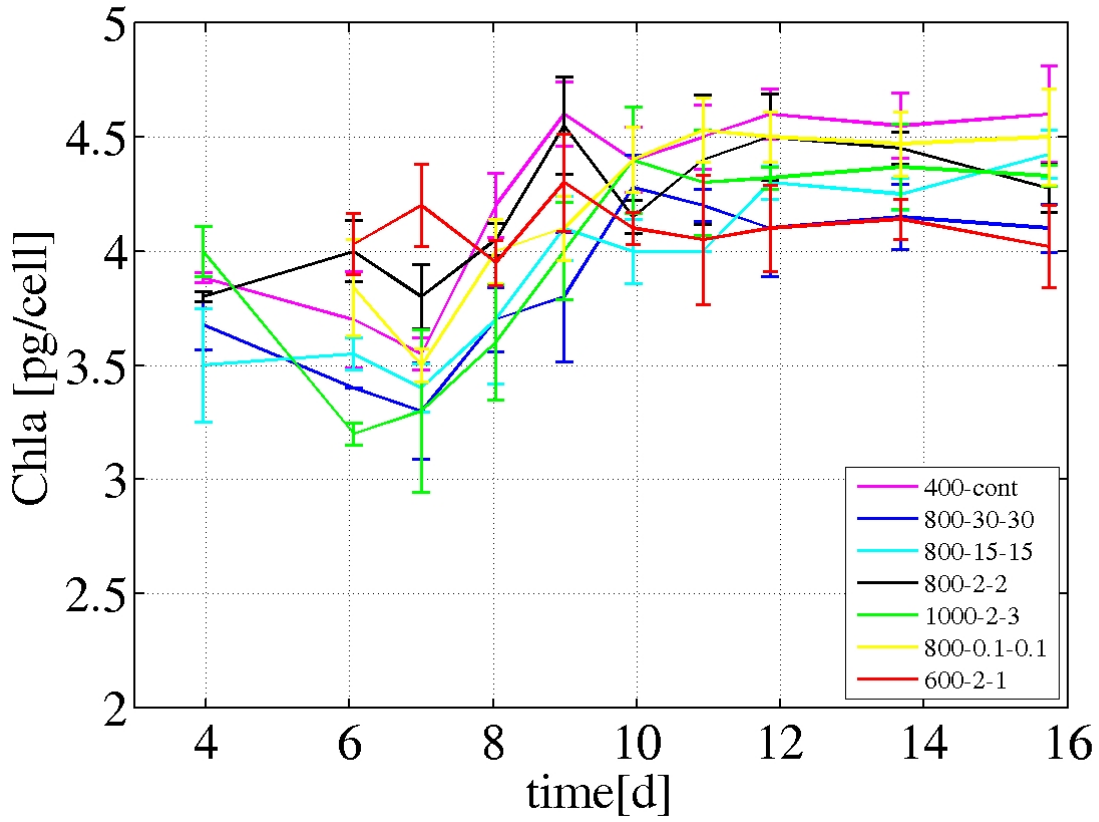

Figure 2: Dynamic effect of various illumination conditions on Chlorophyll *a* content (pg cell^{-1}) of *Dunaliella salina* cells cultivated in turbidostat reactors. Results are provided as average values (± SD) between the two duplicate cultures

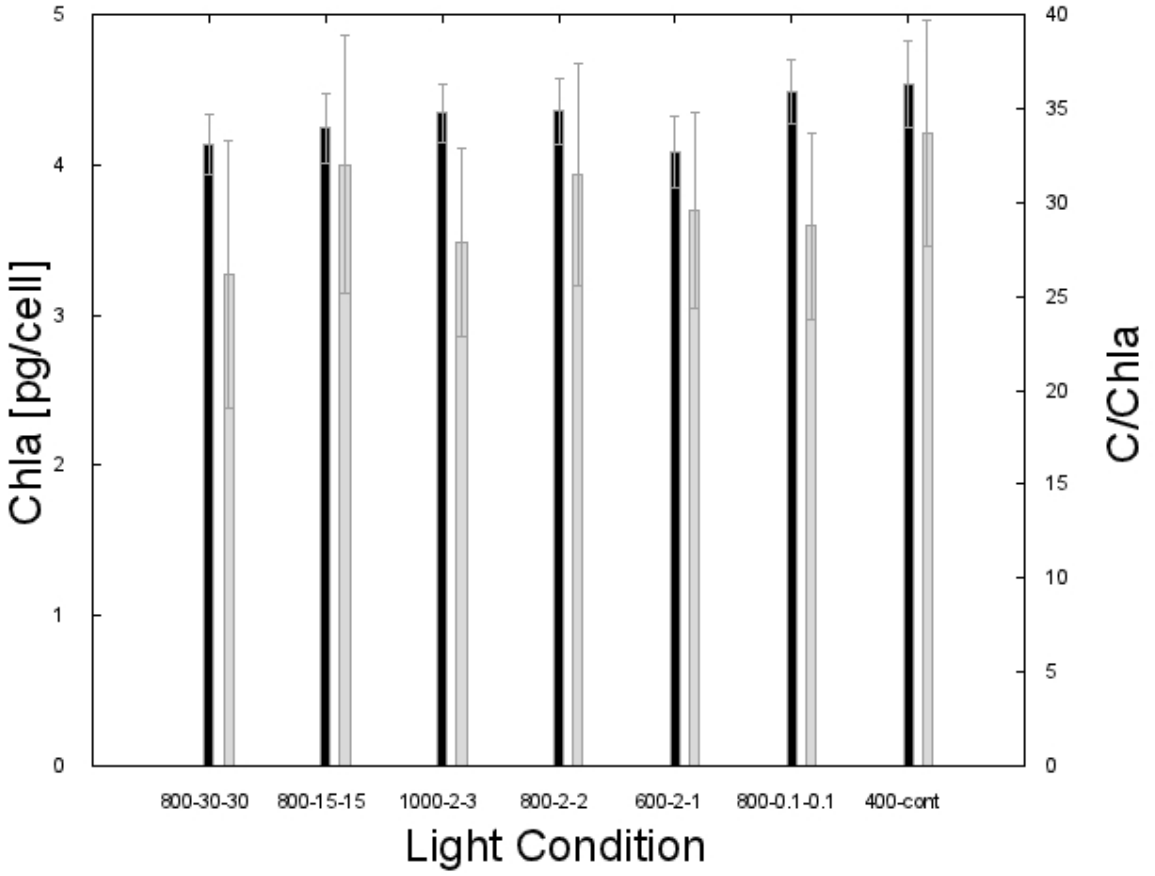

Figure 3: Chlorophyll *a* cell content (pg cell^{-1}) (left ordinate, black bar plots) and C:Chl *a* ratio (right ordinate, grey bar plots) of *Dunaliella salina* under different light regimes for two independent photobioreactor runs. Results are provided as average values (± SD) between the two duplicate cultures after the equilibrium

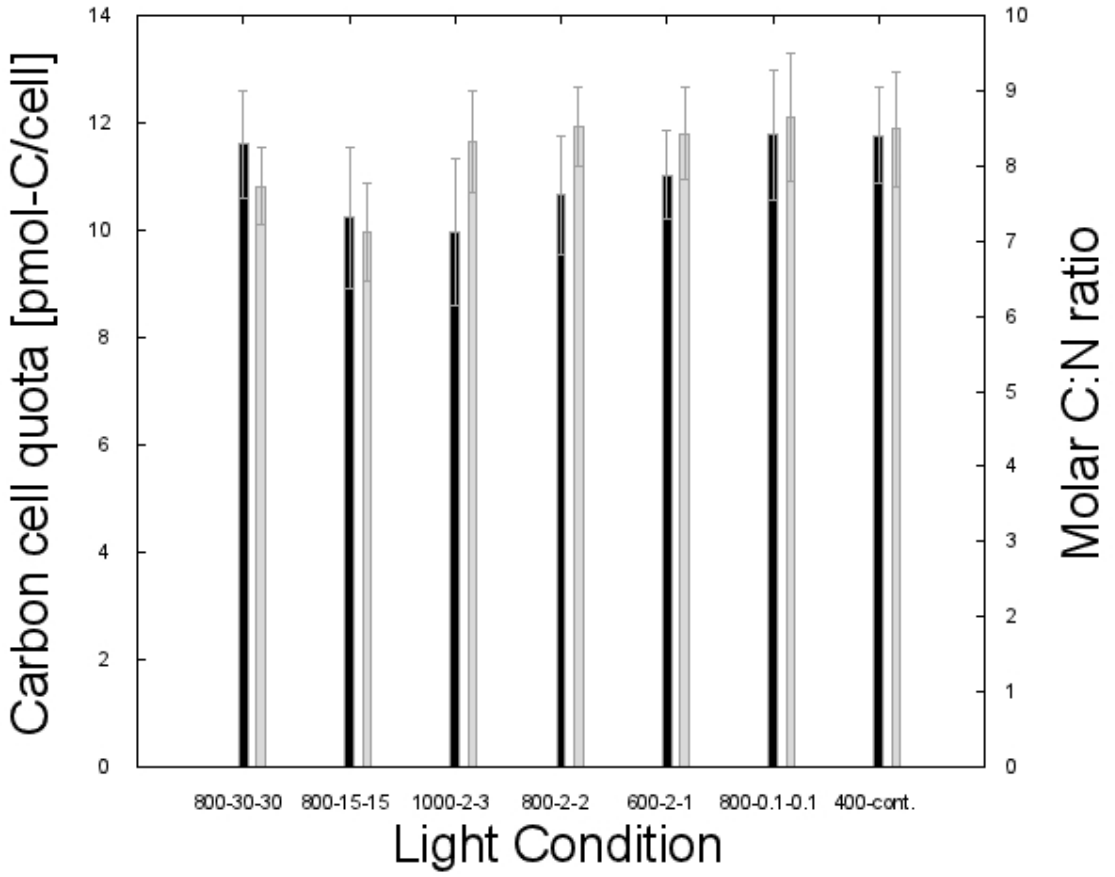

Figure 4: Carbon cell content (pmol-C cell^{-1}) (left ordinate, black bar plots) and molar C:N ratio (right ordinate, grey bar plots) of *Dunaliella salina* under different light regimes for two independent photobioreactor runs. Results are provided as average values (± SD) between the two duplicate cultures after the equilibrium

3.3. Carbon and nitrogen stoichiometry

The same homogeneity is observed in carbon and nitrogen cells content (Fig. 4). Carbon cell content ranged from 9.96 ± 1.37 (FL_{2-3}) to 11.8 ± 1.22 ($FL_{0.1-0.1}$) pmol-C cell^{-1}. The molar C:N ratio of *Dunaliella salina* presented values from 7.73 ± 0.51 (800_{30-30}) to 8.64 ± 0.85 ($800_{0.1-0.1}$).

3.4. Lipid content

In figure 5, the results for the lipids/C (μgLipids/μgC) ratio of *Dunaliella salina* as a function of growth rate μ are presented. The total lipid content increased with the growth rate increase, with a highest value of 0.76 ± 0.09 μgLipids/μgC (mean ± SD, n=4) observed under continuous illumination (μ = 1.03 ± 0.05 day^{-1}). The total lipids content increased from 0.16 ± 0.001 to 0.24 ± 0.004 μgLipids/μgC between 0.25 day^{-1} (800_{30-30}) and 0.73 day^{-1} (800_{2-2}). Finally, between 0.78 day^{-1} (800_{2-1}) and 0.93 day^{-1} ($800_{0.1-0.1}$), cells contained 0.47 ± 0.14 to 0.51 ± 0.086 μg cell^{-1}.

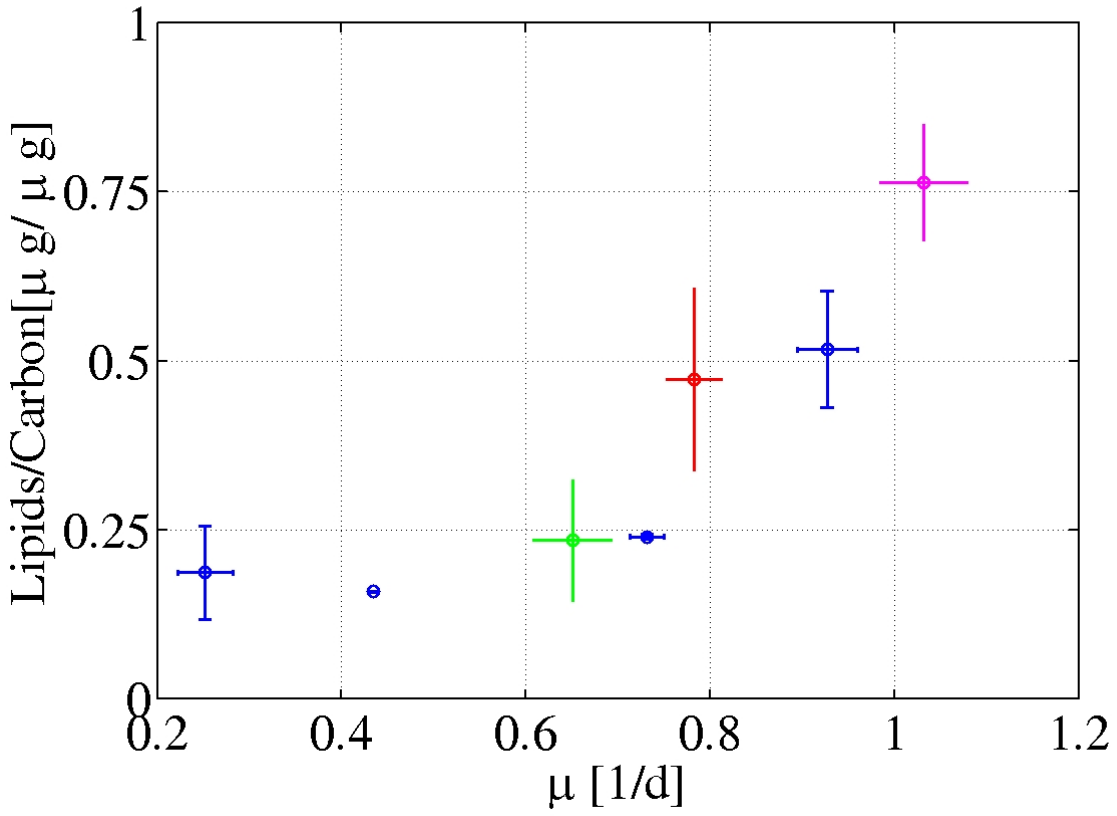

Figure 5: Lipids/C (μgLipids/μgC) ratio of *Dunaliella salina* as a function of growth rate μ. Different colors indicate the light conditions: (blue) 50% illumination, (magenta) continuous light, (green) 2s/3s, (red) 2s/1s

4. Discussion

The data which have been presented in this study investigates important physiological characteristics of *Dunaliella salina* such as growth rate, pigment and lipid content. We carried out the experiments with continuous cultures in turbidostat operation at (constant) low cell density (2 10^5 cells mL^{-1}). Due to the low cell density and the illumination of the culture from different sides, it was possible to maintain homogeneous light distribution in the reactors for the full duration of the experiment (two weeks). Carrying out such experiments in batch mode would not have been possible since variations of cell density, and hence of light distribution would have perturbed the results. Since photoacclimation processes takes more than a week, the turbidostat operation is essential for tracking physiological evolution in a constant cell environment.

4.1. Effect of light flashes frequency on cellular growth of Dunaliella salina

The first clear effect of the light frequency on *Dunaliella salina*, at a given light dose can be observed on the division rate. In turbidostat cultures maintained at equivalent cell densities the specific growth rate increases with increasing flash frequencies (from 0.25 to 0.93 day^{-1}), with continuous light yielding the highest growth rate (1.03 day^{-1}). This maximum growth rate is besides higher than commononly reported in literature, generally less than 0.7 day^{-1} for this species (García et al, 2007; Mendoza et al, 2008).

Flash frequency affects the short term photosynthetic efficiency and has an effect on the long term growth of microalgae. Terry (Terry, 1986) described such improved photosynthetic efficiency with increased light flash frequency as the result of the "light integration effect".

Electron turnover processes are an important mechanism conditioning operations of the photosystems II. These processes are the first step in the electron transport chain and describe cycles between the photon-induced excitation of reaction centres and the subsequent electron separation, which implies de-excitation. After de-excitation the reaction centre is ready for the absorption of a new photon. If new photons are absorbed during the phase of de-excitation, the energy has to be dissipated thermally. The efficiency of the turnover process is optimal if reaction centres always receive photons shortly after de-excitation, while not receiving any in saturated state. The electron turnover, which is the first step in photosynthetic production, has a time scale of about 10 ms (Falkowski and Raven, 1997; Malcata, 2011). For cycle lengths much shorter than 10 ms, full light

integration can be expected. For full light integration, the growth rate for the LD signal equals the growth rate for continuous light with the average light intensity. In our study, full light integration was not achieved, but for the highest frequencies we approximate this condition. Growth rates for the LD signals have been measured inferior to those for continuous illumination, while approaching this value with increasing frequency. For cycle lengths much longer than the electron turnover time the increase in growth rate cannot be explained by the light integration effect alone. One mechanism for lower frequencies is the possibility that the excess energy from the flash might be stored in electron pools which are a part of subsequent reactions. This energy pool can be a combination of the plastoquinone pool, NADPH or reduced compounds of the Calvin cycle (Vejrazka et al, 2011). During the light phase, this pool gets filled and during the dark phase the slower dark reactions synthesize ATP using the stored energy. Furthermore, short term photoprotective mechanisms such as the xanthophyll cycle might intensify efficiency improvements from flashing light. Extended exposure to higher light intensities for lower cycle frequencies can lead to increased thermal dissipation rates and thus lower the photosynthetic efficiency (Casper-Lindley and Bjrkman, 1998; Iluz et al, 2012). In the present study, a deeper analysis of the photosynthetic yield and non photochemical quenching would be necessary to conclusively identify the physiological mechanism behind this growth rate increase.

Mathematical modelling can also help to understand the response to light frequency. Simple models describing the state of the PSU in a caricature way (open, closed, inhibited) have been developed (Eilers, P H C and Peeters, J C H, 1988; Han, B P, 2001). The transition between these theoretical states is straightforwardly related to the incident photon flux. The mathematical analysis of these models reveals that photosynthetic efficiency increases with frequency of light supply (Hartmann et al, 2014). To get a more mathematical intuition of reasons of this increase, two extreme cases can be considered. The first one is an extremely fast alternation between dark and light intensity I, so that the cells cannot make the difference with continuous light. This explains that the growth rate, when frequency is very high, tends to the one obtained with continuous light at the average light intensity $\bar{I} = \frac{I}{2}$. The growth rate (denoted $\mu(I)$ for a constant light intensity I) is then $\mu(\bar{I})$. For a very low frequency, the situation is inverse. Considering a very slow alternation of light and dark periods – for example with light duration in the

range of hours – the transient period between these two regimes can be assumed to be negligible compared to light period. During the light period, growth rate is $\mu(I)$ while it is zero for dark period. Finally, the average growth rate is $\frac{\mu(I)}{2}$. This is the lower limit of the growth rate for very low frequencies. Finally, because of the concavity of the growth response $\mu(I)$ (considering non inhibiting light), the property $\frac{\mu(I)}{2} \leqslant (\frac{I}{2})$ can be verified (Hartmann et al, 2014). This explains why the slow varying regime is less favourable for growth.

This analysis shows that the static growth response to light can explain the observed increased of average growth with cycling frequency. Another way of explaining this, is to consider the yield of light use, defined by $\eta(I) = \frac{\mu(I)}{I}$. Fig. 6 shows the evolution of the photosynthesis yield assuming that the growth rate $\mu(I)$ can be represented by a Haldane model (Bernard, 2011). This yield is constant (and maximum) for low light, and then it decreases with the light intensity. The different lines in the figure indicate the yields during the light phase, for the different light conditions. The expected yield for all flashing conditions is inferior to the continuous light condition (magenta). Distributing double of photon flux ($2I = 800$ μE m^{-2} s^{-1}) with $I =$ continuous illumination $= 400$ μE m^{-2} s^{-1}) on 50% of the time is less efficient as a photon flux which is equally distributed on the time interval: $\eta(2I) < \eta(I)$. As a consequence, the average growth rate $\mu(I) = \eta(I)I$ is lower for the LD signal:

$$\frac{1}{2}\eta(2I)2I = \eta(2I)I < \eta(I)I$$

Analogously, a light signal, of average $\bar{I}$ where a fraction p of the time is illuminated, leads to a light phase intensity $I = \frac{\bar{I}}{p}$. The average growth rate is thus:

$$^{-} = p\eta(\frac{\bar{I}}{p})\frac{\bar{I}}{p} = \eta(\frac{\bar{I}}{p})\bar{I}$$

For constant average light $\bar{I}$, $\bar{\mu}$ is thus an increasing function of the proportion p of the time where light is on. As a consequence, the signal 1000-2-3 should lead to a lower growth rate than the signal 600-2-1. Unfortunately, the experiment 1000-2-3 can only be compared to the experiment 600-2-1 which is at the same time at faster frequency and better yield: the better yield for this 600-2-1 is explained by these two factors which both contribute to photosynthesis enhancement.

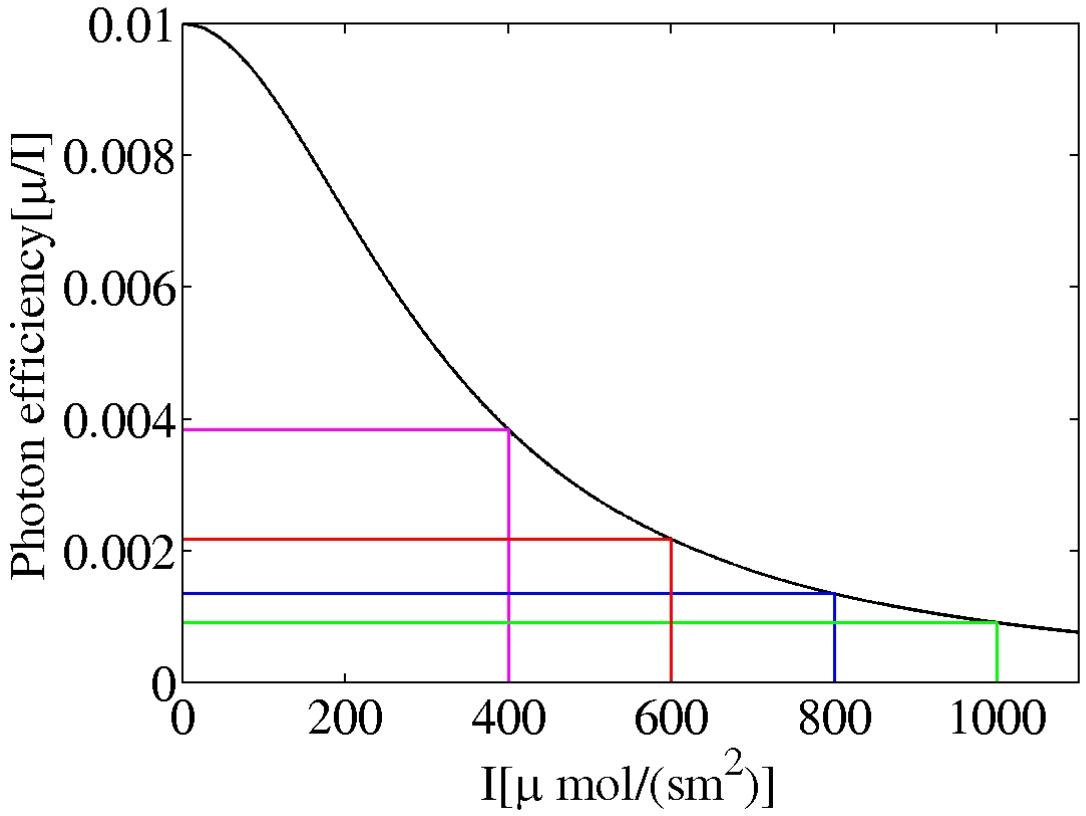

Figure 6: Caricatural representation of the photon efficiency as a function of light intensity following the Haldane model. The different experimental culturing conditions are indicated as lines (magenta) cont., (red) 2s/1s (green) 2s/3s (blue) conditions with LD phases of equal length.

4.2. Effect of flash frequency on pigment content and on the biomass production

In the natural environment, slow light variations induce a physiological response of the photosynthetic system to optimize the light harvesting efficiency of photosynthetic organisms. Photoacclimation describes these phenotypic changes of algae to light variations (Falkowski and LaRoche, 1991). Cells are thus known to actively adapt cell pigmentation, biochemical composition (such as Chl:C and C:N ratios) or structural characteristics such as adjustments in the number and size of photosynthetic units when irradiance is constant for hours to days (Falkowski and Owens, 1980; Herzig and Dubinsky, 1992). An increase in cellular photosynthetic pigment content (such as chlorophyll) is commonly observed in strains grown under low irradiances. Accordingly, pigment content decreases in cells exposed to high irradiances in order to minimize photo-oxidation processes (MacIntyre et al, 2002; Havelková-Doušová et al, 2004). Cellular photosynthetic pigment is thus a main indicator of the state of light acclimation of the cells. This phenomenon has already been documented in continuous irradiance conditions (Herzig and Dubinsky, 1992; MacIntyre et al, 2002). However, acclimation mechanisms and time scales of the photosynthetic apparatus under flashing light had not been studied.

From a dynamical perspective, the results of these experiments highlight the kinetic adaptation in microalgae. The acclimation period until the equilibrium pigment content was reached had a length of nine days for each light conditions. It has – to our best knowledge – never been measured before for a comparative number of different cycle frequencies.

From a static perspective, the presented results show no immediate effect of the LD cycle frequency on the pigment content and therefore the final state of acclimation at same total light dose after equilibrium. Chlorophyll *a* cell content and Chlorophyll/carbon (Chl:C) ratio are independent of light frequency. It can therefore be assumed that for these fast varying light signals only the average light dose matters for the final acclimation state. Exposed to flashing light, cells acclimate to the average light intensity independently from fluctuations. This result coincides with predictions from dynamical models (Bernard, 2011) but is verified experimentally for the first time. Acclimation processes were too slow to follow the light signal generated. Indeed, genetic regulation of pigment synthesis are processes working on time scales which are much slower (hours to days) than the frequencies used in this study (Kana et al, 1997).

Acclimation to average light intensity is also confirmed by the intracellular concentrations of carbon, whose values are independent of light variations after equilibrium. Light is a major determinant not only for carbon (C)-fixation, but also for the cellular content of major elements like nitrogen (N) (Hessen and Anderson, 2008). Carbon/nitrogen (C:N) ratio is used as an indicator of phytoplankton physiological state (Redfield, 1963; Pahlow, 2000). This molar C:N ratio of *Dunaliella salina* has been unaffected by light variation frequency in our study. This result is coherent with model predictions indicating that the ratio is constant and represented as a static function of the mean light intensity (Fasham et al, 1990; Doney et al, 1996; Faugeras et al, 2003).

4.3. Effect of flash frequency on the total lipid content

The relationship between light availability and lipid storage is complex, and many parameters influence the ability of algae to produce lipids. While the effect of nitrogen deprivation on lipid synthesis is well documented (Rodolfi et al, 2009), the influence of flashing lights has been rarely studied.

It seems that total lipid content is directly correlated to the average photosynthetic efficiency (c.f. 5). The highest lipid content appears for continuous light, and in a lesser extend for the high frequency light variation (0.1s/0.1s). The slowest LD alternation provided the lowest lipid amount as it provided the lowest growth rate.

A direct consequence of this point is that optimizing lipid productivity should be carried out in this spirit: the metabolic stress derived from change in light condition should enhance photosynthesis efficiency.

4.4. Upscaling to real systems and future work

Throughout the experiment, LD cycles were used in order to mimic the effect of mixing in large scale culturing systems. In this framework, the cycling frequency represents the mixing speed of the medium. Even though sketchy, this representation helps to understand the complex dynamical processes of photoinhibition and photoacclimation, but it is probably risky to extrapolate to the real smoother light signal perceived by a single cell. Hence, such results may indicate that increasing the mixing rate enhances the photosynthetic yield. However, this increase stays moderate since typical velocities in a raceway are between 0.1 and 0.5 m/s. The extrapolation of the response curve on Figure 1 for L/D in the range of minutes, would imply that while multiplying the frequency by 5, a maximum increase of the growth rate by less than 30% is expected. However, the

energy input for the multiplication of the velocity by 5 – thus increasing the mixer speed – scales superlinearly (energy loss is often assumed to be proportional to the power of three of the fluid velocity). This may reduce the interest of trying to increase productivity in raceway by enhanced hydrodynamics.

5. Conclusion

Data characterizing the long term response of photosynthesis to dynamic light signal are scarce. Such processes are often described along a single factor, such as light intensity, pre-acclimation state or biomass concentration. What reveals this study is that to understand the global picture, these factors must be considered simultaneously, and the response to light pattern must be addressed in a 3 dimensional state-space (acclimation state, light dose, LD cycle frequency). While it is already impossible to cover all possible signals in this framework with ordinary growth experiments, the task becomes infinitely complex when using more realistic light signals i.e. derived from hydrodynamic simulations (Perner-Nochta and Posten, 2007) or adding day night cycles. For the understanding on dynamic effects in photosynthesis, it is thus essential to couple the experimental work to a modelling approach. Indeed, once models have been calibrated (Hartmann et al, 2014), it becomes imaginable to explore this 3D space through extensive simulation, and infer inherent properties on the cell photosynthetic efficiency when faced to realistic dynamic light signals.

References

Amaro HM, Guedes FC, Malcata FX (2011) Advances and perspectives in using microalgae to produce biodiesel. Applied Energy 88(10):3402–3410

Bernard O (2011) Hurdles and challenges for modelling and control of microalgae for CO2 mitigation and biofuel production. Journal of Process Control 21(10):1378–1389

Boulanger AC, Cancès C, Mathis H, Saleh K, Seguin N (2013) OSAMOAL: Optimized Simulations by Adapted MOdels using Asymptotic Limits. ESAIM: Proceedings 38:183–201

Brindley C, Fernández FGA, Fernández-Sevilla JM (2011) Analysis of light regime in continuous light distributions in photobioreactors. Bioresource technology 102(3):3138–3148

Casper-Lindley C, Bjrkman O (1998) Fluorescence quenching in four unicellular algae with different light-harvesting and xanthophyll-cycle pigments. Photosynthesis Research 56:277–289

Chisti Y (2008) Biodiesel from microalgae beats bioethanol. Trends in biotechnology 26(3):126–31

Doney SC, Glover DM, Najjar RG (1996) A new coupled, one-dimensional biological-physical model for the upper ocean: Applications to the JGOFS Bermuda Atlantic Time-series Study (BATS) site. Deep Sea Research Part II: Topical Studies in Oceanography 43(2-3):591–624

Eilers, P H C and Peeters, J C H (1988) A model for the relationship between light intensity and the rate of photosynthesis in phytoplankton. Ecological modelling 42:199–215

Falkowski P, Raven J (1997) Aquatic Photosynthesis. Malden, MA: Blackwell Science.

Falkowski PG, LaRoche J (1991) Acclimation to Spectral Irradiance in Algae. Journal of Phycology 27(1):8–14

Falkowski PG, Owens TG (1980) Light-Shade Adaptation : Two strategies in marine phytoplankton. Plant physiology 66(4):592–595

Fasham M, Ducklow H, McKelvie S (1990) A nitrogen-based model of plankton dynamics in the oceanic mixed layer. Journal of Marine Research 48(3):591–639

Faugeras B, Lévy M, Mémery L, Verron J, Blum J, Charpentier I (2003) Can biogeochemical fluxes be recovered from nitrate and chlorophyll data? A case study assimilating data in the Northwestern Mediterranean Sea at the JGOFS-DYFAMED station. Journal of Marine Systems 40-41:99–125

García F, Freile-Pelegrín Y, Robledo D (2007) Physiological characterization of Dunaliella sp. (Chlorophyta, Volvocales) from Yucatan, Mexico. Bioresource technology 98(7):1359–1365

Garcia-Camacho F, Sánchez-Mirón A, Molina-Grima E, Camacho-Rubio F, Merchuck JC (2012) A mechanistic model of photosynthesis in microalgae including photoacclimation dynamics. Journal of theoretical biology 304:1–15

Gordon JM, Polle JEW (2007) Ultrahigh bioproductivity from algae. Applied microbiology and biotechnology 76(5):969–975

Gordon R SJ (2012) The Science of Algal Fuels: Phycology, Geology, Biophotonics, Genomics and Nanotechnology. Springer

Gouveia L, Oliveira AC (2009) Microalgae as a raw material for biofuels production. Journal of industrial microbiology & biotechnology 36(2):269–274

Grobbelaar JU (2010) Microalgal biomass production: challenges and realities. Photosynthesis research 106(1-2):135–144

Grobbelaar JU, Nedbal L, Tichý V, Grobbelaarl JU, Tichy V (1996) Influence of high frequency light / dark fluctuations on photosynthetic characteristics of microalgae photoacclimated to different light intensities and implications for mass algal cultivation. Journal of Applied Phycology 8(4-5):335–343

Han, B P (2001) Photosynthesis-irradiance response at physiological level: A mechanistic model. J Theor Biol 213:121–127

Hannon M, Gimpel J, Tran M, Rasala B, Mayfield S (2010) Biofuels from algae: challenges and potential. Biofuels 1(5):763–784

Hartmann P, Béchet Q, Bernard O (2014) The effect of photosynthesis time scales on microalgae productivity. Bioprocess and biosystems engineering 37(1):17–25

Havelková-Doušová H, Prášil O, Behrenfeld M (2004) Photoacclimation of Dunaliella tertiolecta (Chlorophyceae) Under Fluctuating Irradiance. Photosynthetica 42(2):273–281

Herzig R, Dubinsky Z (1992) Photoacclimation, photosynthetis, and growth. Israel Journal of Botany 41(4-6):199–212

Hessen DO, Anderson TR (2008) Excess carbon in aquatic organisms and ecosystems: Physiological, ecological, and evolutionary implications. Limnol Oceanography 53(4):16851696

Höök M, Tang X (2012) Depletion of fossil fuels and anthropogenic climate changeA review. Energy Policy 52:797–809

Iluz D, Alexandrovich I, Dubinsky Z (2012) The enhancement of photosynthesis by fluctuating light. InTech

Kana TM, Geider RJ, Critchley C (1997) Regulation of photosynthetic pigments in microalgae by multiple environmental factors: a dynamic balance hypothesis. New phytologist 137(4):629–638

Kok B (1956) Photosynthesis in flashing light. Biochimica et Biophysica Acta 21(2):245–258

Li Z, Wakao S, Fischer BB, Niyogi KK (2009) Sensing and responding to excess light. Annual review of plant biology 60:239–260

Litchman E (2000) Growth rates of phytoplankton under fluctuating light. Cultures 44(2):223–235

MacIntyre HL, Kana TM, Anning T, Geider RJ (2002) Photoacclimation of photosynthesis irradiance response curves and photosynthetic pigments in microalgae and cyanobacteria. Journal of Phycology 38(July 2000):17–38

Malcata FX (2011) Microalgae and biofuels: a promising partnership? Trends in biotechnology 29(11):542–549

Mata TM, Martins AA, Caetano NS (2010) Microalgae for biodiesel production and other applications: A review. Renewable and Sustainable Energy Reviews 14(1):217–232

Matthijs HC, Balke H, van Hes UM, Kroon BM, Mur LR, Binot Ra (1996) Application of light-emitting diodes in bioreactors: flashing light effects and energy economy in algal culture (Chlorella pyrenoidosa). Biotechnology and bioengineering 50(1):98–107

Mendoza H, de la Jara A, Freijanes K, Carmona L, Ramos AA, de Sousa Duarte V, Serafim Varela JaC (2008) Characterization of Dunaliella salina strains by flow cytometry: a new approach to select carotenoid hyperproducing strains. Electronic Journal of Biotechnology 11(4):5–6

Murata N, Takahashi S, Nishiyama Y, Allakhverdiev SI (2007) Photoinhibition of photosystem II under environmental stress. Biochimica et biophysica acta 1767(6):414–421

Nedbal L, Tichy V, Xiong F, Grobbelaar JU (1996) Microscopic green algae and cyanobacteria in high-frequency intermittent light. Journal of Applied Phycology 8:325–333

Nixon PJ, Michoux F, Yu J, Boehm M, Komenda J (2010) Recent advances in understanding the assembly and repair of photosystem II. Annals of botany 106(1):1–16

Pahlow M (2000) Temporal Trends in Deep Ocean Redfield Ratios. Science 287(5454):831–833

Perner-Nochta I, Posten C (2007) Simulations of light intensity variation in photobioreactors. Journal of Biotechnology 131:276–285

Phillips JN, Myers J (1954) Growth Rate of Chlorella in Flashing Light. Plant physiology 29(2):152–161

Posten C (2009) Design principles of photo-bioreactors for cultivation of microalgae. Engineering in Life Sciences 9(3):165–177

Pulz O (2001) Photobioreactors: production systems for phototrophic microorganisms. Applied Microbiology and Biotechnology 57(3):287–293

Redfield AC (1963) The influence of organisms on the composition of sea-water. The Sea pp 26–77

Richardson K, Beardall J, Raven JA (1983) Adaptation of unicellular algae to irradiance: an analysis of strategies. New Phytologist 93(2):157–191

Richmond A (2004) Principles for attaining maximal microalgal productivity in photobioreactors : an overview. Hydrobiologia 512(Table 1):33–37

Rodolfi L, Chini Zittelli G, Bassi N, Padovani G, Biondi N, Bonini G, Tredici MR (2009) Microalgae for oil: Strain selection, induction of lipid synthesis and outdoor mass cultivation in a low-cost photobioreactor. Biotechnology and bioengineering 102(1):100–112

Sarmiento JL, Gruber N (2006) Ocean Biogeochemical Dynamics. Princeton University Press

Sforza E, Simionato D, Giacometti GM, Bertucco A, Morosinotto T (2012) Adjusted light and dark cycles can optimize photosynthetic efficiency in algae growing in photobioreactors. PloS one 7(6):e38,975

Terry KL (1986) Photosynthesis in modulated light: quantitative dependence of photosynthetic enhancement on flashing rate. Biotechnology and bioengineering 28(7):988–995

Vejrazka C, Janssen M, Streefland M, Wijffels RH (2011) Photosynthetic efficiency of Chlamydomonas reinhardtii in flashing light. Biotechnology and bioengineering 108(12):2905–2913

4

THE EFFECT OF PHOTOSYNTHESIS TIME SCALES ON MICROALGAE PRODUCTIVITY

Mathematics is a game played according to certain simple rules with meaningless marks on paper.

David Hilbert

In this chapter, the theoretical response of the photosynthetic apparatus to rapidly varying light signals is studied. The objective is to understand – using a dedicated model for rapid time scales – the impact of the light supply on photosynthesis efficiency and especially the productivity enhancement with increased mixing rate. In this context, we have used the Han model as it is presented in Chapter 1, which considers three possible states of the photosystems: open, closed and inhibited. The transitions between the different states are functions of the photon flux. The mathematical analysis of this model, when considering periodic LD signals gives a hint on the effect of photon supply frequency on productivity and explains the decrease of growth rate at high light intensities. Similar studies have already been carried out by Wu and Merchuk [73] who used the very similar model of Eilers and Peeters [23], to describe the fast time scale processes of photosynthesis. Later on, Papáček et al. [58, 57] provided analytical solutions for periodical LD cycles with any ratio and intensity of the light dark cycles.

The presented approach goes beyond the analysis of the response of the Han model to LD cycles. It also relates photosynthetic activity to growth using the Droop model [20], to account for slower time scales for nitrogen and carbon acquisition processes. The model is finally analyzed assuming (1) slow fast approximation, stating that some fast variables can reach their pseudo steady state during the phases where light is constant (2) averaging properties, stating that slow variables only adapt to the average value of a fast varying signal.

Bioprocess Biosyst Eng (2014) 37:17–25
DOI 10.1007/s00449-013-1031-2

ORIGINAL PAPER

The effect of photosynthesis time scales on microalgae productivity

Philipp Hartmann · Quentin Béchet · Olivier Bernard

Received: 18 February 2013 / Accepted: 21 February 2013 / Published online: 25 August 2013

Abstract Microalgae are often seen as a potential biofuel producer. In order to predict achievable productivities in the so called raceway culturing system, the dynamics of photosynthesis has to be taken into account. In particular, the dynamical effect of inhibition by an excess of light (photoinhibition) must be represented. We propose a model considering both photosynthesis and growth dynamics. This model involves three different time scales. We study the response of this model to fluctuating light with different frequencies by slow/fast approximations. Therefore, we identify three different regimes for which a simplified expression for the model can be derived. These expressions give a hint on productivity improvement which can be expected by stimulating photosynthesis with a faster hydrodynamics.

Keywords Microalgae · Photosynthesis · Modeling · Photoinhibition · Biofuel

P. Hartmann (✉) · O. Bernard
BIOCORE-INRIA, BP93, 06902 Sophia-Antipolis Cedex, France
e-mail: philipp.hartmann@inria.fr

O. Bernard
e-mail: olivier.bernard@inria.fr

P. Hartmann · O. Bernard
UPMC-CNRS LOV, BP28, 06234 Villefranche sur mer, France

Q. Béchet
Massey University, Private Bag 11 222, Palmerston North 4442, New Zealand
e-mail: q.bechet@massey.ac.nz

Introduction

Microalgae have received a specific attention in the framework of biodiesel production and renewable energy generation since a decade. Their high actual photosynthetic yield compared to terrestrial plants (whose growth is limited by CO_2 availability and access to nutrients) could lead to large potential algal biomass productions which is orders of magnitude higher than biofuel from field crops [30].

After a nitrogen limitation, this biomass can reach a very high lipid content (up to 60 % of dry weight [18]). These possibilities have led some authors to consider that microalgae could be one of the main biofuel producers in the future [7, 14]. Moreover, the ability of microalgae to fix CO_2 in a controlled way opens up applications in mitigation systems [1, 20]. Microalgal biofuel production systems could therefore be associated with industrial powerplants with a high CO_2 production. In the same spirit, microalgae could be used to consume inorganic nitrogen and phosphorus, and improve wastewater treatment technology [26].

These advantages put microalgae in a good position for renewable energy production at large scale [7]. In the coming years there might be large scale industrial plants to produce microalgae. However, the culture of algae is not straightforward and suffers from many limitations [5, 22]. As a matter of fact, growth rates in mass cultures are often reduced due to an excess of light which is inhibiting the photosynthesis process. Consequently, productivity is often below its optimal value. Better understanding photoinhibition and therefore improving growth efficiency of the algae is a key issue. The dynamics of photoinhibition has been described by models [10, 11, 13], but its effect on cell cultures is challenging to predict since photoinhibition is a dynamic mechanism. The level of photoinhibition experienced by a cell does not depend only on the level of light

intensity that the cell is exposed to, but as well on the length of exposure. The damaging effect of photoinhibition is counterbalanced by a recovery process that also needs to be considered. In most cultivation systems, the light intensity that cells are exposed to constantly varies as cells move within the culture due to mixing. It should therefore be possible to optimize the hydrodynamics regime to minimize the effect of photoinhibition. Another difficulty is that the level of photoinhibition has an impact on the rate of nitrogen uptake, even under nitrogen-limiting conditions. In order to account for this interaction between photoinhibition and nitrogen absorption, this study aims at analyzing the Han photoinhibition dynamics model coupled with the Droop model for nitrogen consumption.

The Droop model [8, 9] has been widely studied and proved to accurately reproduce situations of nitrogen limitation [4, 9, 25]. The Droop model has been validated for the prediction of microalgal growth in the case of nitrogen limitation for biodiesel production [17].

This paper is organized as follows: In a first part, we recall the Droop model. Secondly, we introduce the light influence in this model. In a third part, we propose analytic approximations of the model for the whole frequency range. In the last part, the applicability of the model and the approximations are discussed.

The Droop model

The Droop model has been proven to appropriately represent the effect of macronutrients, such as nitrogen on the growth rate of microalgae [9]. It is known to predict a unique non trivial equilibrium if the culturing conditions (i.e. influent concentration of nitrogen s_{in} and dilution rate D) are kept constant [3, 15]. In contrast to the simpler Monod model [19], the Droop model considers a dependence of growth on the intracellular nitrogen concentration or quota q. This defines nutrient uptake and growth as uncoupled processes. In the following, the differential equations present a modified version of the Droop model (as in [2]) representing the evolution of the biomass (x) with an inorganic nitrogen substrate s.

$$(D)\begin{cases} \dot{s} = Ds_{in} - \rho(s,q)x - Ds \\ \dot{q} = \rho(s,q) - \mu(q)q \\ \dot{x} = \mu(q)x - Dx \end{cases} \quad (1)$$

In this model the absorption rate $\rho(s, q)$ and growth rate $\mu(q)$ are generally defined as Michaelis–Menten and Droop functions:

$$\rho(s,q) = \rho_0 \frac{s}{s+K_s} \cdot (1 - q/Q_1) \quad (2)$$

$$\mu(q) = \mu_0\left(1 - \frac{Q_0}{q}\right) \quad (3)$$

where K_s is the half saturation constant for substrate uptake and Q_0 the minimal cell quota. At the quota Q_0, the growth rate equals 0. In Eq. (1), a factor $(1 - q/Q_1)$ is introduced to account for the down regulation of the uptake when the quota becomes high. It thus limits the internal quota to the following interval [2]:

$$Q_0 \le q \le Q_m \le Q_1 \quad (4)$$

Q_m is the maximum cell quota which is obtained in conditions where nutrients are not limiting. As a direct consequence, the growth rate is also bound:

$$0 \le \mu(q) < \mu_{\max} = \mu_0(1 - Q_0/Q_m) \quad (5)$$

where μ_m is the maximum growth rate reached in non limiting conditions. The parameters of the Droop model can be estimated well with growth experiments under nutrient limiting conditions [2]. The Droop model has been widely studied [3, 15, 28] and validated [4, 9, 25, 28]. However, it cannot directly be used for the description of photobioreactors or raceways since it does not account for light limitation.

Integration of the photosynthesis time scale

In a microalgae culturing device, the light perception of a cell can vary at a time scale faster than the inherent uptake and growth time scales of the Droop model [16, 21]. The fast dynamics of the photosynthetic processes within the chloroplasts have thus to be taken into account. On a molecular scale two photosystems types (denoted PSI and PSII) are involved in the photon harvesting process [27]. The photosynthetic production is triggered by the simultaneous excitation of both photocenters. In the Han model [12], it is assumed that the activation of the second photosystem (PSII) is the limiting factor in photosynthetic productivity. These photosystems can be damaged by an excess of energy due to an excess of absorbed photons. The key proteins within the photosynthetic units (PSUs) can be however repaired at a slow rate. Photosystem damage and recovery are the two main processes which drive the dynamics of photoinhibition.

The PSII is assumed to be in one of the three states: open (A), closed (B), or inhibited (C). Open PSUs may be excited by photons, trigger the photosynthetic process, and turn to the closed state. The turnover rate for this process is the product of the PSII's cross-section σ and the light intensity I. A closed PSU may return to an open state at the rate $\frac{1}{\tau}$, whereas τ represents the turnover time of the

electron transfer chain. If facing excessive radiation, a closed PSU can also be destroyed by incident light. The rate for photoinhibition processes is defined by the product $k_d\ \sigma\ I$, k_d being the PSII's damage parameter. Inhibited PSUs can be repaired by chemical processes in the cell at a constant rate k_r. The equations for the three states (according to [12]) consequently are:

$$\frac{dA}{dt} = -I\sigma A + \frac{B}{\tau} \tag{6}$$

$$\frac{dB}{dt} = I\sigma A - \frac{B}{\tau} + k_r C - k_d \sigma I B \tag{7}$$

$$\frac{dC}{dt} = -k_r C + k_d \sigma I B \tag{8}$$

A, B, and C are the relative frequencies of the respective states, the sum of A, B, and C is therefore 1 and the system can be completely described by two equations only.

To couple this model with the Droop model, we consider that growth rate results from the product of the total cross-section of the cell PSUs in open state (resulting thus from their number and size) and light. In line with the Droop model, we assume that the PSUs number and size are related to the internal nitrogen quota with a Droop relationship. In that spirit, the Droop relationship can be seen as a factor describing the total cross-section of all PSUs. As a consequence, the total cross-section of productive PSUs is assumed to be proportional to $\sigma\left(1 - \frac{Q_0}{q}\right)A$. The growth rate in terms of inorganic carbon fixation rate is then proportional to the product of the light intensity I with the total cross-section of the active photocenters.

$$\mu(I, A, q) = \mu_m\left(1 - \frac{Q_0}{q}\right) \cdot \sigma I A \tag{9}$$

where μ_m is a parameter such that $\mu_m \sigma I_0 A = \mu_0$ for a constant light I_0, and the associated fraction of open states A.

In the following considerations, only $2T$-periodic light is studied. Assuming state periodicity, we can compute:

$$\int_{2T} \dot{A}dt = -\int_{2T} I\sigma A dt + \int_{2T} \frac{B}{\tau} dt = 0 \tag{10}$$

Since A is periodic, we have then:

$$\overline{IA}\sigma = \bar{B}/\tau$$

where $\overline{IA}$ and $\bar{B}$ denominate the mean values over one period. Following this equation, $\bar{B}$ can be used as an indicator for the photosynthetic productivity; by definition it is bound in the interval [0,1].

$$\bar{B} = \overline{IA}\sigma\tau. \tag{11}$$

In the following section, we will compute $\bar{B}$ as a function of the light intensity and frequency. Depending on the frequency domains, two approximations ($\bar{B}_{slow}$ and $\bar{B}_{fast}$) will be given.

Model analysis

Motivation

In this section, the mathematical behavior of the Droop–Han model under periodic forcing of light is investigated. It is worth noting that the time scales associated with the kinetics of light response and nitrogen consumption differ by several orders of magnitude. Indeed, the excitation/relaxation and photodamage/recovery processes have time scales slower than the hour, while the nitrogen uptake has a time scale of hours to days [2]. As a result, using quasi steady state approximations [24], the analysis of the Droop–Han model will be performed in two steps. First, the light-response will be discussed, and then the effect of nitrogen consumption on this light response will be investigated.

The light response of the model implies two additional time scales of very different magnitude. It can thus be identified as a slow/fast system which can be approximated using singular perturbation theory [24].

Light Response

We rewrite the Han model using $B = 1 - A - C$, it is a system with slow/fast time scales:

$$\frac{dA}{dt} = -(\sigma I + 1/\tau)A + (1 - C)/\tau \tag{12}$$

$$\frac{dC}{dt} = k_d(-(k_r/k_d + \sigma I)C + \sigma I(1 - A)) \tag{13}$$

which can be written in the classical form of a slow/fast system:

$$\dot{\mathbf{x}} = \epsilon \cdot (M\mathbf{x} + \mathbf{b}) \tag{14}$$

$$\epsilon = \begin{pmatrix} 1 & 0 \\ 0 & k_d \end{pmatrix};\ \mathbf{b} = \begin{pmatrix} 1/\tau \\ \sigma I \end{pmatrix};$$
$$M = \begin{pmatrix} -(\sigma I + 1/\tau) & -1/\tau \\ -\sigma I & -(k_r/k_d + \sigma I) \end{pmatrix} \tag{15}$$

Using an exemplary parameter set as shown in Table 1, the absolute values of the entries of M and $\mathbf{b}$ are in the range 0.1–6 whereas k_d is on the order of 10^{-4}.

Table 1 Model parameters according to [31]

Parameter	Value	Unit
k_r	4.8×10^{-4}	s^{-1}
k_d	2.99×10^{-4}	·
$1/\tau$	0.1460	s^{-1}
σ	0.0019	$m^2/(\mu\ mol)$
I_0	2,000	$\mu mol\ s^{-1} m^{-2}$

This shows that the system of Eqs. (13, 14) has a slow/fast dynamics with a time scale ratio of k_d. The dynamics of C is more than a factor 1,000 slower than the dynamics of A. Although the considered parameters depend on the species, this key time scale property remains qualitatively true for any species due to the nature of the involved physiological processes.

In order to study analytically the model response to fluctuating light, we consider a caricatured light pattern as follows:

$$I(t) = \begin{cases} I_0, & \text{for } 0 < t < T \\ 0, & \text{for } T < t < 2T \end{cases} \tag{16}$$

Note that the solution of the Han model (14), at steady state, for a continuous light I_0, can be straightforwardly computed as follows:

$$\bar{B}_{SS}(I_0) = \frac{\sigma I_0 \tau}{1 + \tau\sigma I_0 + k_d/k_r \tau (\sigma I_0)^2} \tag{17}$$

In order to analytically study the model response to various light frequencies, two domains of the light variation frequency have to be distinguished: slow frequencies with $T > 10 \cdot \tau \approx 100\,\text{s}$, and fast frequencies with $T \leq 100$ s.

In the following paragraphs, the approximations for the low and the high frequency domains are given, as shown in Figs. 1 and 2. All approximations consider a forced periodic state of the system.

Low frequencies

For large values of T, the fast dynamics of A (Eq. 12) will reach its slow manifold, given by $(\sigma I + 1/\tau)\, A = (1 - C)/\tau$. The slow dynamics can therefore be represented by

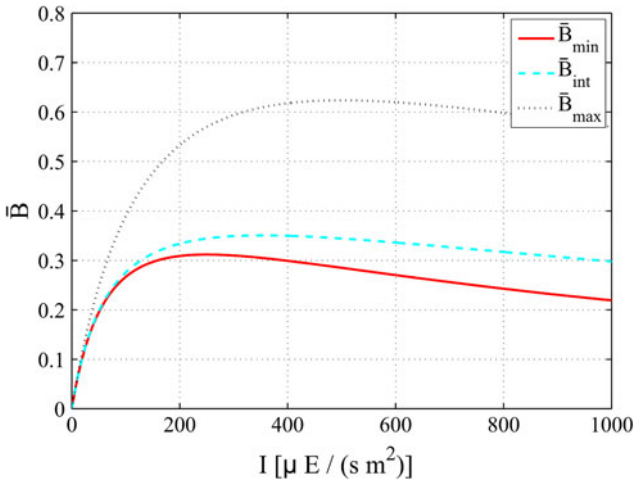

Fig. 1 Direct effect of light on the growth rate: variation of the mean value of B over a period with respect to light intensity. The plot results from the approximations for slow frequency ($\bar{B}_{min}$, *red*), intermediate frequency ($\bar{B}_{int}$, *dashed cyan*) and fast frequency ($\bar{B}_{max}$, *dotted black*) (color figure online)

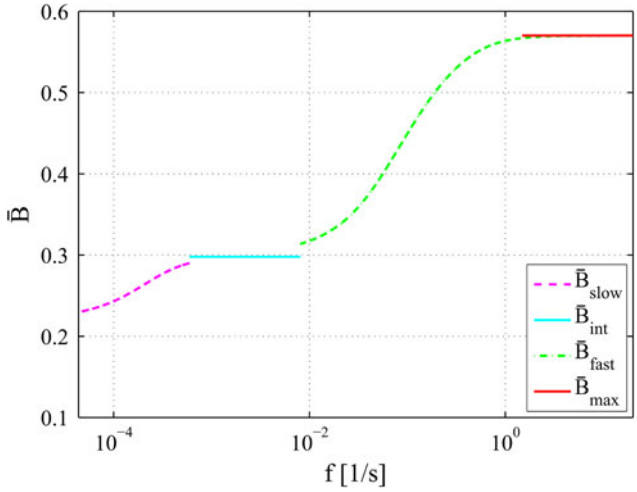

Fig. 2 Approximations of the growth rate over different domains of light frequency ($\bar{B}_{slow}$: *purple dash-line*, $\bar{B}_{int}$: cyan line, $\bar{B}_{fast}$: *green dash-line*, $\bar{B}_{max}$: *red-line*) against LD-frequency $f = 1/T$ on a logarithmic scale (color figure online)

Eq. (13), where A is replaced by its expression with respect to C. An analytical expression can be derived for C (calculation not shown). The average value along the period $2T$ can then be determined (see "Appendix A1"), leading to the following expression for $\bar{B}$:

$$\bar{B}_{slow} = \left(1 + \frac{\delta(I_0)}{k_r}\frac{1}{T}\frac{(1-\gamma(0))(1-\gamma(I_0))}{1-\gamma(0)\gamma(I_0)}\right) \cdot \frac{\bar{B}_{SS}(I_0)}{2} \tag{18}$$

with

$$\delta(I) = \frac{kd\tau\frac{(\sigma I)^2}{1+\tau\sigma I}}{k_r + \frac{(\sigma I)^2}{1+\tau\sigma I}} \tag{19}$$

$$\gamma(I) = e^{-\left(kr + kd\frac{(\sigma I)^2}{1+\tau\sigma I}\right)T} \tag{20}$$

High frequencies

For small T, the dynamics of C in Eq. (13) is so slow that C stays approximately constant over one period. As a consequence, Eq. (13) leads thus to a value of C as a function of the mean value of I and IA on one period. This value can then be used in Eq. (12) and defines the dynamics of B, as shown in "Appendix A2".

$$\bar{B}_{fast} = \frac{\sigma I_0}{2}\frac{\eta - \theta + \tau\eta\theta}{\eta^2 + \frac{kd(\sigma I_0)^2}{2k_r}(\eta - \theta)} \tag{21}$$

$$\eta = (\sigma I_0 + 1/\tau) \tag{22}$$

$$\theta = \frac{1}{T}\frac{(1-\alpha(0))(1-\alpha(I_0))}{1-\alpha(I_0)\alpha(0)} \tag{23}$$

$$\alpha(I) := e^{-(1/\tau + \sigma I)T} \tag{24}$$

Monotony of the productivity with respect to light period

Property *The approximated growth rate response composed by* $\bar{B}_{\text{fast}}$, $\bar{B}_{\text{slow}}$ *reproduces a continuous and decreasing function in T from* $B_{\text{ss}}(I_0/2)$ *down to* $B_{\text{ss}}(I_0)/2$. *The results obtained through this approximation are represented on Fig.* 2.

Proof First, let us show that the successive approximations continuously join up together. Using the rule of de l'Hôpital, the limits of $\bar{B}_{\text{slow}}$ can be estimated for $T \to 0$ and $T \to \infty$:

$$\lim_{T\to 0} \bar{B}_{\text{slow}} = \bar{B}_{\text{int}} = \frac{\sigma I_0 \tau}{(2 + 2\tau\sigma I_0 + k_{\text{d}}/k_{\text{r}}\tau(\sigma I_0)^2)} \tag{25}$$

$$\lim_{T\to \infty} \bar{B}_{\text{slow}} = \bar{B}_{\text{min}} = B_{\text{SS}}(I_0)/2 \tag{26}$$

The limit for long periodicities is the steady state solution, i.e. 0 during night period and $\bar{B}_{\text{SS}}$ during light. Finally, the average response is $\bar{B}_{\text{min}} = B_{\text{SS}}/2$. Considering $\bar{B}_{\text{fast}}$, the same type of calculation leads to:

$$\lim_{T\to 0} \bar{B}_{\text{fast}} = \bar{B}_{\text{max}} = \frac{\tau\sigma\frac{I_0}{2}}{\left(1 + \tau\sigma\frac{I_0}{2} + k_{\text{d}}/k_{\text{r}}\tau(\sigma\frac{I_0}{2})^2\right)} \tag{27}$$

$$\lim_{T\to \infty} \bar{B}_{\text{fast}} = \bar{B}_{\text{int}} \tag{28}$$

The limit of $\bar{B}_{\text{fast}}$ for low frequencies coincides with the limit of $\bar{B}_{\text{slow}}$ for high frequencies. The limit of $\bar{B}_{\text{fast}}$ for high frequencies is the steady state solution for continuous illumination with the mean intensity $\bar{I} = I_0/2$. As shown in "Appendix A3", both approximations $\bar{B}_{\text{fast}}$ and $\bar{B}_{\text{slow}}$ are decreasing functions with respect to T. The monotonic behavior of the functions in respect to T is presented in Fig. 2.

Dynamics of the Droop variables

In most cultivation systems, algae are cultivated under nutrient-saturating conditions to maximize the productivity. Consequently, we assume $s \gg K_{\text{s}}$, and the nitrogen absorption rate, as given by Eq. (2) is only a function of q. The dynamics of q in system Eq. (1) does only depend on q, and this stable linear equation can be solved at steady state. The intracellular concentration of nitrogen can be determined, by calculating the equilibrium value of q (Q_{eq}):

$$Q_{\text{eq}} = \frac{\rho_0 + \mu_m \bar{B}(I,T) Q_0}{\frac{\rho_0}{Q_1} + \mu_{\text{m}} \bar{B}(I,T)} \tag{29}$$

where $\bar{B}(I,T)$ is the mean photosynthetic productivity and can stand for any of the presented approximate values. The growth rate can then be computed as follows:

$$\begin{aligned}\mu &= \mu_{\text{m}}\left(1 - \frac{Q_0}{Q_{\text{eq}}(I,T)}\right)\bar{B}(I,T)/\tau \\ &= \mu_{\text{H}}(I,T)\left(1 - \frac{Q_0}{Q_{\text{eq}}(I,T)}\right)\end{aligned} \tag{30}$$

Figure 3 shows the resulting growth rate μ as defined in Eq. (30) the theoretical photosynthetic productivity neglecting any nitrogen limitation μ_{H} and the equilibrium value for the intracellular nitrogen Q_{eq} as defined in Eq. 29. The function $\bar{B}(I,T)$ was assumed to be equal to $B_{\text{slow}}(I, T)$. As presented, high light conditions lead to a lowered Q and therefore a slight reduction of the growth rate, compared to the photosynthetic efficiency only considered with the Han model. Further more, the influence of the steady state value Q_{eq} turns to a constant factor for intermediate and high productivities. Therefore, in the case of non limiting nitrogen, it can be disregarded.

Parameter identification

From measurements of substrate, biomass and intracellular nitrogen under different conditions, the key parameters of Droop's model can be identified [2]. As it has been discussed, the limited nitrogen quota fluctuation due to light (when nitrogen is not limiting) hardly influences growth rate.

Assuming that the growth rate response for continuous illumination $\bar{B}_{\text{SS}}(I)$ (Haldane curve) is available, two parameters can be determined. The parameters g_1 and g_2 can be estimated by a least-square fit of the function $\bar{B}_{\text{SS}}(I)$, as it is defined in Eq. (17), normalized by the value of its maximum:

$$\bar{B}_{\text{SS}} = \frac{\sigma I_0 \tau}{1 + g_1 I_0 + g_2 I_0^2} \tag{31}$$

with

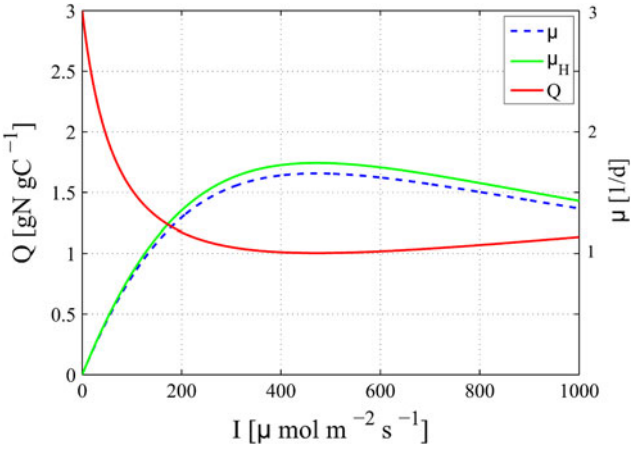

Fig. 3 Intracellular nitrogen ratio at equilibrium (Q_{eq}, *red*) in respect to irradiance at steady state for the slow frequency approximation $\bar{B}_{\text{min}}$ (Eq. 29). The growth rate μ given by the Droop–Han model (*blue dash-line*) is compared to the growth rate μ_{H} computed without the Droop term (*green line*) (cf. Eq. 9) (color figure online)

$$g_1 = \tau\sigma \tag{32}$$

$$g_2 = k_d/k_r\tau\sigma^2 \tag{33}$$

In order to calculate the independent values of τ and σ, the following quantity can be calculated for different values of I_0:

$$F_1(I_0) = I_0 \cdot \left(\frac{1}{\bar{B}_{min}(I_0)} - \frac{1}{\bar{B}_{int}(I_0)}\right) = \frac{1.5}{\sigma} + 1.5\tau I_0 \tag{34}$$

As F_1 is a linear function of I_0, a linear regression enables the determination of the values of τ and σ. As a consequence, σ, τ and $\frac{kd}{kr}$ can be determined by measuring $\bar{B}_{min}$ and $\bar{B}_{int}$ with respect to I_0 only. To get the absolute values of k_d and k_r, a possible approach is to use the productivity response $\bar{B}_{slow}$ as a function of T. Since the system has only one remaining degree of freedom, a least-square fitting can provide this value.

With the proposed method, measuring the growth rate response for various irradiances and light–dark (LD) frequencies leads to the identification of all the model parameters.

Preliminary validation of the Droop–Han model

The methodology presented in the previous section is only valid in the case of a simple square signal with light and dark periods of equal length. Furthermore, it is necessary to use diluted cultures to ensure a homogeneous light distribution within the reactor and avoid an additional flashing effect. In recent experiments, Vejrazka et al. [29] provided data for the growth of *Chlamydomonas reinhardtii* in LD cycles at a LD ratio of 0.1. Although, their experimental setup differs from the preconditions in the presented approach, Vejrazka's results are in agreement with the prediction of the Droop–Han model as can be seen in Fig. 4. The "inflexion point" can therefore be identified for this experiment between 10 and 50 Hz. The growth rate for 100 Hz is equal to the growth rate under continuous light with average light intensity. These results meet very well the predictions of the Droop–Han model and its analytical approximations for established periodic regimes. Nevertheless, data covering more variations of I_0 and T would allow a better model calibration and a more quantitative validation.

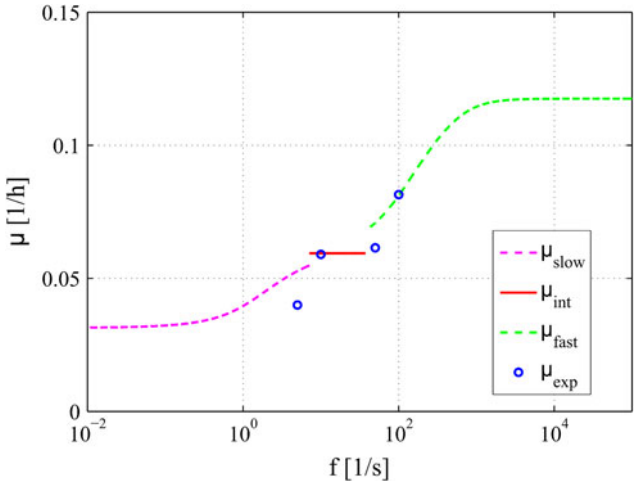

Fig. 4 Growth rate as a function of the frequency of the light signal in the case of a simple square signal (*plain lines*: theoretical prediction using the Han model; *blue circles*: experimental data from Vejrazka et al [29]) (color figure online)

Discussion

With the proposed coupled model, new insights about microalgal response to varying light signals have been obtained. When algae are exposed to periodic flashing light, the Droop–Han model predicts that the growth rate is an increasing function of the light frequency as shown in Fig. 2. It includes plateaus for very low and very high frequencies. A plateau or inflexion point is obtained in a intermediate domain. This specific shape seems to be compatible with the experimental results of Vejrazka et al. [29], then supporting the model validity, as illustrated on Fig. 4.

The characteristic shape directly illustrates key properties of the Han model: the two gradients in growth rate correspond to the two time scales of the inhibition-repair process and the activation–relaxation process. For very slow light variations, growth is limited by strong inhibition during the light phase. With increasing frequency, the degree of inhibition turns to a constant equilibrium throughout each LD cycle. As a result, for increased frequency, there is less photoinhibition during the light phase, which results in an increased productivity of the photosystem. With further increasing frequency, the degree of photoinhibition remains constant, while the open-closed dynamics changes from two alternating states to a constant equilibrium value throughout the entire LD cycle. The equilibrium state reached for high frequencies leads to an increased growth rate compared to the very slow alternating state. The maximum growth rate is the one obtained for a constant illumination with the mean light intensity $I_0/2$. This latter point coincides with the theoretical proof of Celikovsk, et al. [6]. The inhibition at $I_0/2$ is of course lower than the inhibition at I_0. It is less clear that, with a Haldane model, the growth rate at $I_0/2$ is always greater than half the value of the growth rate at I_0:[1]

[1] This property can be shown by remarking that the Haldane curve $B_{SS}(I)$ is always under its initial tangent for $I = 0$. Straightforward geometrical considerations based on Thales Theorem prove this result.

$$\frac{\mu_{\mathrm{H}}(I_0)}{2} \leq \mu_{\mathrm{H}}\left(\frac{I_0}{2}\right) \tag{35}$$

This effect is even stronger for the portion of the Haldane curve far from the initial tangent i.e. for photoinhibiting light intensities.

This point is important, since it provides an estimation of the flashing effect scale at a given flashing light intensity I_0. The possible productivity gain between a process where the cells stay too long exposed to a high light and a process where the alternation is fast is the difference between $B_{\mathrm{ss}}(I_0/2)$ and $B_{\mathrm{ss}}(I_0)/2$. For algae whose photoinhibition is low (at this light intensity), the increase in productivity will then be very low and it will not compensate for the additionally invested mixing energy. This effect can however be stronger when photoinhibition is higher. An efficient management procedure could therefore consist in increasing the agitation velocity only at high light, when the microalgae experience a strong photoinhibition.

It is also interesting to note that the intermediate growth rate for which a plateau, or simply an inflexion point is obtained, corresponds to the Haldane model $B_{\mathrm{ss}}(I_0/2)$, but for which the inhibition term has been doubled ($k_{\mathrm{d}}/k_{\mathrm{r}}$ in the model). This provides a hint on the respective effect of the flashing effect for low and high frequencies.

Conclusion

The model properties have been derived analytically using a slow/fast approximation. The resulting formulas have a very simple form compared to the exact solution of the Han model [6]. Based on these formulas, a measurement protocol has been proposed to deduce the parameters of the model which relies on the dependency between growth rate and cycle frequency. It can also be derived from the link between growth rate and the maximum light intensity I_0. Concerning the physiological parameters describing the photosynthetic system, the proposed method for parameter identification varies fundamentally in complexity from other approaches, as proposed by [23] and [31]. Our approach is a simple procedure implying neither a tricky numerical integration of the system nor additional off line measurements. This simplifies the experimental protocol and the calculation. In addition, our simple analytical expression allows for a better estimation of the approximation error.

The resulting formulas for the growth rate do not only allow for the determination of the physiological parameters, they also show a characteristic dependency between signal frequency and growth rate which enables an easy experimental validation of the model. The shape of the curve explains the "Flashing Light Effect" and shows that the increase of growth rate with fluctuation frequency is not linear but shows a very characteristic saturation for intermediate frequencies. Only a weak increase in growth rate can be expected with frequency augmentation in this domain. This insight can lead to important consequences for the design of raceways and photobioreactors. The dynamics of nitrogen assimilation and nutrient limited growth play an inferior role under the conditions we were assuming.

The proposed model is suitable to investigate the effect of the hydrodynamic regime on the growth rate of microalgae cultures due to photoinhibition. Regarding biofuel production with raceways and photobioreactors, the light variability on faster time scales is typically caused by mixing. The results from this study give important insights and are a first step in understanding the coupling of physical and biological models. With further research on the Droop–Han model, the light intensity dynamics at the scale of the microalgae can be optimized by the design of the process and an increased productivity can be achieved using the same total light dose. Increasing efficiency in biomass production by optimized photobioreactors is an important step on the way to the industrial use of microalgae.

Acknowledgements This work was carried out in the framework of the ARC Nautilus funded by INRIA.

Appendix A: analytical derivation

A1. Low frequency signal

Equation (11) is taken as an expression for the productivity of the photosynthetic system and the mean value during one period is taken. The domain of the integral can be restricted to the light phase of the cycle only, since during the dark phase $B = 0$.

$$\bar{B}_{\mathrm{slow}} = \frac{1}{2T}\int_T B\mathrm{d}t \tag{36}$$

By replacing A by $1 - B - C$, and assuming that A rests in its equilibrium while C is periodically oscillating:

$$B = \tau\sigma I A \tag{37}$$

we get:

$$\bar{B}_{\mathrm{slow}} = \frac{1}{2}\frac{\tau\sigma I_0}{1+\tau\sigma I_0}\left(1 - \frac{1}{T}\int_T C\mathrm{d}t\right) \tag{38}$$

Analogously, the differential equation for C can be reformulated

$$\dot{C} = -\left(k_{\mathrm{d}}\tau\frac{(\sigma I_0)^2}{1+\tau\sigma I_0}+k_{\mathrm{r}}\right)C+\frac{(\sigma I_0)^2}{1+\tau\sigma I_0} \tag{39}$$

This equation can be easily solved. C_0 is determined by applying the periodic boarder condition. Several simplification steps lead to the following expression for the integral:

$$\int_T C\mathrm{d}t = \frac{C_0-\delta(I)}{\epsilon}(1-\gamma(I)+\delta(I)T) \tag{40}$$

Using expression Eq. (38), we get expression Eq. (18).

A2. High frequency signal

Under the precondition that the periodicity of the signal is short, we already showed that the dynamics of C is negligible. In contrast, the transition process of A and B has to be taken into account. The expression for the mean growth rate has to account for the entire period, since $B \geq 0$ during the dark phase. The expression for the growth rate turns to:

$$\bar{B}_{\mathrm{fast}} = \frac{1}{2T}\left(\int_0^T B\mathrm{d}t+\int_T^{2T} B\mathrm{d}t\right) \tag{41}$$

The first integral being during the light period and the second during the dark period. To solve the integrals, an expression for $A(t)$ has to be determined from the differential equation. By assumption that C is a constant value and with periodical boarder conditions, Eq. (13) can be solved with the result:

$$A(t) = \left(A_0+\frac{1-C}{1+I_0\sigma\tau}\right)e^{\left(-\frac{t}{\tau}-I_0\sigma\zeta t\right)} - \frac{1-C}{1+I_0\sigma\tau}, \quad \text{for } t\in[0,T] \tag{42}$$

$$A(t) = \left(A_T+1-Ce^{\left(-\frac{t-T}{\tau}\right)}\right)-1-C, \quad \text{for } t\in[T,2T] \tag{43}$$

With Eqs. (42) and (13), periodical boarder conditions and the assumption $\dot{C}=0$, a value for C can be determined to:

$$C = \frac{kd(\sigma I)^2}{2Tk_{\mathrm{r}}}\frac{T\eta-T\theta}{\eta^2+\frac{kd(\sigma I)^2}{2Tk_{\mathrm{r}}}(T\eta-T\theta)} \tag{44}$$

with the expressions:

$$\eta = \frac{1}{\tau}+\sigma I_0, \quad \theta = \frac{(1-\alpha_0)(1-\alpha I)}{T(1-\alpha_0\alpha_{\mathrm{I}})}, \quad \alpha_{\mathrm{I}} = e^{-\left(\frac{1}{\tau}+\sigma I_0\right)T}, \quad \alpha_0 = e^{-\frac{T}{\tau}} \tag{45}$$

Knowing the value of C, the integrals in Eq. (41) can be resolved and B can be formulated as:

$$\bar{B}_{\mathrm{fast}} = \frac{\sigma I_0}{2}\frac{\eta-\theta+\tau\delta\theta}{\eta^2+\frac{kd(\sigma I)^2}{2k_{\mathrm{r}}}(\eta-\theta)} \tag{46}$$

A3. Proof of monotony

Low frequency

It can be shown, that the function:

$$\Phi(x,a,b) = \frac{(1-e^{-ax})(1-e^{-bx})}{x(1-e^{-(a+b)x})} \tag{47}$$

is strictly monotonic decreasing in x and it holds $\Phi(x,a,b)>0$ for $a>0$, $b>0$, $x>0$.

Further, $\bar{B}_{\mathrm{slow}}(I,T)$ can be defined as follows:

$$\bar{B}_{\mathrm{slow}}(I,T) = \left(1+\frac{\delta(I)}{k_{\mathrm{r}}}\Phi(T,k_{\mathrm{r}},\chi)\right)\cdot\bar{B}_{\mathrm{SS}}/2 \tag{48}$$

with $\chi = k_{\mathrm{r}}+k_{\mathrm{d}}\frac{(\sigma I)^2}{1+\tau\sigma I}$, consequently, $\bar{B}_{\mathrm{slow}}$ is strictly monotonic decreasing in T.

High frequency

$\bar{B}_{\mathrm{fast}}$ can be written as:

$$\bar{B}_{\mathrm{fast}} = \frac{\sigma I_0}{2}\frac{\eta-\Phi(1/\tau,\eta,T)+\tau\eta\Phi(1/\tau,\eta,T)}{\eta^2+\frac{k_{\mathrm{d}}(\sigma I)^2}{2k_{\mathrm{r}}}(\eta-\Phi(1/\tau,\eta,T))} \tag{49}$$

Derivation with respect to T yields:

$$\frac{\partial\bar{B}_{\mathrm{fast}}}{\partial T} = \frac{\eta^2\left(\frac{k_{\mathrm{d}}\sigma I^2}{2k_{\mathrm{r}}}+\sigma I\tau\right)}{\left(\eta^2+\frac{k_{\mathrm{d}}(\sigma I)^2)^2}{2k_{\mathrm{r}}}(\eta-\Phi(1/\tau,\kappa,T))\right)^2}\cdot\frac{\partial\Phi(1/\tau,\eta,T)}{\partial T} \tag{50}$$

Taking into account the parameters, it is clear that the fraction is positive. With the property $\frac{\partial\Phi(1/\tau,\eta,T)}{\partial T}<0$, it is shown that $\bar{B}_{\mathrm{fast}}$ is strictly monotonic decreasing with respect to T.

References

1. Benemann JR (1997) CO_2 mitigation with microalgae systems. Energy Convers Manag 38:475–479
2. Bernard O (2011) Hurdles and challenges for modelling and control of microalgae for CO2 mitigation and biofuel production. J Process Control 21(10):1378–1389
3. Bernard O, Gouzé JL (1995) Transient behavior of biological loop models, with application to the Droop model. Math Biosci 127(1):19–43
4. Bernard O, Gouzé JL (1999) Nonlinear qualitative signal processing for biological systems: application to the algal growth in bioreactors. Math Biosci 157:357–372

5. Carvalho AP, Meireles LA, Malcata FX (2006) Microalgal reactors: areview of enclosed system designs and performances. Biotechnol Prog 22(6):1490–1506
6. Celikovsk S, Stys D, Papacek S, Celikovsky S, Ruiz-Leon J (2007) Bilinear system as a modelling framework for analysis of microalgal growth. Kybernetika 43(1):1–20
7. Chisti Y (2007) Biodiesel from microalgae. Biotechnol Adv 25:294–306
8. Droop MR (1968) Vitamin B_{12} and marine ecology. The kinetics of uptake growth and inhibition in *Monochrysis lutheri*. J Mar Biol Assoc 48(3):689–733
9. Droop MR (1983) 25 Years of algal growth kinetics, a personal view. Bot Mar 16:99–112
10. Eilers PHC, Peeters JCH (1988) A model for the relationship between light intensity and the rate of photosynthesis in phytoplankton. Ecol Model 42(3–4):199–215
11. Eilers PHC, Peeters JCH (1993) Dynamic behavior of a model for photosynthesis and photoinhibition. Ecol Model 69(1–2): 113–133
12. Han BP (2001) Photosynthesis-irradiance response at physiological level: a mechanistic model.J Theor Biol 213:121–127
13. Han BP (2002) A mechanistic model of algal photoinhibition induced by photodamage to photosystem-II. J Theor Biol 214(4):519–527
14. Huntley M, Redalje DG (2007) CO_2 mitigation et renewable oil from photosynthetic microbes: a new appraisal. Mitig Adapt Strateg Glob Chang 12:573–608
15. Lange K, Oyarzun FJ (1992) The attractiveness of the Droop equations. Math Biosci 111:261–278
16. Luo HP, Al-Dahhan MH (2004) Analyzing and modeling of photobioreactors by combining first principles of physiology and hydrodynamics. Biotechnol Bioeng 85:382–393
17. Mairet F, Bernard O, Masci P, Lacour T, Sciandra A (2011) Modelling neutral lipid production by the microalga *Isochrysis affinis galbana* under nitrogen limitation. Biores Technol 102:142–149
18. Metting FB (1996) Biodiversity and application of microalgae. J Ind Microbiol Biotechnol 17:477–489
19. Monod J (1950) La technique de culture continue. théorie et applications. Annales de L'intiut Pasteur 79:390–410
20. Olaizola M (2003) Commercial development of microalgal biotechnology: from the test tube to the marketplace. Biomol Eng 20:459–466
21. Perner-Nochta I, Posten C (2007) Simulations of light intensity variation in photobioreactors. J Biotechnol 131:276–285
22. Pulz O (2001) Photobioreactors: production systems for phototrophicmicroorganisms. Appl Microbiol et Biotechnol 57:287–293
23. Rehak B, Celikovsky S, Papcek S (2008) Model for photosynthesis and photoinhibition: parameter identification based on the harmonic irradiation O_2 response measurement. IEEE Trans Autom Control 53(special Issue):101–108
24. Sari T (2007) Averaging for ordinary differential equation and functional differential equations. In: van den Berg I, Neves V (eds) The strength of nonstandard analysis, Springer, New York, p 286–305
25. Sciandra A, Ramani P (1994) The limitations of continuous cultures with low rates of medium renewal per cell. J Exp Mar Biol Ecol 178:1–15
26. Sialve B, Bernet N, Bernard O (2009) Anaerobic digestion of microalgae as a necessary step to make microalgal biodiesel sustainable. Biotechnol Adv 27:409–416
27. Prezlin V (1981) Light reaction in photosynthesis. Can. J Fish Aquat Sci 210:1–43
28. Vatcheva I, de Jong H, Bernard O, Mars NJL (2006) Experiment selection for the discrimination of semi-quantitative models of dynamical systems. Artif Intel 170:472–506
29. Vejrazka C, Janssen M, Streefland M, Wijffels R (2011) Photosynthetic efficiency of *Chlamydomonas reinhardtii* in flashing light. Biotechnol Bioeng 108(12):2905–2913
30. Wijffels RH, Barbosa MJ (2010) An outlook on microalgal biofuels. Science 329(5993):796–799
31. Wu X (2001) A model integrating fluid dynamics in photosynthesis and photoinhibition processes. Chem Eng Sci 56(11): 3527–3538

5

DYNAMIC COUPLING OF PHOTOACCLIMATION AND PHOTOINHIBITION IN A MODEL OF MICROALGAE GROWTH

Nature is relentless and unchangable, and it is indifferent as to whether its hidden reasons and actions are understandable to man or not.

Galileo Galilei

In the previous chapter, effects of short-term light fluctuations were studied based on a model for nutrient uptake and photoinhibition. In raceway systems, the received light signals not only consist of high changing frequencies. Due to the exponential light gradient, the fastest variations of the light signal appear close to the surface. In the darker regions of the volume, the rate of changes in light intensity are much lower considering a comparable movement speed of the particles. Apart from this, the external conditions of the raceway system such as weather, the diel cycle or seasonal changes impose mid- to long-term changes of the light signal. This motivates the development of models including short term and long term reactions of the photosynthetic production capacity. The key process for long term adaption is photoacclimation.

As presented in ch. 1, there are different approaches for modeling photoacclimation [30, 7]. While there are also approaches providing models for phtoinhibition and acclimation at the same time [29, 25], they are not adapted for the application with raceway cultures. The approach of Esposito et al. does not account for an adaption due to acclimation processes on the scale of the photocenter while the approach of Garcia-Camacho et al. has a very complex structure and many parameters.

In the following chapter, we present a dynamical model including photoacclimation, photoinhibition and nutrient limitation while maintaining a very simple structure. The model is based on two well-studied models for photo-acclimation [7] and inhibition [36]. It is formulated according to the widely discussed assumption that the initial slope of the PI Curve is independent from the chlorophyll content of the cells.

Dynamic Coupling of Photoacclimation and Photoinhibition in a Model of Microalgae Growth

Philipp Hartmann[a,b,c,*], Andreas Nikolaou[d,*], Antoine Sciandra[b,c], Benoît Chachuat[d], Olivier Bernard[a,b,c,**]

[a] *BIOCORE-INRIA, BP93, 06902 Sophia-Antipolis Cedex, France*
[b] *Sorbonne Universités, UPMC Univ Paris 06, UMR 7093, LOV, Observatoire océanologique, F-06230, Villefranche/mer, France*
[c] *CNRS, UMR 7093, LOV, Observatoire océanologique, F-06230, Villefranche/mer, France*
[d] *Centre for Process Systems Engineering (CPSE), Department of Chemical Engineering, Imperial College London, London SW7 2AZ, UK*

[*] Equal contributors
[**] Corresponding author

Abstract

The development of mathematical models that can predict photosynthetic productivity of microalgae under transient conditions is crucial for enhancing large-scale industrial culturing systems. Particularly important in outdoor culture systems, where the light irradiance varies greatly, are the processes of photoinhibition and photoacclimation, which can affect photoproduction significantly. The former is caused by an excess of light and occurs on a fast time scale of minutes, whereas the latter results from the adjustment of the light harvesting capacity to the incoming irradiance and takes place on a slow time scale of days. In this paper, we develop a dynamic model of microalgae growth that simultaneously accounts for the processes of photoinhibition and photoacclimation, thereby spanning multiple time scales. The properties of the model are analysed in connection to PI-response curves, under a quasi steady-state assumption for the fast processes and by neglecting the slow dynamics. For validation purposes, the model is calibrated and compared against multiple experimental data sets from the literature. In particular, these calibration results provide a means of distinguishing between the s-strategy and the n-strategy of photosystem adaptation, thereby shedding light on the mechanisms that underlie photoacclimation.

Keywords: photoinhibition, photoacclimation, photosynthesis, modeling, dynamic, biofuel

1. Introduction

Microalgae are often considered a promising alternative for production of renewable energy (Wijffels and Barbosa, 2010). Claimed advantages of this approach are a higher actual photosynthetic yield compared to field crops, a reduction in fresh water consumption, and independence to agriculturally usable land (Williams and Laurens, 2010). These advantages could lead to large-scale production of algal biomass that is not in direct competition with food production. Moreover, microalgae culture systems can be coupled with wastewater treatment technologies (Sialve et al., 2009), can produce high added-value products such as cosmetics, pharmaceuticals and nutraceuticals (Brennan and Owende, 2010), and can even contribute to CO_2 mitigation due to their inherent ability to fix carbon during photosynthesis (Talec et al., 2013). Nonetheless, numerous problems need to be overcome on the path to a sustainable large-scale biofuel production. Optimizing the entire production chain in order to reduce the production costs as well as the environmental impact presents many challenges, and among them improving the algal biomass production efficiency has top priority. As well as developing a better understanding of the key mechanisms underlying photosynthesis, the development of more accurate mathematical models combining mass-conservation principle and phenomenological knowledge holds much promise in this context.

Two key processes are involved in the way light conditions affect the photosynthetic yield. *Photoinhibition* causes a loss of photosynthetic yield due to an excess of photons, which damage some of the key proteins in the photosynthetic apparatus. *Photoacclimation*, the process by which microalgae adjust their pigment content and composition to light intensity, alters the rate of photosynthetic production. These two processes act on different time scales: photoinhibition occurs on a time scale of minutes, whereas photoacclimation acts on a time scale of days. In order to achieve optimal microalgae productivity, understanding the processes of nutrient assimilation, photoinhibition and photoacclimation, together with their interactions, is thus paramount. A number of mathematical models are available that account for photoacclimation at the slow time scale (Geider et al., 1997; Bernard, 2011; Geider et al., 1998), yet they neglect the photoinhibition processes. Conversely, models have also been proposed which describe photoinhibition in the fast time scale (Eilers and Peeters, 1993b; Han, 2001), but they do not account for photoacclimation.

It is the main objective of this paper to develop a dynamic model of microalgae growth that couples photoinhibition and photoacclimation with carbon and nitrogen uptake. We rely on

existing and validated models wherever possible and couple them so as to preserve biophysical consistency. Nutrient assimilation is described by the well-accepted and validated Droop model (Droop, 1983). Photoinhibition is described by the model proposed by Han (Han, 2001), originating in the work of Eilers and Peeters (1993b) who first introduced the concept of photosynthetic factories (also known as photosynthetic units). A related, yet simpler, coupling between a photoinhibition model and the Droop model has been studied by Hartmann et al. (2014). An extension of this coupling that incorporates photoacclimation processes constitutes the main novelty of the developed model. Specifically, we propose a modification of the photosynthesis rate and pigment synthesis rate expressions to account for photoacclimation effects, and we express both the effective cross section and the number of photosynthetic units—which are parameters in the Han model—as functions of the chlorophyll content by means of empirical relations (Falkowski and Raven, 2007). This approach leads to a simple expression for the photosynthesis rate, which is readily amenable to mathematical analysis under a quasi-steady-state approximation.

The remainder of this paper is organized as follows. Existing models of slow and fast processes, including nutrient limited growth, photoacclimation and photoinhibition, are first reviewed in Sect. 2. The dynamic model coupling these processes is described in Sect. 3, and the properties of the resulting PI-response model are analyzed. A calibration of the coupled model against several experimental data sets from the literature is presented in Sect. 4, followed by a discussion in Sect. 5. Finally, Sect. 6 concludes the paper and draws future research directions.

2. Modelling of Slow and Fast Processes in Microalgae

2.1. Nutrient-Limited Growth – The Droop Model

Droop (1968) observed that microalgae keep growing for some time after nutrients have been depleted. Monod kinetics are unable to model this behavior and therefore are not suitable for predicting microalgae growth under nutrient limitation. A better way to represent nutrient-limited growth is by separating the nutrient uptake rate, denoted by ρ hereafter, from the growth rate, denoted by μ. This idea was followed by Droop (1968, 1983) in relating the growth rate to the internal elemental nutrient quota. Since its introduction, the Droop model has been widely studied (Lange and Oyarzun, 1992; Bernard and Gouzé, 1995; Vatcheva et al., 2006) and thoroughly validated (Droop, 1983; Sciandra and Ramani, 1994; Bernard and Gouzé, 1999; Vatcheva et al., 2006).

In a continuous and homogeneous microalgae culture, the mass-balance equations for the nutrient (inorganic nitrogen) concentration s in the bulk phase, the biomass concentration x, and the carbon-specific nitrogen quota q of the cells (in units of $\mathrm{g_N/g_C}$) are given by

$$\begin{aligned} \dot{s} &= D\, s_{\mathrm{in}} - \rho(s,q)\, x - D\, s \\ \dot{x} &= \mu(q,\cdot)\, x - D\, x - R\, x \\ \dot{q} &= \rho(s,q) - \mu(q,\cdot)\, q\,, \end{aligned} \tag{1}$$

with D and R denoting the dilution rate and the endogenous respiration rate, respectively; and s_{in}, the nutrient concentration in the feed.

Recently, an extension of the Droop model has been proposed by Bernard (2011) for accounting the effect of light conditions on the growth rate μ in the form

$$\mu(q,\cdot) = \bar{\mu}\, \left(1 - \frac{Q_0}{q}\right)\, \phi(\cdot), \tag{2}$$

where $\bar{\mu}$ stands for the maximum growth rate, i.e., the growth rate reached under non-limiting conditions; Q_0, the minimal cell quota, so that $\mu(Q_0,\cdot) = 0$ and $q \geq Q_0$; and, $\phi(\cdot)$ is a saturation function. In particular, an expression of $\phi(\cdot)$ will be developed in Sect. 3 that accounts for the state of the photosystem units.

The nutrient uptake rate ρ, on the other hand, can be expressed as (Geider et al., 1998)

$$\rho(s,q) = \bar{\rho}\, \frac{s}{s+k_s}\, \left(1 - \frac{q}{Q_l}\right), \tag{3}$$

where $\bar{\rho}$ stands for the maximum nutrient uptake rate; k_s, the half-saturation constant for substrate uptake; and Q_l, the limit quota for the nitrogen uptake, so that $\rho(s,Q_l) = 0$ and $q \leq Q_l$, with equality corresponding to nutrient-replete conditions.

2.2. Pigment Content

Photoacclimation is the mechanism by which both the chlorophyll content and the pigment composition change in response to variations in the light irradiance. Such changes take place on a time scale of days, and it has been suggested that microalgae use photoacclimation as a means to optimize their growth at low irradiance as well as to minimize damage at high irradiance (Falkowski and Raven, 2007).

One way to describe photoacclimation is by accounting for the change in the chlorophyll content over time. Following Bernard (2011), the chlorophyll content, c, is assumed to be proportional to cellular protein content as a first approximation, which is itself represented by

the particulate nitrogen content $x\,q$:

$$c = \gamma(I_g)\, x\, q, \tag{4}$$

where I_g represents the light irradiance at which the cells are acclimated, also called *growth irradiance*. Introducing the carbon-specific chlorophyll quota $\theta := c/x$ (in units of $\mathrm{g_{chl}/g_C}$), the foregoing relation can be rewritten in the form

$$\theta = \gamma(I_g)\, q\,. \tag{5}$$

Here, we choose to express $\gamma(\cdot)$ in the form of the hyperbolic function

$$\gamma(I_g) = \bar{\gamma}\frac{k_I}{I_g + k_I}, \tag{6}$$

with parameters $\bar{\gamma}$ and k_I. Moreover, the dynamic evolution of I_g is related to the current light irradiance I by the following equation

$$\dot{I}_g = \delta\ \mu(q,\cdot)\ (I - I_g)\,, \tag{7}$$

thereby assuming that the adaptation speed is proportional to the irradiance difference $(I - I_g)$ as well as to the current growth rate $\mu(\cdot)$, with the constant proportionality coefficient δ. On the whole, a change in the current irradiance I affects I_g via (7), which in turn modifies the chlorophyll quota θ via (5).

2.3. Photosynthetic Production and Photoinhibition – The Han Model

The Han model (Han, 2001), which is inspired by the model of Eilers and Peeters (1993a), describes the effect of light irradiance on microalgae growth. This model considers the damage of key proteins in photosynthetic units to be the main contribution to photoinhibition. Particularly appealing in the Han model is the description of complex photosynthetic processes in terms of three possible states of the photosystem II (PSII) unit only, namely: open, A; closed, B; and, inhibited, C.

The equations giving the rates of change in the fractions of open, closed and inhibited PSUs are:

$$\begin{aligned}
\dot{A} &= -I\,\sigma\,A + \frac{B}{\tau} \\
\dot{B} &= I\,\sigma\,A - \frac{B}{\tau} + k_r\,C - k_d\,\sigma\,I\,B \\
\dot{C} &= -k_r\,C + k_d\,\sigma\,I\,B\,,
\end{aligned} \tag{8}$$

with initial conditions such that $A(0) + B(0) + C(0) = 1$. A number of remarks are:

- Photosynthetic production is described by the transition between open state and closed state. Excitation is assumed to occur at a rate of σI, with σ being the effective cross section of the photosynthetic unit (PSU), whereas deexcitation is assumed to occur at a rate of $\frac{1}{\tau}$, with τ the turnover time of the electron transport chain.

- Photoinhibition occurring at high light irradiance corresponds to the transition from closed state to inhibited state. This process is assumed to occur at a rate of $k_d \sigma I$. The reverse transition from inhibited state to closed state accounts for the repair of damaged PSUs by enzymatic processes in the cell, a mechanism that is assumed to occur at a constant rate k_r.

Interestingly, expressions for the fractions of open, closed and inhibited states at steady state as a function of the irradiance I can be obtained via basic algebraic manipulation of (8). For instance, the steady-state expression A^∞ for the open state A is given by:

$$A^\infty(I) = \frac{1}{1 + \tau\,\sigma\,I + K\,\tau\,\sigma^2\,I^2}\,, \tag{9}$$

with $K := k_d/k_r$.

3. Multi-Scale Model of Microalgae Growth Coupled with Photoinhibition and Photoacclimation

The proposed model couples three dynamic processes, namely (i) the dynamics of PSUs, (ii) the dynamics of intracellular nitrogen content, and (iii) the dynamics of chlorophyll content. These processes span four different timescales ranging from milliseconds for the open-closed dynamics of the PSUs up to several days for the dynamics of intracellular nitrogen quota q.

3.1. Coupling Between Growth, Photoinhibition and Photoacclimation

Our model builds upon the Droop-Han model of Hartmann et al. (2014) and incorporates photoacclimation processes via the dynamics of the chlorophyll quota θ introduced in Sect. 2.2. More specifically, we account for two possible ways that the term $\phi(\cdot)$ in (2) can depend on θ. The first effect is a direct linear dependency of photosynthesis efficiency on the chlorophyll content, which is in agreement with the work of Faugeras et al. (2004). Since the probability of a photon encountering an open state is proportional to $A\,I$, a second, indirect effect is via the dependence of the dynamics of A on θ. This latter dependency results from the fact that the parameter σ introduced in the Han model (8) can itself depend on the current acclimation state. Indeed, Falkowski and Raven (2007) describe photoacclimation as a process that can follow

either one of two strategies: the *n-strategy* corresponds to a change in the density (per biomass unit) of PSUs, denoted by N subsequently; the *s-strategy* corresponds to a change in the size of the PSU, and is thus directly related to the functional cross section σ. In practice, chlorophyll is thus used either to build new PSUs or to increase the size of the antenna in existing PSUs. These two acclimation strategies run concurrently, and both can be described by defining $N(\cdot)$ and $\sigma(\cdot)$ as functions of the chlorophyll quota θ. Such relationships are further investigated in Sect. 3.3.

Based on the above considerations, the growth rate μ can be modeled as:

$$\mu(q,\theta,I) = \bar{\alpha}\,\left(1-\frac{Q_0}{q}\right)\,\theta\,A(I,\theta)\,I\,,$$

where $\bar{\alpha}$ is a constant parameter. At this point, we shall introduce the rate of carbon uptake per chlorophyll unit, μ_{chl}, as

$$\mu_{\mathrm{chl}}(q,\theta,I) = \frac{\mu(q,\cdot)}{\theta} = \bar{\alpha}\,\left(1-\frac{Q_0}{q}\right)\,A(I,\theta)\,I\,, \tag{10}$$

which is also known as the chlorophyll-specific photosynthesis rate.

3.2. Structural Analysis of the PI Response

In experiments assessing photosynthetic efficiency of microalgae, the cells are photoacclimated to a given light intensity for a sufficiently long time and under nutrient replete conditions, before exposing them to a series of varying light irradiances I. The instantaneous growth rates obtained under these conditions—ideally via consideration of the carbon fixation rate, but often based on the O_2 production rate too—are measured and yield the so-called PI-response curve when plotted against I.

A common assumption about PI-response curve experiments is that they are fast enough for photoacclimation, substrate internalization and growth to be negligible; that is, variations in the variables θ, q and x can all be neglected. In contrast, variations in the fractions of open, closed and inhibited states in the Han model can be considered fast in the time scale of PI-response curve experiments, and one can thus assume that the variables A, B and C reach their steady states as in (9), without significantly impairing the PI response predictions (quasi-steady-state approximation). Both approximations of the slow and fast dynamics can be tested via numerical simulation, and they lead to the following expression of the chlorophyll-specific growth rate:

$$\mu^{\mathrm{PI}}_{\mathrm{chl}}(\theta,I) = \bar{\alpha}\,\left(1-\frac{Q_0}{Q_{\max}(\cdot)}\right)\,\frac{I}{1+\tau\,\sigma(\theta)\,I+K\,\tau\,\sigma^2(\theta)\,I^2}\,, \tag{11}$$

where $Q_{\max}(\cdot)$ denotes the maximal value of the nitrogen internal quota q under nutrient replete conditions, a value that typically depends on the growth irradiance I_g (Bernard, 2011). A further simplification gives

$$\mu_{\text{chl}}^{\text{PI}}(\theta, I) = \alpha(\cdot)\, \frac{I}{1 + \tau\, \sigma(\theta)\, I + K\, \tau\, \sigma^2(\theta)\, I^2}\,, \tag{12}$$

with $\alpha(\cdot) := \bar{\alpha}\left(1 - \frac{Q_0}{Q_{\max}(\cdot)}\right)$ denoting the initial slope of the PI response curve, i.e., the rate of change of μ_{chl} with respect to the light irradiance I for a vanishing irradiance.

Many authors concur to say that, for many microalgae species, the initial slope $\alpha(\cdot)$ can be considered to be independent of the value of θ (MacIntyre et al., 2002). Nonetheless, we like to note that the constant initial slope assumption is still debated; see, for instance, the paper by Richardson et al. (1983), where microalgae acclimation strategies are divided into six different categories based on photosynthesis-irradiance response data. We shall come back to this important point later on in Sect. 5, where it is argued that certain variations in initial slopes may as well be explained by transients effects in the fraction of inhibited PSUs.

In the remainder of this subsection, we investigate structural properties of the PI-response curve under the foregoing assumptions of time-scale separation and constant initial slope. The optimal irradiance value $I^\star$ maximizing μ_{chl} can be determined from (12) as

$$I^\star(\theta) := \frac{1}{\sigma(\theta)\sqrt{K\tau}}\,. \tag{13}$$

In turn, the maximal productivity rate $\mu_{\text{chl}}^{\text{PI}\star}$ can be expressed in the form

$$\mu_{\text{chl}}^{\text{PI}\star}(\theta) := \alpha\, \frac{\sqrt{K\tau}}{\tau + 2\sqrt{K\tau}}\, I^\star(\theta)\,. \tag{14}$$

The following property follows readily from (14), provided that the Han model parameters τ and K are independent of the acclimation state:

Property 1. *The maximal growth rate $\mu_{\text{chl}}^{\text{PI}\star}$ is proportional to the optimal irradiance $I^\star$ regardless of the pre-acclimated state or the growth irradiance.*

Although a direct consequence of the constant initial slope assumption, this property does not depend on a particular choice of the relationship between $\sigma(\cdot)$ and θ. Moreover, it is readily tested using data from experimental PI curves corresponding to different acclimation states.

3.3. Quantitative Analysis of the PI Response

In order to make quantitative predictions of the PI-response curve or, more generally, for numerical simulation of the coupled model, relationships must be specified for $\sigma(\cdot)$ and $N(\cdot)$ in terms of the chlorophyll quota θ.

We start by noting that $\sigma(\cdot)$ and $N(\cdot)$ can both be related to the average chlorophyll content of a single PSU, denoted by $\Gamma(\cdot)$ subsequently. An immediate relation for $N(\cdot)$ is:

$$\Gamma(\theta)\, N(\theta) = \theta\,. \tag{15}$$

On the other hand, we choose to express $\sigma(\cdot)$ in the form of a power law of Γ as:

$$\sigma(\theta) \;=\; \sigma_0\, \Gamma(\theta)^{\gamma}\,,$$

where the exponent γ depends on the geometric shape of the photosynthetic antenna; for instance, $\gamma = 2/3$ in the idealized case that a PSU is assimilated to a sphere. In most of the data set that we considered, it was not possible to estimate γ, therefore the value $2/3$ has been taken.

Now, assuming a general power law relationships between σ and θ as:

$$\sigma(\theta) = \beta\, \theta^{\kappa}\,, \tag{16}$$

and using (15), a relationship between N and θ follows in the form:

$$N(\theta) = \left(\frac{\sigma_0}{\beta}\right)^{1/\gamma} \theta^{1-\kappa/\gamma}\,. \tag{17}$$

Besides their simplicity, expressions of $\sigma(\theta)$ and $N(\theta)$ in the form of power laws are also plausible from a biophysical standpoint. It is indeed expected that $\sigma(\theta)$ should be a monotonically increasing function of θ, as the size of the PSUs typically increases with an increasing chlorophyll quota θ. In contrast, the expression of $N(\theta)$ in (17) remains flexible enough to predict either an increase or a decrease in the number of PSUs with respect to θ. This way the proposed acclimation model allow distinguishing between the s-strategy and the n-strategy of PSU adaptation.

Substituting the power law (16) in the expression of $I^{\star}$ in (13), and log-linearizing the resulting expression yields

$$\log I^{\star}(\theta) = -\kappa\, \log\theta - \log(\beta\sqrt{K\tau})\,. \tag{18}$$

The following property follows directly from (18):

Property 2. *The exponent κ in the power laws* (16) *corresponds to the (negative of the) slope in a log-log plot of $I^\star$ versus θ.*

Like Property 1, the linearity of the relationship between $\log I^\star$ and $\log \theta$ can be readily tested using data from experimental PI curves corresponding to different acclimation states.

To summarize, a complete expression of the model predicting the PI responses of a given microalgae at various pre-acclimated states is:

$$\mu_{\mathrm{chl}}^{\mathrm{PI}}(q,\theta,I) = \bar{\alpha}\,\left(1-\frac{Q_0}{Q_{\max}(\cdot)}\right)\,\frac{I}{1+\tau\,\beta\,\theta^{\kappa}\,I+K\,\tau\,\beta^2\,\theta^{2\kappa}\,I^2}\,. \tag{19}$$

This expression is of the Haldane type and comprises the following parameters: K and τ from the Han model; β and κ from the acclimation model; and the initial slope $\bar{\alpha}$ together with the minimal and maximal nitrogen quotas Q_0 and $Q_{\max}$—or alternatively α in the simplified version.

4. Calibration and Validation Results using Data Sets from the Literature

A calibration of the new features in the coupled model is carried out using experimental data sets from the works of Anning et al. (2000) and Falkowski and Owens (1980). The focus is on the chlorophyll-specific photosynthesis rate (19) as well as on the saturation function γ in the nitrogen-quota-to-chlorophyll-quota relationship (5).

4.1. Data for Skeletonema costatum

Experimental data by Anning et al. (2000) are for the diatom *Skeletonema costatum*. They comprise two acclimation states at different growth irradiances I_g, namely $50\ \mu\mathrm{E\ m^{-2}\ s^{-1}}$ (LL) and $1500\ \mu\mathrm{E\ m^{-2}\ s^{-1}}$ (HL). The LL irradiance corresponds to a chlorophyll quota of $\theta = 0.082\ \mathrm{g_{chl}\ g_C^{-1}}$, and the HL irradiance to $\theta = 0.018\ \mathrm{g_{chl}\ g_C^{-1}}$.

Calibration of PI-Response Curves. We neglect variations of the term α in (19) as a first approximation, and we consider a nonlinear regression approach based on least-square minimization to estimate the values of parameters β, κ and α. On the other hand, we use default values for the Han model parameters k_r, k_d and τ; these values are obtained by averaging over the parameter ranges reported in (Han et al., 2000) and can be found in Table 1.

In order to certify global optimality of the parameter estimates, we use the global optimization solver BARON (Tawarmalani and Sahinidis, 2005) in the GAMS modelling environment. The

Table 1: Default parameter values in the Han model and Parameter estimates in the photosynthesis rate (19) for the data by Anning et al. (2000).

Parameter	Value	Origin
τ	5.5×10^{-3} s	default
k_r	1.4×10^{-4} s^{-1}	default
k_d	5.0×10^{-8} –	default
α	0.0160 $\mathrm{g_C\ g_{chl}^{-1}\ \mu E^{-1}\ s\ m^2}$	estimated from Anning et al. (2000)
β	0.492 $\mathrm{\mu E^{-1}\ m^2\ s\ g_{chl}^{1/\kappa}\ g_C^{-1/\kappa}}$	estimated from Anning et al. (2000)
κ	0.469 –	estimated from Anning et al. (2000)

resulting parameter estimates are given in Table 1, and the fitted PI-response curves (19) are plotted against the available experimental data in Fig. 1. The predictions are in excellent agreement with this experimental data sets at both light irradiances, also with regards to Property 1, thereby providing a first validation of the structural assumptions in (19).

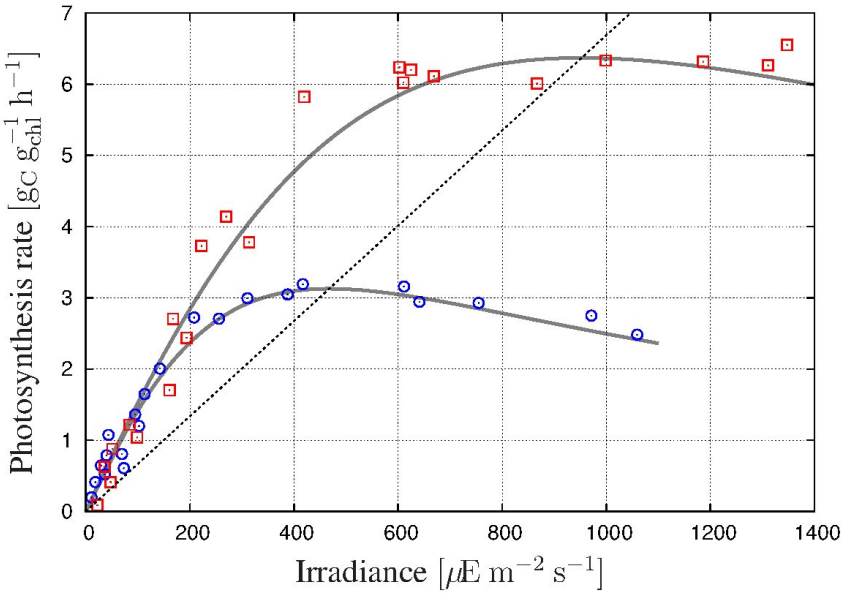

Figure 1: PI-response curves for *Skeletonema costatum* based on the data by Anning et al. (2000). The blue and red points correspond to acclimation at HL and LL, respectively. The predicted PI responses are depicted in gray solid lines. The dashed line connects the maxima of both PI curves per Property 1.

Confidence Analysis of PI-Response Curves. In order to assess the confidence of the parameter estimates in Table 1, we apply guaranteed parameter estimation in the bounded-error sense (Jaulin and Walter, 1993). To conduct the analysis, we consider variations around the available photosynthesis rate measurements, here variations of $\pm 5\%$. A large number of scenarios is generated by sampling the resulting measurement ranges—using Sobol sequences and assuming no correlation between the different measurements—and globally optimal estimates for β,

κ and α are then computed for every scenario. This way, we obtain the set of all possible parameter values that are consistent with the available measurements within a $\pm 5\%$ error.

The results obtained for the data set by Anning et al. (2000) are shown in Fig. 2. Projections of the confidence region onto the (β, κ), (β, α) and (κ, α) subspaces provide parameter confidence ranges as $\beta \in [0.45, 0.54]$, $\kappa \in [0.44, 0.5]$ and $\alpha \in [0.0158, 0.0172]$. Moreover, these projections reveal the existence of a significant correlation between the parameters β and κ of the acclimation model, whereas correlations of β or κ with α are rather weak. The envelopes of both PI-response curves obtained for parameter values in the confidence region are shown on the bottom-right plot of Fig. 2 as well, confirming the good agreement with the experimental data.

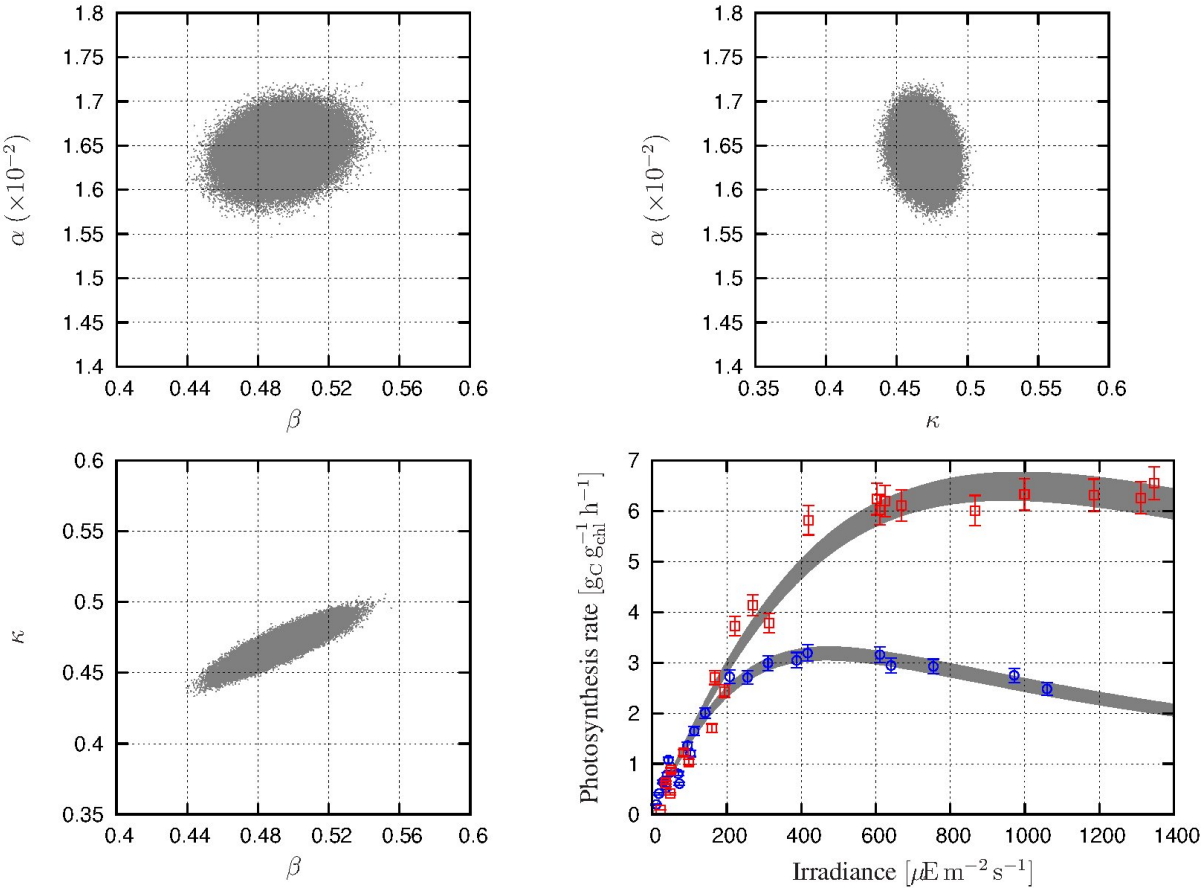

Figure 2: Confidence region of the parameter estimates β, κ and α for $\pm 5\%$ deviations from the measurement data by Anning et al. (2000) and corresponding envelopes of PI curves.

4.2. Data for Dunaliella tertiolecta

Experimental data by Falkowski and Owens (1980) are for the chlorophyte *Dunaliella tertiolecta*. Amongst the available data, four PI curves are selected that were not affected by 'bleaching', corresponding to acclimation states at growth irradiances I_g of 60 μE m^{-2} s^{-1}

(LL_1), 120 $\mu\mathrm{E}\,\mathrm{m}^{-2}\,\mathrm{s}^{-1}$ (LL_2), 200 $\mu\mathrm{E}\,\mathrm{m}^{-2}\,\mathrm{s}^{-1}$ (LL_3), and 400 $\mu\mathrm{E}\,\mathrm{m}^{-2}\,\mathrm{s}^{-1}$ (LL_4). Measurements of carbon, nitrogen and chlorophyll content per cell are also available for all four acclimation states, based on which lower and upper ranges for both the nitrogen quota q and the chlorophyll quota θ can be determined, as given in Table 2.

Table 2: Ranges of nitrogen and chlorophyll quotas from the measurement data by Falkowski and Owens (1980) at acclimation states LL_1, LL_2, LL_3 and LL_4.

Growth irradiance I_g $[\mu\mathrm{E}\,\mathrm{m}^{-2}\,\mathrm{s}^{-1}]$	Nitrogen quota $Q_{\max}$ $[\mathrm{g_N}\,\mathrm{g_C}^{-1}]$	Chlorophyll quota θ $[\mathrm{g_{chl}}\,\mathrm{g_C}^{-1}]$
LL_1: 60	$Q_{\max} \in [0.250, 0.357]$	$\theta \in [0.0774, 0.0820]$
LL_2: 120	$Q_{\max} \in [0.222, 0.323]$	$\theta \in [0.0654, 0.0682]$
LL_3: 200	$Q_{\max} \in [0.213, 0.286]$	$\theta \in [0.0436, 0.0453]$
LL_4: 400	$Q_{\max} \in [0.172, 0.208]$	$\theta \in [0.0355, 0.0373]$

Calibration of PI-Response Curves. Since experimental information is available for the nitrogen quota q in all acclimation states, variations of the term $(1 - Q_0/Q_{\max})$ in (19) can be accounted for with this data set—we consider a value of $Q_0 = 0.05\ \mathrm{g_N}\,\mathrm{g_C}^{-1}$ for the minimum nitrogen quota throughout (Geider et al., 1998; Bernard, 2011). Like previously, we use a nonlinear regression approach based on least-square minimization to estimate the values of parameters $\bar{\alpha}$, β and κ, and we define extra variables for the nitrogen and chlorophyll quotas in the regression problem with bounds as defined in Table 2. As far as the Han model parameters are concerned, we use the default values of τ and k_r in Table 1. On the other hand, the default value for k_d is not deemed suitable as photoinhibition effects are not observed on the available PI-curve data, so k_d is considered an extra variable in the regression problem with bounds $[0, 10^{-7}]$ initially.

Table 3: Parameter estimates in the photosynthesis rate (19) for the data by Falkowski and Owens (1980).

Param.	Value	Nitrogen quota	Chlorophyll quota
$\bar{\alpha}$	$0.055\ \mathrm{g_C}\,\mathrm{g_{chl}}^{-1}\,\mu\mathrm{E}^{-1}\,\mathrm{m}^2$	$Q_{\max}^{60} = 0.250\ \mathrm{g_N}\,\mathrm{g_C}^{-1}$	$\theta^{60} = 0.082\ \mathrm{g_{chl}}\,\mathrm{g_C}^{-1}$
β	$54.8\ \mu\mathrm{m}^{1/\kappa}\,\mathrm{g_{chl}}^{1/\kappa}\,\mathrm{g_C}^{-1/\kappa}$	$Q_{\max}^{120} = 0.322\ \mathrm{g_N}\,\mathrm{g_C}^{-1}$	$\theta^{120} = 0.065\ \mathrm{g_{chl}}\,\mathrm{g_C}^{-1}$
κ	1.54 –	$Q_{\max}^{200} = 0.266\ \mathrm{g_N}\,\mathrm{g_C}^{-1}$	$\theta^{200} = 0.045\ \mathrm{g_{chl}}\,\mathrm{g_C}^{-1}$
k_d	1.27×10^{-8} –	$Q_{\max}^{400} = 0.208\ \mathrm{g_N}\,\mathrm{g_C}^{-1}$	$\theta^{400} = 0.036\ \mathrm{g_{chl}}\,\mathrm{g_C}^{-1}$

The solver BARON (Tawarmalani and Sahinidis, 2005) in the GAMS modelling environment is again used to guarantee globally optimal parameter estimates. These estimates are reported in Table 3, and the fitted PI-response curves (19) are plotted against the available experimental

data in Fig. 3 in gray solid lines. The predicted responses are generally in good agreement with the experimental data, thereby confirming the ability of the model to capture the photosynthetic activity of *Dunaliella tertiolecta*.

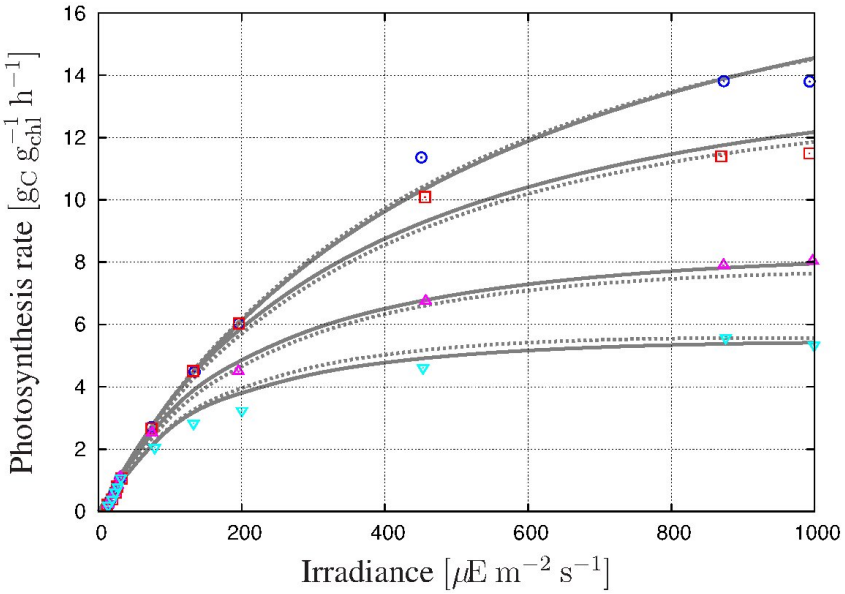

Figure 3: PI-response curves for *Dunaliella tertiolecta* based on the data by Falkowski and Owens (1980). The light blue, magenta, red, and blue points correspond to acclimation at LL_1, LL_2, LL_3 and LL_4, respectively. The predicted PI responses are depicted in gray lines, with and without accounting for variations of the term $(1 - Q_0/Q_{\max})$ in solid lines and dotted lines, respectively.

For sake of comparison, we also plot in gray dotted lines on Fig. 3 the fitted PI responses without accounting for variations of the term $(1 - \frac{Q^0}{Q_{\max}})$ in (19); that is, the parameter α is estimated in lieu of $\bar{\alpha}$. These fits, although slightly degraded, remain accurate. Moreover, the corresponding parameter estimates, $\beta \approx 32.4$, $\kappa \approx 1.4$, and $\alpha \approx 0.042$, are in good agreement with the values in Table 3 as well as with the confidence analysis that follows. This shows that the PI-response model (19) is robust towards uncertainty in the nitrogen maximal quota $Q_{\max}$.

Confidence Analysis of PI-Response Curves. As previously, we assess the confidence of the estimates obtained for the acclimation parameters $\bar{\alpha}$, β and κ in Table 3. We consider variations of $\pm 5\%$ around the available photosynthesis rate measurements and we apply guaranteed parameter estimation to obtain the set of all possible values for $\bar{\alpha}$, β and κ that are consistent with these measurement-error ranges.

The results obtained for the data set by Falkowski and Owens (1980) are shown in Fig. 4. Projections of the confidence region onto the (β, κ), $(\beta, \bar{\alpha})$ and $(\kappa, \bar{\alpha})$ subspaces provide parameter confidence ranges as $\beta \in [32, 65]$, $\kappa \in [1.35, 1.6]$ and $\bar{\alpha} \in [0.052, 0.058]$. These projections also reveal the existence of a strong correlation between the parameters β and κ, which is likely

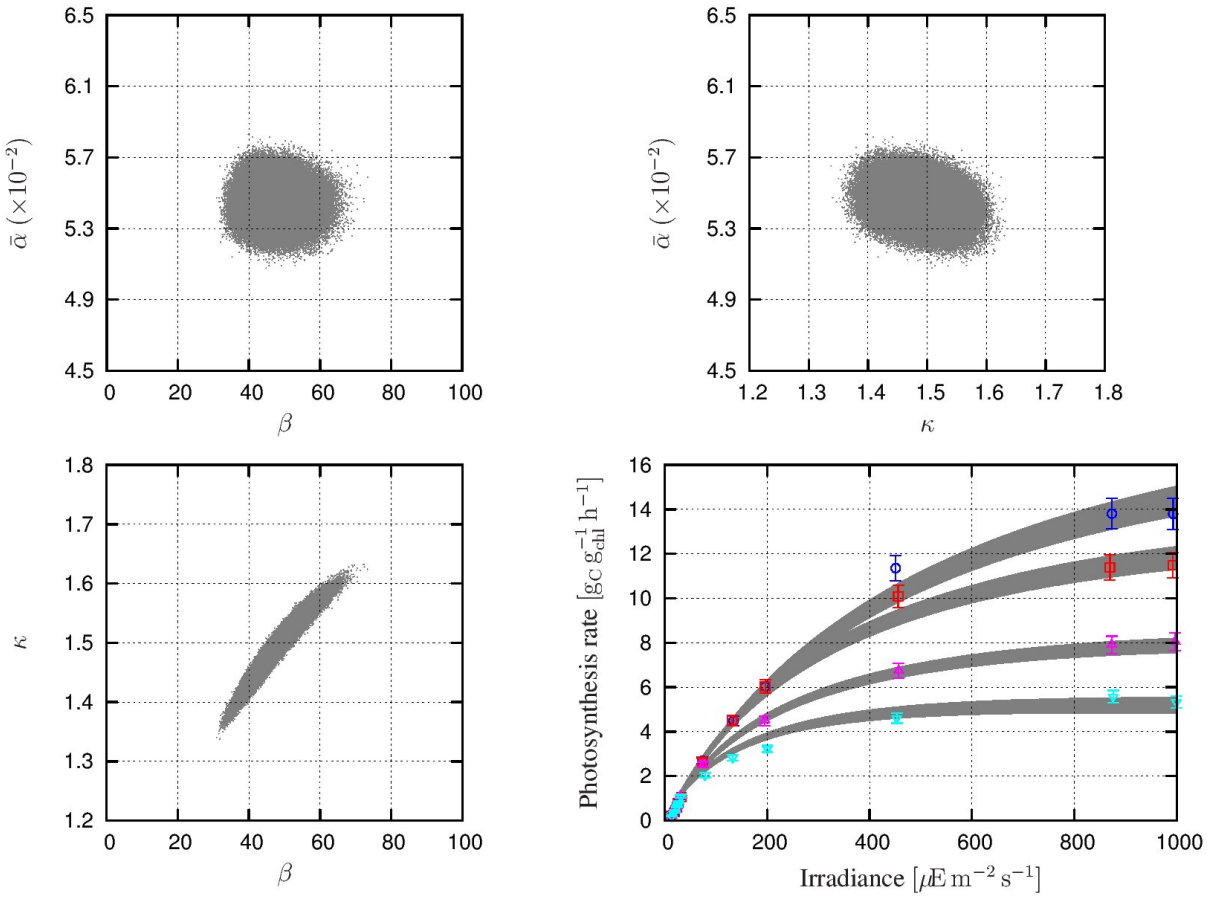

Figure 4: Confidence region of the parameter estimates $\bar{\alpha}$, β and κ for $\pm 5\%$ deviations from the measurement data by Falkowski and Owens (1980) and corresponding envelopes of PI curves.

due to the absence of photoinhibition effects in this data set. In contrast, the correlations of β or κ with $\bar{\alpha}$ appear to be rather weak. The envelopes of all four PI-response curves obtained for parameter values in the confidence region are shown on the bottom-right plot of Fig. 2 and confirm the good agreement with the experimental data.

Calibration of Nitrogen-Quota-to-Chlorophyll-Quota Relationship. Since experimental information is available for both the nitrogen quota q and the chlorophyll quota θ in all four acclimation states, values of the parameters $\bar{\gamma}$ and k_I in the nitrogen-quota-to-chlorophyll-quota relationship (5),(6) can be estimated from this data set too. Note that these relationships can be rewritten in the form

$$\bar{\gamma}\frac{q}{\theta} - \frac{1}{k_I} I_g = 1\,, \tag{20}$$

thus making it possible to use a simple linear regression approach for estimating the values of $\bar{\gamma}$ and $\frac{1}{k_I}$. For consistency with the foregoing PI-curve calibration, we use the estimated values of nitrogen and chlorophyll quotas in Table 2 to carry out the estimation.

Table 4: Parameter estimates in the nitrogen-quota-to-chlorophyll-quota relationship (5),(6) for the data by Falkowski and Owens (1980).

Parameter	Value
$\bar{\gamma}$	0.31 $\mathrm{g_{chl}\,g_N^{-1}}$
k_I	440 $\mu\mathrm{E\,m^{-2}\,s^{-1}}$

The computed estimates for $\bar{\gamma}$ and k_I are given in Table 4, and the nitrogen-quota-to-chlorophyll-quota predictions (black points) are plotted against the available experimental data (red circles) in Fig. 5; the gray dotted line on this plot is merely an interpolation between the predictions, since nitrogen or chlorophyll quotas are not available at intermediate irradiances. Despite some discrepancies at higher light irradiances, these results confirm the ability of the acclimation model (5),(6) to capture the general trend of the data.

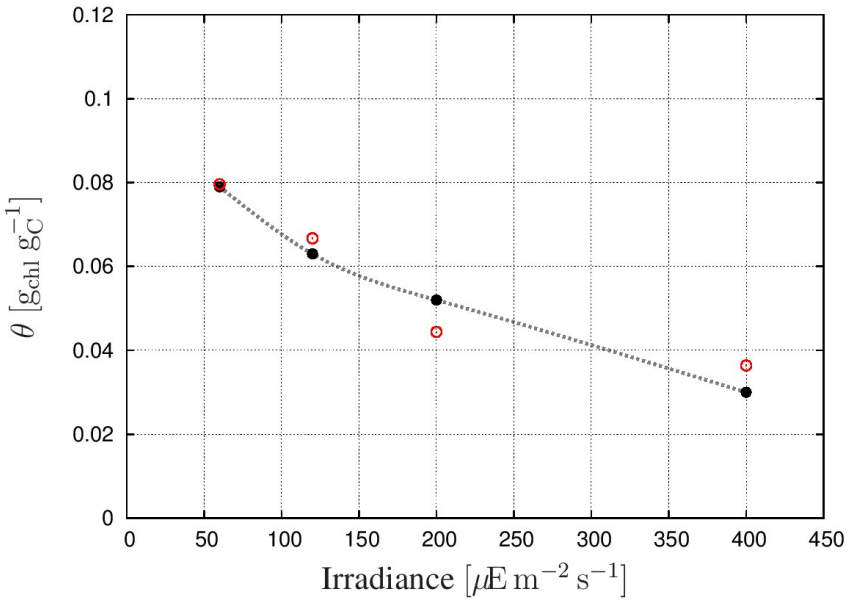

Figure 5: Relation between chlorophyll quota and growth irradiance for *Dunaliella tertiolecta*. The red circles correspond to measurements by Falkowski and Owens (1980) at acclimation states LL_1, LL_2, LL_3 and LL_4, respectively. The black points are computed from the calibrated nitrogen-quota-to-chlorophyll-quota relationship (5),(6), interpolated by the gray dotted line.

Confidence Analysis of Nitrogen-Quota-to-Chlorophyll-Quota Relationship. Following a guaranteed parameter estimation approach, confidence in the foregoing parameter estimates is assessed by computing the set of all values for $\bar{\gamma}$ and k_I that are consistent with the available measurement ranges of the nitrogen quota q and of the chlorophyll quota θ at all four acclimation states. The resulting confidence region is shown on the left plot in Fig. 6, providing parameter confidence ranges as $\bar{\gamma} \in [0.2, 0.35]$ and $k_I \in [400, \infty)$. The bounds on $\bar{\gamma}$, although

wide, confirm the order of magnitude for this parameter. On the other hand, k_I can take on arbitrary large values, a result which is best understood from the upper-right plot in Fig. 6, where a horizontal line can indeed be seen to provide a good fit of the data point due to the large uncertainty in the nitrogen-quota measurements. This uncertainty is also reflected in the rather loose model-prediction envelopes on the lower-right plot.

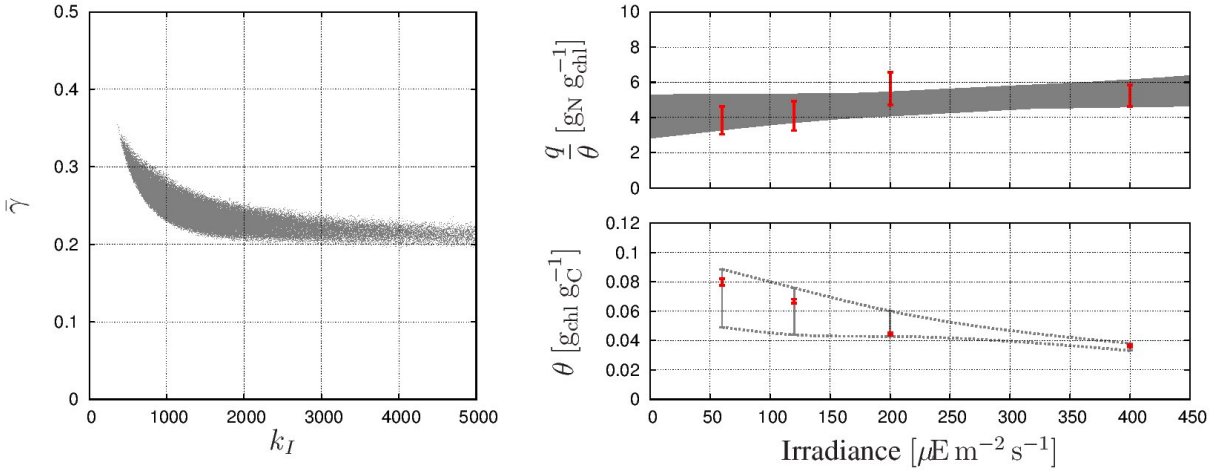

Figure 6: Confidence region of the parameter estimates $\bar{\gamma}$ and k_I for the measurement data ranges of nitrogen and chlorophyll quotas given in Table 2 (left plot) and corresponding fit envelopes (right plots).

5. Discussion

The fits obtained by estimating the parameters β, κ and $\bar{\alpha}$ (or α) in the chlorophyll-specific photosynthesis rate (19) are found to be in good agreement with the two data sets by Anning et al. (2000) (Fig. 1) and Falkowski and Owens (1980) (Fig. 3). Moreover, the resulting parameter estimates are found to be rather reliable in view of the confidence regions (Figs. 2 and 4), despite the presence of a significant correlation between the acclimation parameters β and κ.

- For *Skeletonema costatum* (Anning et al., 2000), the estimated value of $\kappa = 0.47$ and corresponding confidence range of $[0.45, 0.54]$ suggest that the functional cross section σ—and hence the size of the PSUs—is an increasing function of θ per (16), although the rate of increase σ' is slowing down with θ (concave shape). Considering (17) now, assuming a value of $\gamma = 2/3$ leads to variations of the exponent $(1 - \kappa/\gamma)$ in a positive range, thereby suggesting that the density of PSUs N follows a similar trend as σ with increasing θ. This behavior can thus be interpreted as a mixed n-s acclimation strategy of *S. costatum*.

- For *Dunaliella tertiolecta* (Falkowski and Owens, 1980), the estimated value of $\kappa = 1.54$ and corresponding confidence range of $[1.35, 1.6]$ suggest that σ is increasing with θ, but the rate of increase σ' is itself increasing (convex). This seemingly counter-intuitive behavior is made possible by a reduction in PSU density with increasing θ, since a typical value of $\gamma \approx 2/3$ now leads to variations of $(1 - \kappa/\gamma)$ in a negative range. This analysis therefore suggests that *D. tertiolecta* would preferentially follow the s-strategy of photoacclimation.

In sum, the calibration results for either microalgae species illustrate well the potential of the proposed model to distinguish between competing adaptation strategies for their light harvesting capacity at various irradiance levels. Additional experiments where proxies of σ and N are measured should be carried out in the future to support these preliminary interpretations.

Likewise, the fits obtained by estimating the parameters $\bar{\gamma}$ and k_I in the nitrogen-quota-to-chlorophyll-quota relationship (5),(6) show a good agreement with the data sets by Falkowski and Owens (1980) (Fig. 5). It is worth mentioning here that the estimated values of k_I and $\bar{\gamma}$ (Table 3) are consistent with those reported in previous work (e.g., Bernard, 2011). Nonetheless, a more careful confidence analysis (Fig. 6) reveals that the nitrogen-quota measurements carry too much uncertainty to determine reliable estimates, especially for the parameter k_I whose confidence range happens to be unbounded. These calibration results, although promising, clearly delineate the need for more accurate and richer data sets in order to fully validate the proposed model.

5.1. Can the Dynamic Model Predict the Data of Neidhardt et al. (1998)?

Experimental data by Neidhardt et al. (1998) are for the microalgae *Dunaliella salina*. They comprise two acclimation states at different growth irradiances of 50 μE m^{-2} s^{-1}) (LL) and $2000-2500$ $\mu\mathrm{E}\,\mathrm{m}^{-2}\,\mathrm{s}^{-1}$ (HL). Estimation of primary production is via the O_2 production rate by exposing the pre-acclimated microalgae to a sequence of increasing light irradiances between 4.7 and 4900 μE m^{-2} s^{-1}, during 150 s at each irradiance level. Moreover, neither the nitrogen quotas nor the chlorophyll quotas are reported.

As seen from Fig. 7, the initial slopes of the PI-response curves for cultures pre-acclimated at LL and HL differ greatly, which is in apparent contradiction with the constant initial slope assumption discussed in Sect. 3.2. Also reported on this figure (solid lines) are the results of a preliminary calibration showing that such a variation in initial slope can nonetheless be predicted accurately by the proposed model. More specifically, we simulated the experimental

protocol in Neidhardt et al. (1998), to more accurately account for the actual repair dynamics. In this context, it is not assumed that a quasi steady state is reached. The calibration procedure was carried out on this basis. It is important to do so here, because each stage of the PI-response protocol (150 s) may be too short for the dynamics of PSU inhibition to fully equilibrate, especially for a larger chlorophyll quota (LL pre-acclimated state). Indeed, the initial slope is reduced when A is still smaller than one despite the very low light (since a fraction of C is still not fully repaired). The initial slope expression is given by (10), with $A = 1 - C$. The lower slope is thus an index of the fraction of damaged PSU. The simulations on fig. 7 show that, respecting the exact experimental protocol, this behaviour can be reproduced by the model.

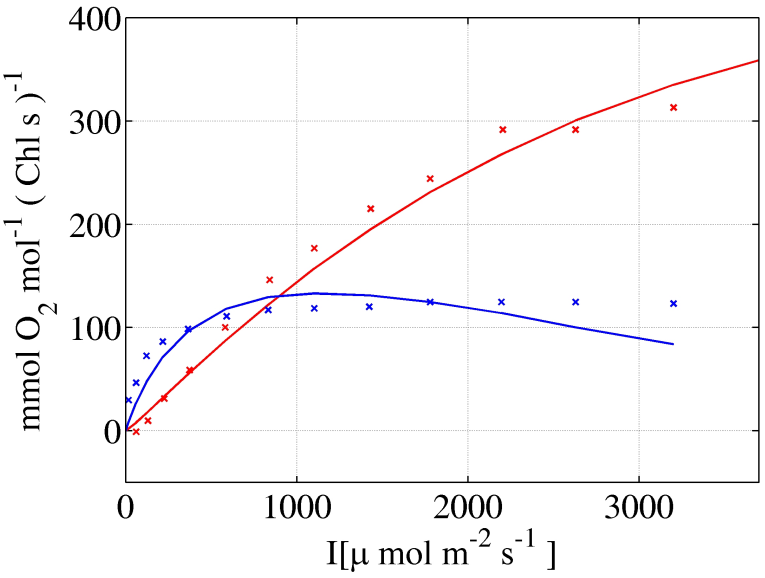

Figure 7: Dependency between growth rate and acclimation for *Dunaliella salina* (Neidhardt et al., 1998). (blue crosses) experimental data for LL acclimation (blue curve) model simulations for LL acclimation (red crosses) experimental data for HL acclimation (red curve) model simulation for HL acclimation.

6. Conclusions and Future Directions

The dynamic model presented in this paper couples photosynthetic processes that act on different time scales. Photosynthetic production and inhibition act on fast time scales of seconds or minutes, while the dynamics of intracellular nitrogen and chlorophyll contents are bound to slow time scales of hours or days. Our model builds upon the well-accepted Droop model describing nitrogen utilization and microalgae growth, together with the Han model describing photoproduction and photoinhibition in terms of PSU states. The main novelty lies in the use of the chlorophyll quota to relate both the acclimation and growth processes with the states of

the PSUs. Combined with previous (validated) models describing the dynamics of the PSUs (Han model), nitrogen content (Droop model), and chlorophyll content (Geider et al. (1997); Bernard (2011)), our model is the first of its kind to link photoinhibition, photoacclimation and nutrient-limited growth all together.

Preliminary calibrations and confidence analyses based on PI response data from the literature give encouraging results. By making the link among different PI curves, while preserving a simple structure, the proposed model can serve as a tool for hypothesis testing. Particularly insightful in this context is the ability to distinguish between the s-strategy and the n-strategy of PSU adaptation, which sheds light on the mechanisms that underly photoacclimation in various microalgae species. In order to further discriminate between the n-strategy and s-strategy of photoacclimation, more experimental data would be needed nonetheless, especially data covering a wider range of acclimation states and other species. Measuring a larger set of physiological variables, such as the functional cross section (Huot and Babin, 2010), would also be helpful. Another valuable insight from the proposed model has been that the experimental protocols used for producing PI response curves may not allow enough time at each irradiance level for the photoinhibition dynamics to fully develop. In practice, this may lead to overestimating the actual rate of photosynthesis and could explain the variations in initial slopes that are observed between PI response curves at different acclimation states in some experimental studies. Finally, a mathematical analysis of the proposed model could provide valuable insight into the inherent trade-offs and eventually help to identify strategies for enhancing microalgae productivity in large-scale industrial systems.

Acknowledgments

This work was supported by the ANR-13-BIME-0004 Purple Sun together with the INRIA Project Lab Algae in silico. AN and BC gratefully acknowledge financial support from Marie Curie under grant PCIG09-GA-2011-293953.

References

Anning, T., MacIntyre, H. L., Pratt, S. M., Sammes, P. J., Gibb, S. and, R. J., 2000. Photoacclimation in the marine diatom *Skeletonema costatum*. Limnology & Oceanography 45, 1807–1817.

Bernard, O., 2011. Hurdles and challenges for modelling and control of microalgae for CO_2 mitigation and biofuel production. Journal of Process Control 21 (10), 1378–1389.

Bernard, O., Gouzé, J. L., 1995. Transient behavior of biological loop models, with application to the Droop model. Mathematical Biosciences 127 (1), 19–43.

Bernard, O., Gouzé, J. L., 1999. Nonlinear qualitative signal processing for biological systems: application to the algal growth in bioreactors. Mathematical Biosciences 157, 357–372.

Brennan, L., Owende, P., 2010. Biofuels from microalgaea review of technologies for production, processing, and extractions of biofuels and co-products. Renewable and Sustainable Energy Reviews 14 (2), 557 – 577.

Droop, M. R., 1968. Vitamin B_{12} and marine ecology. The kinetics of uptake, growth and inhibition in *Monochrysis lutheri*. Journal of the Marine Biological Association of the United Kingdom 48 (3), 689–733.

Droop, M. R., 1983. 25 years of algal growth kinetics – A personal view. Botanica Marina 16, 99–112.

Eilers, P., Peeters, J., 1993a. Dynamic behaviour of a model for photosynthesis and photoinhibition. Ecological Modelling 69 (1-2), 113–133.

Eilers, P. H. C., Peeters, J. C. H., 1993b. Dynamic behavior of a model for photosynthesis and photoinhibition. Ecological Modelling 69 (1-2), 113–133.

Falkowski, P. G., Owens, T. G., 1980. Light–shade adaptation: Two strategies in marine phytoplankton. Plant Physiology 66, 592–595.

Falkowski, P. G., Raven, J. A., 2007. Aquatic Photosynthesis, 2nd Edition. Princeton University Press.

Faugeras, B., Bernard, O., Sciandra, A., Levy, M., 2004. A mechanistic modelling and data assimilation approach to estimate the carbon/chlorophyll and carbon/nitrogen ratios in a coupled hydrodynamical-biological model. Nonlinear Processes in Geophysics 11, 515–533.

Geider, R. J., MacIntyre, H. L., Kana, T. M., 1997. Dynamic model of phytoplankton growth and acclimation: responses of the balanced growth rate and the chlorophyll a:carbon ratio to light, nutrient-limitation and temperature. Marine Ecology Progress Series 148, 187–200.

Geider, R. J., MacIntyre, H. L., Kana, T. M., 1998. A dynamic regulatory model of phytoplanktonic acclimation to light, nutrients, and temperature. Limonology And Oceanography 43 (4), 679–694.

Han, B. P., 2001. Photosynthesis-irradiance response at physiological level: A mechanistic model. Journal of Theoretical Biology 213, 121–127.

Han, B. P., Virtanen, M., Koponen, J., Straskraba, M., 2000. Effect of photoinhibition on algal photosynthesis: a dynamic model. Journal of Plankton Research 22 (5), 865–885.

Hartmann, P., Béchet, Q., Bernard, O., 2014. The effect of photosynthesis time scales on microalgae productivity. Bioprocess and biosystems engineering 37 (1), 17–25.

Huot, Y., Babin, M., 2010. Chlorophyll a Fluorescence in Aquatic Sciences: Methods and Applications. Springer, Dordrecht, The Netherlands.

Jaulin, L., Walter, E., 1993. Set-inversion via interval analysis for nonlinear bounded-error estimation. Automatica 29 (4), 1053–1064.

Lange, K., Oyarzun, F. J., 1992. The attractiveness of the Droop equations. Mathematical Biosciences 111, 261–278.

MacIntyre, H. L., Kana, T. M., , T., Geider, R. J., 2002. Photoacclimation of photosynthesis irradiance response curves and photosynthetic pigments in microlagae and cyanobacteria. Journal of Phycology 38 (1), 17–38.

Neidhardt, J., Benemann, J., Zhang, L., Melis, A., 1998. Photosystem-ii repair and chloroplast recovery from irradiance stress: relationship between chronic photoinhibition, light-harvesting chlorophyll antenna size and photosynthetic productivity in dunaliella salina (green algae). Photosynthesis Research 56 (2), 175–184.

Richardson, K., Beardall, J., Raven, J., 1983. Adaptation to unicellular algae to irradiance: An analysis of strategies. New Phytologist 93, 175–191.

Sciandra, A., Ramani, P., 1994. The limitations of continuous cultures with low rates of medium renewal per cell. Journal of Experimental Marine Biology & Ecology 178, 1–15.

Sialve, B., Bernet, N., Bernard, O., 2009. Anaerobic digestion of microalgae as a necessary step to make microalgal biodiesel sustainable. Biotechnology Advances 27, 409–416.

Talec, A., Philistin, M., Ferey, F., Walenta, G., Irisson, J. O., Bernard, O., Sciandra, A., 2013. Effect of gaseous cement industry effluents on four species of microalgae. Bioresource Technology 143, 353–359.

Tawarmalani, M., Sahinidis, N. V., 2005. A polyhedral branch-and-cut approach to global optimization. Mathematical Programming 103 (2), 225–249.

Vatcheva, I., deJong, H., Bernard, O., Mars, N. J. L., 2006. Experiment selection for the discrimination of semi-quantitative models of dynamical systems. Artificial Intelligence 170, 472–506.

Wijffels, R. H., Barbosa, M. J., 2010. An outlook on microalgal biofuels. Science 329 (5993), 796–799.

Williams, P. J. l. B., Laurens, L. M. L., 2010. Microalgae as biodiesel and biomass feedstocks: Review and analysis of the biochemistry, energetics and economics. Energy & Environmental Science 3, 554–590.

The following section proposes a deeper insight into the validation of the model with the data of [55]. Here we show more detailed than in the preceding section [37] that these data is not in contradiction with the hypothesis that the initial slope of the chlorophyll specific PI curve is constant, as it could appear at first glance.

Neidhardts' data shows a significant difference in the initial slope of PI curves for pre-acclimated cultures at high light (HL: 2000-2500 $\mu mol\, m^{-2}\, s^{-1}$) and at low light (LL: 50 $\mu mol\, m^{-2}\, s^{-1}$). In these experiments, primary production was estimated by oxygen evolution using a protocol of 2.5 minutes of illumination for a series in the interval from 4.7 to 4900 $\mu mol\, m^{-2}\, s^{-1}$. Since values for θ are not reported by [55], we used the coupled model to simulate the experimental protocol.

The fit obtained after a calibration of the PI Curves is presented in Fig. 12. Fig. 13 presents the fit and the data for the product of the number of photosystems and the effective cross section and fig. 14 shows the time evolution of the cellular chlorophyll content. The corresponding parameter values are reported in tab. 3.

The fit was obtained by step-wise adjustment of three groups of parameters while minimizing square-distance cost functions. In a first step, the parameters of the Han model –including two values for σ respectively for HL and LL acclimation– were deduced in order to fit the two PI curves. The PI curves are a result of a numeric integration of the eq. 8 based on Neidhardt's PI measurement protocol. No steady state assumption has been taken at this point (which is necessary, if the exact protocol for the PI curve measurement is unknown). Secondly, the parameters for the chlorophyll evolution

Table 3: Parameters for the fit of the data of [55]

Parameter	Value	
$\bar{\mu}$	0.52	s^{-1}
$\bar{\rho}$	0.073	$g_N\, g_C^{-1}\, s^{-1}$
Q_l	0.25	$g_N\, g_C^{-1}$
Q_0	0.05	$g_N\, g_C^{-1}$
τ	6.04×10^{-3}	s
k_d	1.37×10^{-6}	–
kr	$7.61 \cdot 10^{-5}$	–
β	0.00919	$(g_N/g_C)^{1/\kappa}$
κ	1.82	–
k_I	1915	$E\, m^{-2}\, s^{-1}$
$\bar{\gamma}$	5093.1	$10^{-16} mol/(g_N \cdot cell \cdot h)$
$\tilde{\beta}$	172.745	$1/cell$
γ	0.791807	–

have been deduced by fitting the data in fig. 14. In a third step, the parameters κ and γ have been deduced based on the evolution of $N \cdot \sigma$ and the two values for σ from the PI curve fits, using eq. 16 and 17. Finally, the parameters for the Droop model have been estimated based on the values given in [7] and the maximum growth rates found for the two acclimation states.

For the PI curves, the calibrated model reproduces the general trend of the data well, despite the apparent contradiction that the initial PI curve slope is not independent from the acclimation state. This results from the fact that the fit is not based on the steady state assumption (for which the θ-independent initial slope is characteristic) but integrates the PI measurement protocol given by Neidhardt. For the calculation only the fast variables A and B were considered to reach their equilibrium as a function of the dynamic variable C. If we assume:

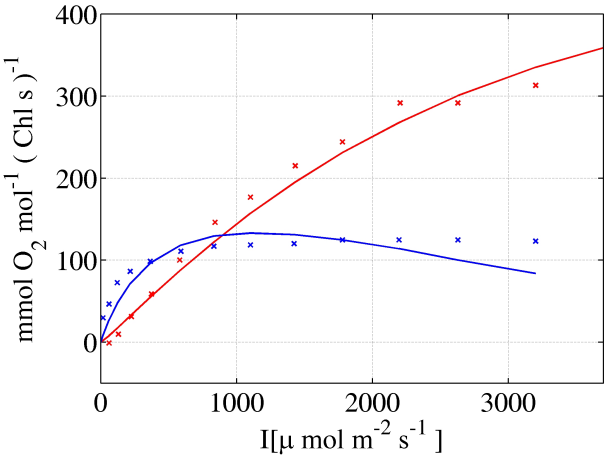

Figure 12: Dependency between growth rate and acclimation for *Dunaliela salina* [55]. The blue curve and the crosses are for LL acclimation and the red curve and crosses are for HL acclimation.

$$C(0)_{LL} = C_{inf}(50\mu mol/(m^2 s)) \tag{5.1}$$

$$C(0)_{HL} = C_{inf}(2000\mu mol/(m^2 s)) \tag{5.2}$$

$$\Rightarrow C(0)_{LL} < C(0)_{HL} \tag{5.3}$$

due to the preacclimation period, and

$$\dot{A} = \dot{B} = 0 \tag{5.4}$$

$$\Leftrightarrow A = \frac{B}{I\sigma\tau} = \frac{1 - A - C}{I\sigma\tau} \tag{5.5}$$

$$\Leftrightarrow A = \frac{1 - C}{I\sigma\tau + 1} \tag{5.6}$$

Due to the fast kinetics of A/B transitions compared to C evolution.

For μ_{chl} we consequently get:

$$\mu_{chl} = \bar{\alpha}\left(1 - \frac{Q_0}{q}\right)\frac{1 - C}{I\sigma\tau + 1} \tag{5.7}$$

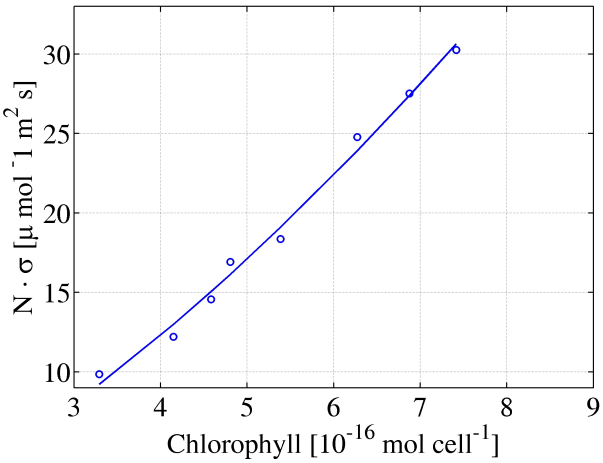

Figure 13: Dependency between the product of number of Photosystems and the effective cross section as a function of the cellular chlorophyll content. The blue curve is the fit of the model and the open circles is the measured data.

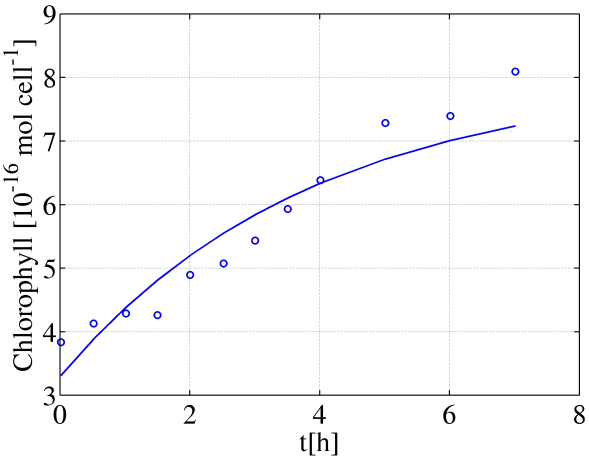

Figure 14: Time evolution of the Chlorophyll content of the data from Neidhard et al. The blue line is model prediction, the crosses are measured data.

with the initial slope

$$\left.\frac{\partial \mu_{chl}(C,q)}{\partial I}\right|_{I=0} = \bar{\alpha}\left(1-\frac{Q_0}{q}\right)\frac{1-C}{I\sigma\tau+1} \tag{5.8}$$

which yields with eq. 5.3

$$\left.\frac{\partial \mu_{chl}(C(0)_{LL},q)}{\partial I}\right|_{I=0} > \left.\frac{\partial \mu_{chl}(C(0)_{HL},q)}{\partial I}\right|_{I=0} \tag{5.9}$$

As shown, our model yields the different initial growth rate as a response due to the inhibited state of the algae after the pre-acclimation period, which reduces the efficiency of photsynthesis and. Due to the dynamics of the photoinhibition and repair a part of the inhibited photocenters get repaired throughout the measurement, which explains that no maximum for the photosynthetic productivity is obtained for the HL PI curve.

Neidhardt et al. interpret the differnet initial slope of the LL and HL PI curve as a result of acclimation to the high light signal implying smaller chlorophyll antennas (which in our model would be equivalent to a smaller cross section σ_{HL}). This interpretation is not supported by the analysis with our model.

We identified Neidhardt's spectroscopic measurement of thylakoid number (denominated as Q_A in his work) as $N \cdot \sigma$. The model describes very well the dependency of the $N \cdot \sigma$ as a function of chlorophyll content (see fig. 13). With the information about σ at LL and HL acclimation, this allows to well characterize the acclimation behaviour by the parameters γ and κ. The temporal evolution of chlorophyll (see fig. 14) is also well described. Overall, the values of the parameters utilized for this fit are reasonable. Since there is no explicit information for cellular nitrogen content available, the data is not sufficient for a certain estimate the parameters for the Droop

model. The value of $\kappa = 1.82$ is relatively high. In the context of our model this means that the algae highly prioritize increasing the size of the photocenter antennas while trading of their number for high chlorophyll content.

6

GROWTH RATE ESTIMATION OF ALGAE IN RACEWAY PONDS: A NOVEL APPROACH

I was born not knowing and have had only a little time
to change that here and there.
Richard P. Feynman

In the previous chapters the dynamic effects of photosynthesis have been studied theoretically and experimentally. The presented studies give insights on short term and long term effects on the photosynthetic apparatus. The dynamics of photoinhibition, photoacclimation and nutrient uptake in varying conditions have been studied and formulated in models.

The consecutive step for growth rate prediction on the scale of a full size industrial culture is the integration of realistic hydrodynamic models in a comprehensive approach. Pruvost et al. [62] presented an approach for growth rate estimation in toric photobioreactors using trajectories from a hydrodynamic model in order to deduce light signals for the biological model. For the solution of the hydrodynamics they used the commercial software FLUENT. The volume of their reactor is small and the fluid circulates at rapid velocities. Therefore, it is sufficient to solve the model for several seconds of real time evolution. The volume of a raceway system is several magnitudes larger than the small reactor, while the water flow is a lot slower. This leads to the fact that at least 20 hours of real time have to be simulated.

In order to handle this enormous computational task, the following chapter uses a hydrodynamic model relying on a multi-layer Saint-Venant approach. This approach is well adapted to the characteristics of the raceway system, such as the z-invariant geometry and the open water surface. Based on the generated trajectories, light signals are generated and the growth rate of the raceway is estimated. In this framework, the influence of the standard deviation of LD cycles on the growth rate is investigated.

Growth Rate Estimation of algae in Raceway Ponds: A novel Approach

Philipp Hartmann [*] **David Demory** [**] **Charlotte Combe** [**]
Raouf Hamouda [***] **Anne-Céline Boulanger** [***]
Marie-Odile Bristeau [***] **Jacques Sainte-Marie** [***]
Bruno Sialve [****] **Jean-Philippe Steyer** [****] **Sophie Rabouille** [**]
Antoine Sciandra [**] **Olivier Bernard** [*]

[*] *INRIA Sophia Antipolis, 2004, Route des Lucioles, B.P 93, 06902 Sophia Antipolis, France*
[**] *UPMC, BP 28, Chemin du Lazaret, 06234 Villefranche sur Mer, France*
[***] *INRIA Paris-Rocquencourt Domaine de Voluceau, B.P. 105, 78153 Le Chesnay Cedex, France*
[****] *INRA, UR050, Laboratoire de Biotechnologie de l'Environnement, Avenue des Etangs, F-11100 Narbonne, France*

Abstract: Microalgae mass cultiviation is a promising future source of biomass for energy and food production. In order to optimize productivity of large scale plants and to make them environmentally and economically sustainable, energy requirements have to be minimized. In particular, mixing of the growth medium is a major energy input, and its effect on overall productivity should be better understood. Several dynamic models have been developed to represent the effect of a rapidly varying light on the photosynthesis process especially for the effect of photoinhibition on growth. In order to assess the mixing effects in a complex hydrodynamic regime, we propose to reconstruct the light profile received by a single cell. A multi-layer Saint-Venant approach is used to simulate the hydrodynamics of the system. It allows for the computation of Lagrangian trajectories, and finally, when knowing the light distribution, the light pattern perceived by a cell. This pattern is then used with the dynamical model for photosynthesis. In a last step, the growth rate of the whole system is estimated as the average over a set of trajectories.

Keywords: modelling, biofuel, raceway, hydrodynamics, microalgae, optimization

1. INTRODUCTION

Microalgae are considered a new source of biomass and renewable energy since the 70s (Sheehan et al., 1998). Advantages of microalgae cultivation compared to terrestrial plants are a high photosynthetic yield, independence from fertile soil and a possibly reduced freshwater consumption (Williams and Laurens, 2010). These advantages can lead to a large algal biomass production which is not in direct competition with food production. Improving biofuel production and energy generation from microalgae receives increasing attention over the last years. Increased Lipid productivity can be obtained in special conditions of nutrient limitation and high light illumination. It has been reported that after a nitrogen limitation microalgae can reach a very high lipid content (more than 50% of dry weight) (Metting, 1996).

In a wider perspective, the consumption of CO_2 during photosynthesis can contribute to carbon mitigation (Talec et al., 2013) . There are also combined approaches for wastewater treatment technologies (Sialve et al., 2009) and for a production of high value products such as cosmetics and pharmaceuticals (Wijffels and Barbosa, 2010). All these possibilities have put microalgae in a favorable position for the integration in biorefinery concepts.

For large scale production of microalgal biofuel, many problems have to be addressed. Light conditions and nutrient supply affect the photosynthetic yield, and two key processes are involved. Among them, photoinhibition diminishes of photosynthetic yield due to an excess of irradiance which destroys some key proteins of the photosynthetic apparatus. This can be represented by models that take into account the dynamics of the photosynthetic reaction centers which are represented in resting (or open) state or active (closed) state. The dynamics of open/closed transition occurs at a fast time scale (within seconds), while photoinhibition occurs in the time scale of minutes. In order to achieve optimal biomass productivities, it is very important to understand the effects of dynamical light patterns on photosynthesis dynamics, and especially on the mechanisms which lead to photoinhibition.

In this work, we propose an integrated approach for the estimation of growth rate of an open-channel raceway microalgae culture. In a first step, numerical integration of an approximation of the Navier-Stokes equation by a multilayer Saint-Venant approach is carried out in order to

predict the trajectories of single algae cells in the medium (Bernard et al., 2013). In a second step, a dynamical model for photoinhibition (Han, 2001) is calibrated using experimental data. This model gets numerically integrated using light profiles corresponding to different trajectories and calculate the average among them. This average value is considered to be an estimation of the growth rate of the complete raceway pond.

2. METHODS & RESULTS

The presented approach for the estimation of the growth rate of raceway ponds consists of three steps:

(1) Computation of the trajectories and light profiles of individual algae cells within the raceway volume
(2) Growth rate estimation for each trajectory using a photosynthesis model
(3) Averaging of the growth rate among individual trajectories resulting in an estimation for the entire system

In the following paragraph we present the hydrodynamic model presented by Bernard et al. (2013), the Photosynthesis model of Han (2001) and how the average growth rate for the entire system is calculated. We finally present structural properties of the model of Han leading to a non-linear growth response to dynamic light signals.

2.1 Hydrodynamics and single cell trajectories computation

An approximation of the Navier-Stokes equations has been proposed by Audusse et al. (2011a), which is well adapted to the conditions in an open raceway pond. Compared to former multilayer models that are adapted for non miscible fluids, the so-called multilayer Saint-Venant system with mass exchanges is a good approximation of the Navier-Stokes equations. The accuracy and the stability properties of the multilayer approach have been demonstrated in Audusse et al. (2011a,b).

Moreover the multilayer model has been successfully confronted with analytical solutions of the hydrostatic Euler and Navier-Stokes systems with free surface (Boulanger and Sainte-Marie (2013)). The multilayer model consists in Galerkin type approximation along the vertical axis of the Navier-Stokes sytem, it results in a set of partial differential equations with hyperbolic features and written over a fixed mesh.

The system is numerically solved by considering a 2D triangular mesh of the ground surface, the layers defined by the water depth giving the third spatial dimension. The discretization technique used a finite volume scheme based on a kinetic interpretation of the equations. A specific forcing term mimicking the effect of the paddle wheel was added (Bernard et al., 2013). The impact of the wheel on the fluid is considered as a normalized force applied by the wheel's blade and equal to the square of the velocity at each point. Here, a 3D extension to the model presented in Bernard et al. (2013) was used. The used meshing represents a real raceway pond of the Environmental Biotechnology Laboratory of INRA Narbonne (see Figure 1).

Finally, Lagrangian trajectories of several particles are reconstructed by integrating the velocity field for various

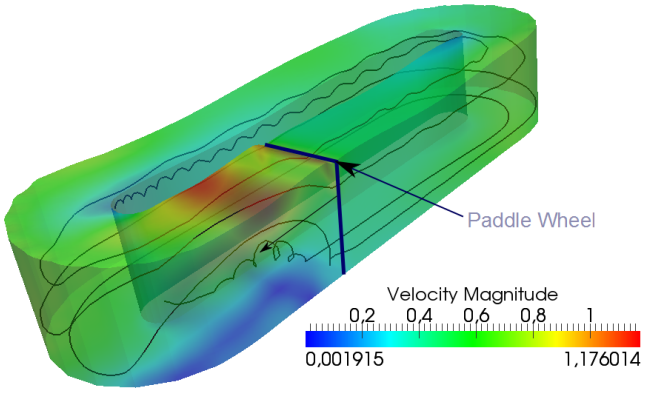

Fig. 1. 3D representation of the water volume and its velocity field in the numerical simulation. A particular trajectory is also represented.

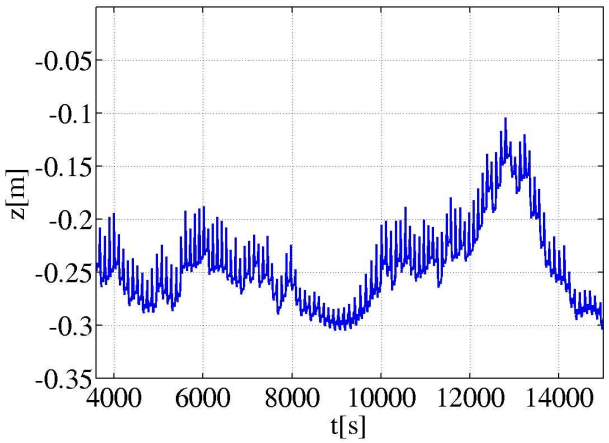

Fig. 2. Depth of a single particle as a function of time

initial conditions of the particles. In addition, a Brownian motion model is applied to better represent the local diffusion effect.

The raceway simulation has been run for 15 000 seconds. The simulation starts with static non agitated medium, and the paddle wheel is immediately set on. Consequently, the first 3600 seconds of simulation were disregarded, in order to reach a stabilisation period.

The time dependent depth coordinate for an exemplary trajectory is presented in fig. 2.

Light intensity profiles are calculated from the trajectories by applying the law of Beer-Lambert for light attenuation. The attenuation coefficient was chosen to be a fixed constant which leads to 5 % of the incident light intensity at the bottom of the raceway. Consequently, the light intensity as a function of the water depth z above the particle is:

$$I(z) = I_0 \cdot e^{-\gamma \cdot (z)} \tag{1}$$

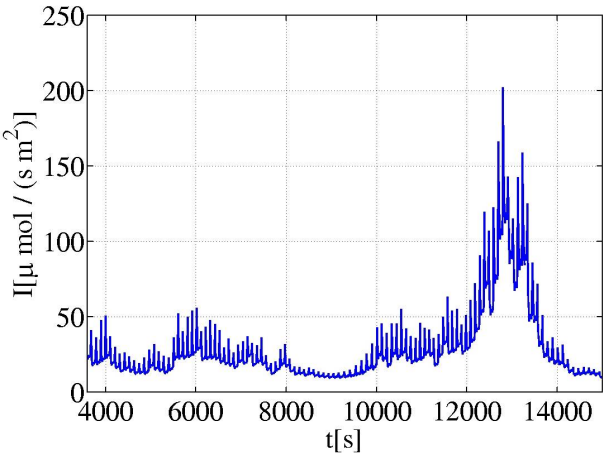

Fig. 3. Light signal received by a single cell as a function of time

Taking into account the depth of the culture of $0.3m$, we can deduce a value of $15.35m^{-1}$ for the parameter γ. A typical light pattern is presented on fig. 3.

2.2 The Han Model

Han (2001) presented a mechanistic model for photosynthesis which includes dynamical effects of photoinhibition. This model represents the dynamics of the photosystems depending of light flux. Photosystems are the first units involved in photosynthesis, they collect photons and transfer electrons to the rest of the system. They can have three possible states: open (A) and relaxed, closed while they are processing photons (B) or inhibited (C) when they received an excess of photons.

Dynamic processes are represented by the transition between the states and depend on the photon flux. Primary production is described by the transition between A and B. Excitation is assumed to occur at a rate of σI, with σ being the functional cross section of the photosynthetic unit (PSU). De-excitation is assumed to occur at a rate of $\frac{1}{\tau}$, with τ being the turnover time of the electron transport chain.

At higher irradiation photoinhibition, occurs: PSII's pass over from closed to inhibited state at a rate $k_d \sigma I$. At the same time a repair mechanism compensates this effect at a constant rate k_r.

The equations describing the rates of change in the fractions of open, closed and inhibited states are given by:

$$\begin{aligned} \dot{A} &= -I\,\sigma\,A + \frac{B}{\tau} \\ \dot{B} &= I\,\sigma\,A - \frac{B}{\tau} + k_r\,C - k_d\,\sigma\,I\,B \\ \dot{C} &= -k_r\,C + k_d\,\sigma\,I\,B. \end{aligned} \tag{2}$$

Expressions giving the fractions of open, closed and inhibited states at steady state as a function of the irradiance I can be derived explicitly from 2. The steady-state expression A^∞ for the open state A is given by:

$$A^\infty(I) = \frac{1}{1 + \tau\,\sigma\,I + k_d/k_r\,\tau\,\sigma^2\,I^2}, \tag{3}$$

Parameter	Value	Unit
k_r	$2 \cdot 10^{-4}$	s^{-1}
k_d	$1.82 \cdot 10^{-16}$	.
τ	0.667	s
σ	0.0143	$m^2/(\mu mol)$
R	4.9250	mol 10^{-6} cells $\min^{-1}$

Table 1. Estimated model parameters based on experimental data by (Park et al., 2013) and data by Combe et al. (2013)

Finally, growth rate is described by a function proportional to IA. At steady state, this corresponds to a Haldane type curve:

$$\mu^\infty(I) = \bar{\mu}\frac{I}{1 + \tau\,\sigma\,I + k_d/k_r\,\tau\,\sigma^2\,I^2}, \tag{4}$$

2.3 Parameters identification

In order to identify the parameters of the Han model for the species *Dunaliella salina* completely it was necessary to use data from different studies. The light response curve was taken from Park et al. (2013) describing the photosynthetic response of microalgae (measured by oxygen evolution) to different light intensities. With this data, we fitted a well-parametrized form of eq. 4 by Bernard and Rémond (2012) In a second step, experiments consisting of measuring the growth rate for different crenellated light/dark alternation frequencies have been done. For such caricatural light signals varying at high frequencies, approximation of the response of the Han model can be obtained (Hartmann et al., 2013). Such approximations responses were used to fit the model to data measured by Combe et al. (2013). It leads to a value for τ and the respiration rate R.

The increase of the Quantum yield after light to dark tranistion as published by Neidhardt et al. (1998) imposes a time scale for the repair process of the photocenters. From this we deduced the value for k_r. However, according to the data of Park et al. (2013), inhibition plays a minor role within natural values for the light intensity. Thus the values for k_d and k_r have negligible impact on the model behaviour in real-life conditions.

After a least square fit on the data presented in paragraph 2.3, the parameters turned out as in tab. 1. The fit of the experimental data is presented in figures 4 and 5.

2.4 Simple factors in light signal affecting productivity

In a preliminary study, the effect of the paddle wheel on the light received by a cell was studied by a caricatural light/dark signal with equal periods of light (at intensity I_0) and darkness. In the work of Hartmann et al. (2013), the effect of the light/dark frequency ω is studied. It is shown that the average growth rate $\mu(I_0, \omega)$ is an increasing function of ω, and that the growth rate is bound within:

$$\frac{1}{2}\mu^\infty(I_0) \leq \mu(I_0, \omega) \leq \mu(\frac{I_0}{2}, +\infty) = \mu^\infty(\frac{I_0}{2}) \tag{5}$$

This means that for very low frequencies, the system can be approximated by a system where half of the time growth rate is obtained for a continuous light at I_0, while there is

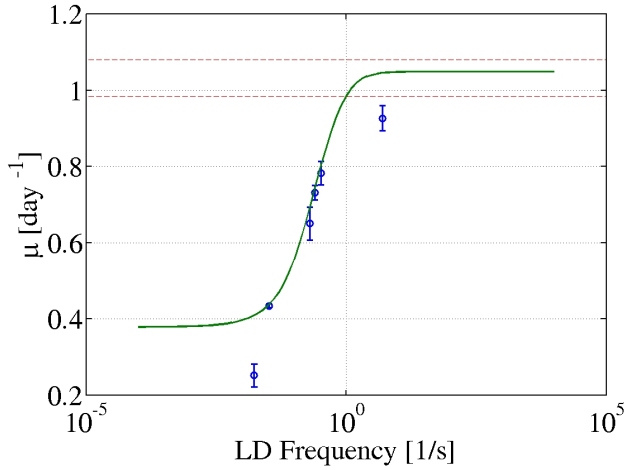

Fig. 4. Dependency between Frequency and Growth rate. Frequency on a logarithmic scale, Circles show measured values of data by Combe et al. (2013), lines show model predictions according to Hartmann et al. (2013)

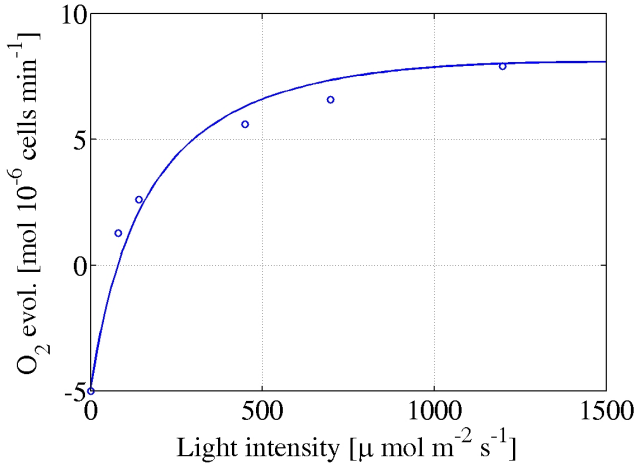

Fig. 5. Steady state Light response curve for the utilized parameters

no growht the rest of the time. For a very fast frequency, much faster that the time scales of the Han model, the light signal is averaged into a light $\frac{I_0}{2}$.

The next step is to test this effect with a more realistic light pattern, derived from a trajectory computed with our hydrodynamical approach.

Firstly, the effect of the signal variance on the growth rate at steady state is analysed. Given different signals with alternation of constant light periods of same length, between $I-\delta I$ and $I+\delta I$; The previously considered case is a specific case for $\delta I = I$.

Hypothesis 1. (H1) Assuming that $I+\delta I$ is in the convex part of the Han equation (4). In other words:

$$\frac{d^2\mu^\infty}{dI^2}(I+\delta I) < 0 \tag{6}$$

Property 1. In order to optimize productivity of large scale plants and to make them environmentally and econolically

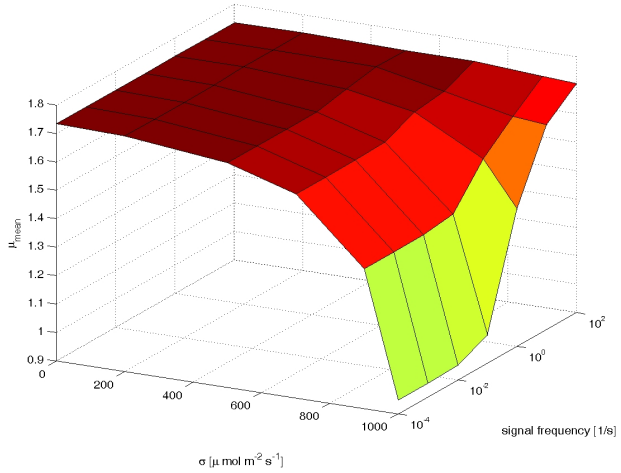

Fig. 6. Average growth rate based on the Han model using rectangular light signals with different variance and frequency

sustainalbe, energy requirements have to be minimized Under Hypothesis H1, we have

$$\frac{\mu^\infty(I+\delta I)+\mu^\infty(I-\delta I))}{2} \leq \mu^\infty(I)$$

Proof: This Property is easily proven when considering the decreasing function (Hypothesis (H1)) $\frac{d\mu^\infty}{dI}\mu^\infty(I)$. We have

$$\frac{d\mu^\infty}{dI}(I) \leq \frac{d\mu^\infty}{dI}(I-\delta I)$$

Integrating this expression between I and $I+\delta I$, we get

$$\mu^\infty(I+\delta I)-\mu^\infty(I) \leq \mu^\infty(I)-\mu^\infty(I-\delta I)$$

This provides the result.

As a consequence, any light signal varying at very low frequency between $I-\delta I$ and $I+\delta I$ would lead to an average growth rate lower than the growth rate for the average light I.

The same reasoning holds for δI: increasing δI (provided that μ^∞ stays in a region where it is convex) leads to a reduced growth rate. This reasoning highlights the two effects affecting growth:

- Signal frequency which tends to increase growth rate
- Variance of the Light signal which, at low frequency, tends to decrease the growth rate

Fig. 6 shows results for numerical integrations of the Han model based on a rectangular signals with different signal variance and frequency. Coherently with the analytical prediction, it can be observed that the growth rate increases with frequency and decreases with increasing variance.

In the next paragraph, a reference trajectory is used so that the second effect is eliminated and and the result depends only on the frequency of light dark succession.

2.5 Effect of the paddle wheel velocity

In a simple approach, in order to understand the effect of the paddle wheel on productivity, it is assumed that

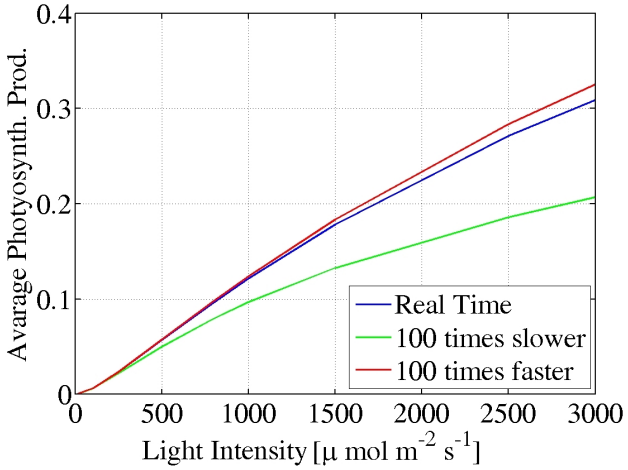

Fig. 7. Steady state Light response curve for the utilized parameters, exemplary trajectory

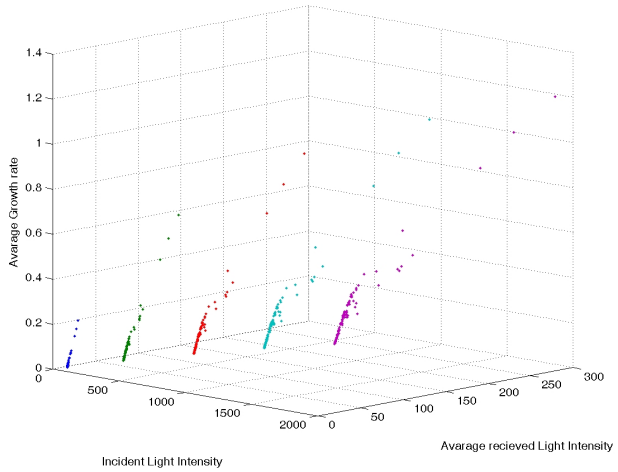

Fig. 8. Average received light intensity and growth rate as a function of surface light intensity. Each color of points refers to one surface light intensity.

increasing mixing intensity is equivalent to contraction and dilatation of the time axis of the cell trajectory. This corresponds to a linearisation of the paddle wheel effect. Considering one reference trajectory, means that different mixing intensities are represented by dilation factors of the time axis. Increased paddle wheel mixing thus corresponds to a time-contracted reference trajectory.

Based on the light signals the mean photosynthetic productivity is calculated from the Han model over the full trajectory. The travel time has been contracted and dilated down by a factor of 100. Moreover, together with the travel time, we simultaneously considered the effect of incident light irradiation I_0 on productivity. The results are presented in fig. 7.

As it can be observed, a reduced travelling time yields only about 70 % of the productivity at the original traveling time for 1000 $\mu mol/s^{-1}m^{-2}$) surface light intensity. There is only an insignificant difference between the result for the light profile passing a 100 times faster and the original speed.

2.6 Growth rate prediction for the mixed Culture

In order to estimate the growth rate of the entire culture, we calculated the average growth rate of all 460 trajectories for different light intensities at the surface. For the total average growth rate μ_{av} we get consequently:

$$\mu_{av} = \frac{\sum_{i=1}^{n} \bar{\mu}(z_i)}{n} \tag{7}$$

With z_i being the time dependent depth coordinate for the ith trajectory.

The resulting average photosynthetic productivity as a function of incident light intensity of the culture is presented in Fig. 9. The individual growth rate of all single trajectories are presented in Fig. 8. The growth rate and the average received light intensity of each trajectory is represented by one point in the 3D Coordinate system.

The average growth rate (fig. 8) of the culture increases linearly with the surface light intensity. However, due to a

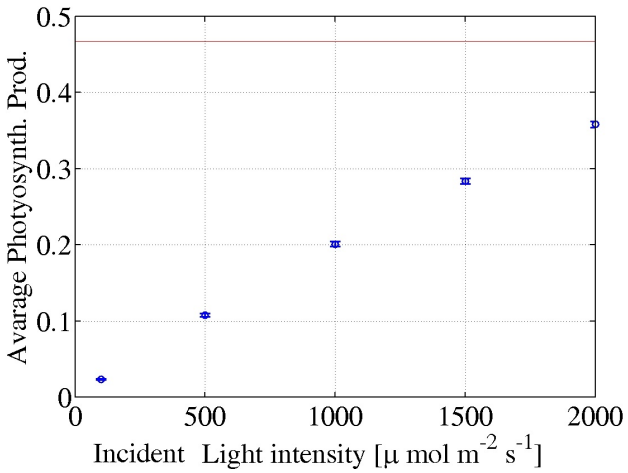

Fig. 9. Average Value of gross Growth rate between the 460 trajectories for different incident illuminations (blue dots). The red line indicates the respiration rate.

special characteristics in the hydrodynamic simulation the average received light intensity has significant variability among the trajectories (compare fig. 8) for the same surface intensity.

3. DISCUSSION

With the presented approach, we can estimate the growth rate of the raceway pond based on the growth response of individual algae cells. Contrary to similar approaches, we did not rely on rectangular light signals, but on light profiles which have been calculated from the hydrodynamics of the system.

For the calibration of the Han Model for *Dunaliella salina*, data from three different studies have been used. The increasing productivity as a function of cycle frequency in the data of Combe et al. (2013) has been identified as an effect of the open/closed dynamics, which is directly linked to the value of the parameter τ. Since this increase can

be observed at frequencies of about 1 Hz, the parameter τ has been estimated as 0.67 s. This value, unusually high, is slower than what is considered a typically in the literature (cf. Falkowski and Raven (2007)). Nevertheless, the study follows an experimental protocol presented by Falkowski and Raven (2007), which allows for direct determination of this physiological parameter. This result might therefore be taken as a hint for an unusual behaviour of *Dunaliella salina* in flashing light conditions.

Structural properties of the Han model show that the growth response depends not only on the average light intensity, but also on the frequency and the shape of the received light profile. This leads to the conclusion that considering only the frequency of the light signal is not enough to estimate the photosynthetic efficiency. Contrarily to several works studying the growth response as a function of flash frequency, predictions of actual productivity should also be based on the variance of the signal. With the proposed approach we suggest a new paradigm to treat this problem by reconstructing realistic trajectories.

In order to predict the growth rate within the aggregate system, the average growth rate has been deduced from 460 trajectories. A linear relation between surface light intensity and aggregated growth rate is found. This could be interpreted similarly to the average growth rate computed in Bernard (2011), when averaging the Han static response over the depth of the culturing system. Analytical computation in this simplified case shows that this is similar to shifting the optimal light intensity towards higher light, and reducing the maximum growth rate. Shifting the maximum of the curve on fig. 5 is similar to zooming the response curve for low light intensity, ending up with a response that becomes approximatively linear.

When regarding the individual values for average growth rate and depth for different trajectories, there is a significant spread for the average depth of the particles. This indicates, that the simulation time is not sufficient in order to show the ergodicity of the system.

At the current state of this study, we suspect that a numerical artefact in the integration of the hydrodynamics leads to an overestimated spatial probability for the particles at the bottom of the raceway. This imposes consequently an offset for the average received light intensity of the particles and leads to growth rates which are underestimated. In the context of the high respiration – which was found for our calibration – the growth rates are even below respiration. It should be pointed out that – to our best knowledge – at present no studies exist which evaluate the spatial distribution of particles in a hydrodynamic raceway simulation for sufficiently long simulation time.

4. CONCLUSION

This work investigates how hydrodynamics impacts biology in microalgae culture ponds. The actual effect on photosynthetic efficiency is assessed by coupling the Lagrangian trajectories computed from a multi-layer Saint-Venant hydrodynamical model, to a dynamical model representing the fast time scales of photosynthesis. Such study highlights the idea that experiments conducted to assess the effect of light/dark frequency on photosynthesis are not sufficient to characterize the mixing effect in a raceway. More work is required to better study the impact of the paddle wheel, by ensuring that basics statistical properties of Lagrangian trajectories (average depth, equirepartition of the particules) are not affected by the wheel velocity. This approach is also the foundation for the development of a computer driven approach able to optimize the design of raceways and increase the ratio between the recovered biofuel from the microalgae and energy consumption for mixing.

REFERENCES

Audusse, E., Bristeau, M.O., Pelanti, M., and Sainte-Marie, J. (2011a). Approximation of the hydrostatic navier–stokes system for density stratified flows by a multilayer model: Kinetic interpretation and numerical solution. *Journal of Computational Physics*, 230(9), 3453–3478.

Audusse, E., Bristeau, M.O., Perthame, B., and Sainte-Marie, J. (2011b). A multilayer saint-venant system with mass exchanges for shallow water flows. derivation and numerical validation. *ESAIM: Mathematical Modelling and Numerical Analysis*, 45(01), 169–200.

Bernard, O. (2011). Hurdles and challenges for modelling and control of microalgae for CO_2 mitigation and biofuel production. *Journal of Process Control*, 21(10), 1378–1389.

Bernard, O., Boulanger, A.C., Bristeau, M.O., and Sainte-Marie, J. (2013). A 2d model for hydrodynamics and biology coupling applied to algae growth simulations. *ESAIM: Mathematical Modelling and Numerical Analysis*, 47, 1387–1412. doi:10.1051/m2an/2013072.

Bernard, O. and Rémond, B. (2012). Validation of a simple model accounting for light and temperature effect on microalgal growth. *Bioresource Technology*.

Boulanger, A.C. and Sainte-Marie, J. (2013). Analytical solutions for the free surface hydrostatic Euler equations. *Commun. Math. Sci.*, 11(4), 993–1010.

Combe, C., Bernard, O., and Rabouille, S. (2013). *Etude exp érimentale de la réponse adaptative de Dunaliella salina a des signaux lumineux haute fréquence*. Master's thesis.

Falkowski, P.G. and Raven, J.A. (2007). *Aquatic Photosynthesis*. Princeton University Press, 2nd edition.

Han, B.P. (2001). Photosynthesis-irradiance response at physiological level: A mechanistic model. *Journal of Theoretical Biology*, 213, 121–127.

Hartmann, P., Béchet, Q., Bernard, O., et al. (2013). The effect of time scales in photosynthesis on microalgae productivity. *Bioprocess and Biosystems Engineering*.

Metting, F.B. (1996). Biodiversity and application of microalgae. *Journal of Industrial Microbiology & Biotechnology*, 17, 477–489.

Neidhardt, J., Benemann, J., Zhang, L., and Melis, A. (1998). Photosystem-ii repair and chloroplast recovery from irradiance stress: relationship between chronic photoinhibition, light-harvesting chlorophyll antenna size and photosynthetic productivity in *dunaliella salina* (green algae). *Photosynthesis Research*, 56(2), 175–184. doi:10.1023/A:1006024827225.

Park, S., Lee, Y., and Jin, E. (2013). Comparison of the responses of two Dunaliella strains, *Dunaliella salina*

CCAP 19/18 and *Dunaliella bardawil* to light intensity with special emphasis on carotenogenesis. *Algae*, 28(2), 203–211. doi:10.4490/algae.2013.28.2.203.

Sheehan, J., Dunahay, T., Benemann, J., and Roessler, P. (1998). A Look Back at the U.S. Department of Energy's Aquatic Species Program – Biodiesel from Algae. Technical report, U.S. Department of Energy.

Sialve, B., Bernet, N., and Bernard, O. (2009). Anaerobic digestion of microalgae as a necessary step to make microalgal biodiesel sustainable. *Biotechnology Advances*, 27, 409–416.

Talec, A., Philistin, M., Ferey, F., Walenta, G., Irisson, J.O., Bernard, O., and Sciandra, A. (2013). Effect of gaseous cement industry effluents on four species of microalgae. *Bioresource Technology*, 143, 353–359.

Wijffels, R.H. and Barbosa, M.J. (2010). An outlook on microalgal biofuels. *Science*, 329(5993), 796–799.

Williams, P.J.l.B. and Laurens, L.M.L. (2010). Microalgae as biodiesel and biomass feedstocks: Review and analysis of the biochemistry, energetics and economics. *Energy & Environmental Science*, 3, 554–590.

7

DISCUSSION

One never notices what has been done; one can only see what remains to be done.

Marie Curie

The previous chapters have described the photosynthesis behavior both from experimental and theoretical point of views. Each chapter has presented a specific aspect of the system while drastically simplifying its complexity. In the following paragraphs the results of these works are extended and discussed. Some new interpretations are presenting important aspects of photosynthesis research from a new perspective while opening opportunities for investigative lab experiments to productivity prediction at the raceway scale.

7.1 YIELD OF THE PHOTOSYNTHETIC APPARATUS AS A RESPONSE TO LD FREQUENCY

The analysis of the Han model (but similar results could be obtained with other fast time scale models such as. [23]) has investigated the way photosynthesis reacts to LD cycles. In response to such periodic light signals, the open (A) closed (B) and inhibited (C) fractions of PSUs follow a periodic dynamic.

For some changing frequencies the obtained results are intuitive. If the cycle frequency is much slower than the time scales of the system, we can assume that the variables reach their pseudo equilibrium within the light and dark phase. Also, the timespans for approximating these states are only a small percentage of the entire cycle. This means that the resulting growth rate is $\mu(I_0)$ during the (long lasting) light periods and 0 during the dark periods. It results that the average growth rate is $\mu(I_0)/2$.

If the light frequency is much faster than the involved time scales, the fractions of open, closed and inhibited photocenters reach a constant equilibrium which does not change throughout a cycle. It should be remarked, that physically – due to the quantum nature

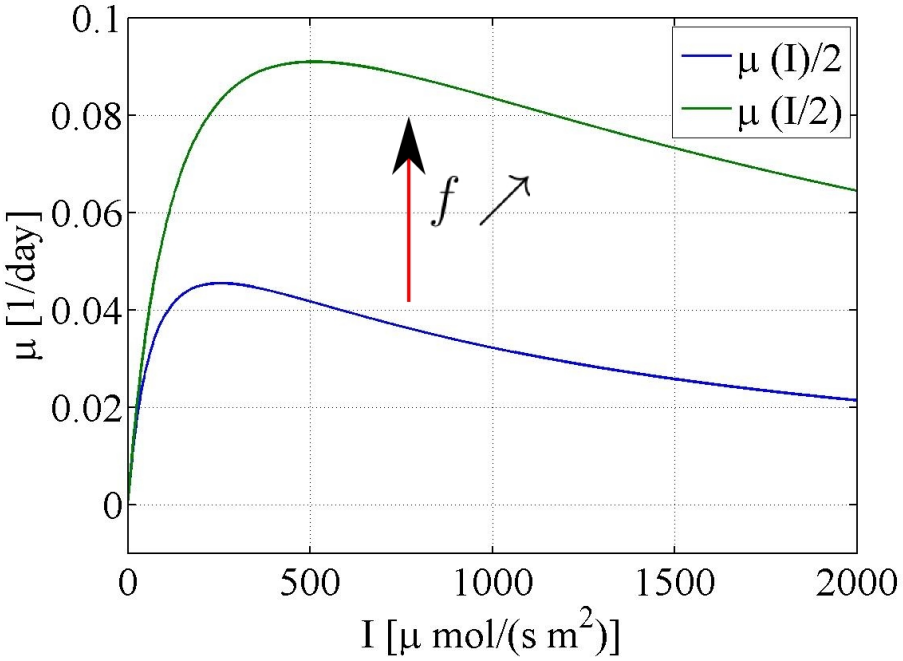

Figure 15: $\mu(I_0)/2$ and $\mu(I_0/2)$ describing the growth rate improvement with cycling frequency of a LD signal

of light – there is no difference between flashing light with infinite frequency and continuous light with average intensity. According to the calculation, the resulting growth rate equals that of continuous illumination with average intensity. With the average value of the light $I_0/2$, the mean growth rate is $\mu(I_0/2)$ in this case. This value is always higher than $\mu(I_0)/2$ because of the concavity of the growth curve (cf. fig. 15). This can be easily shown using property 1 in ch. 6.

In fig. 16, the evolution of the periodic state of the Han model for LD cycles with increasing cycling frequency is presented. For low frequencies, the number of inhibited photosystems C decreases during the dark phase and increases during the light phase. With increasing cycle frequency the value of C stabilizes at an average level. This leads to an increased efficiency of the photosysthetic production, because C_{av} is lower during the light phase, which allows

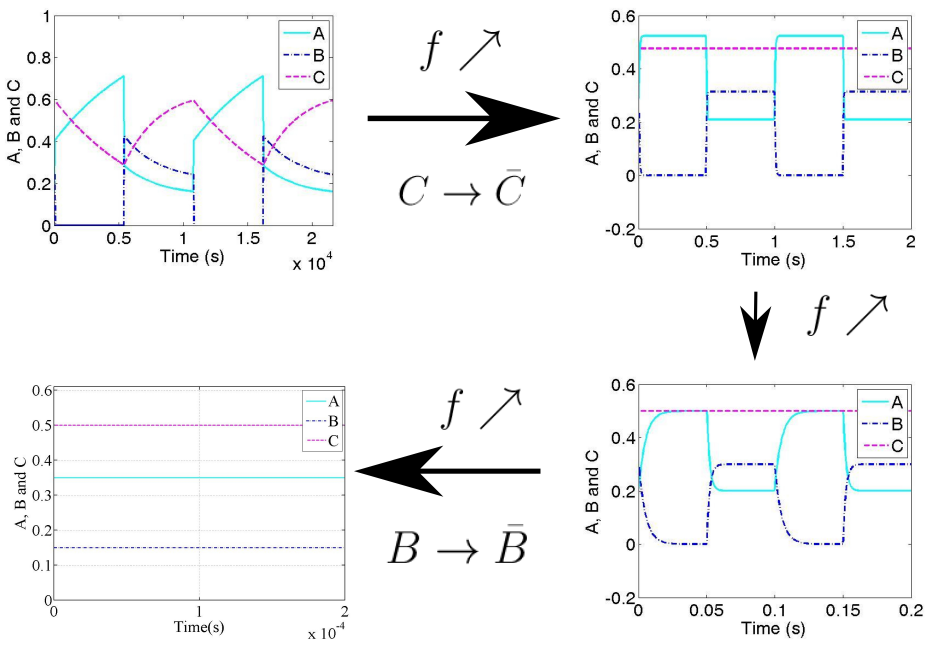

Figure 16: Synthetic Scheme describing the response of the variables of Han model to LD cycles with increasing frequency. In the lower left: A PI curve indicating the evolution from $\mu(I_0)/2$ to $\mu(I_0/2)$

for an increased productivity. For these intermediate frequencies, we found a plateau in the dependency of the photosynthetic production rate from the cycling frequency. For very high cycling frequencies, the fast variables A and B no longer follow the light transitions. Consequently, A and B turns to a average equilibrium values $\bar{B}$ and $\bar{A}$.

For intermediate flashing frequencies, the dynamics of the fast open/closed subsystem reaches its steady state during each period, while the slow closed/inhibited system reaches a global constant value. In this case, the average value of the growth rate can still be computed and compared with the two other values for extreme frequencies:

$$\mu_{SS} < \mu_{int} < \mu_{max} \tag{7.1}$$

This property directly follows from the result in ch. 4. The intermediate regime is of particular importance, since this is the one that is expected under raceway conditions, where time constants of the hydrodynamics (cf ch. 6) mainly stimulate the dynamics of the photoinhibited state.

7.2 DO WE PROPERLY CHARACTERIZE THE RESPONSE WITH LD EXPERIMENTS

In the field of photosynthesis research, experimental studies using LD cycles are a regularly used setup. Corresponding to this, modelling efforts are also often focused on this kind of light signals. When considering real outdoor conditions and the insights about the influence on hydrodynamics we achieved in ch. 6 ,it becomes clear that the representation of mixing effects using LD cycles is far from reality. While not simulating realistic conditions, LD signals have two important properties: (1) Easy repeatability and comparability of different studies and (2) mathematical accessibility for modelling efforts. Both of these properties are invaluable when aiming on validation and parameter identification for mechanistic models.

In ch. 6 we have investigated numerically the response of the Han model to cycles with two different light intensities. The results showed that there is not only a dependency of the growth rate on cycling frequency but also on the amplitude, respectively the standard deviation of the signal (see ch. 6, fig. 6). A step towards a more realistic behavior could consist in a piecewise constant signal, without zero illumination and with unequal duration of high and low light. When limiting the signal structure to two consecutive light intensities I_{low} and I_{high}, while the length of the high light phases

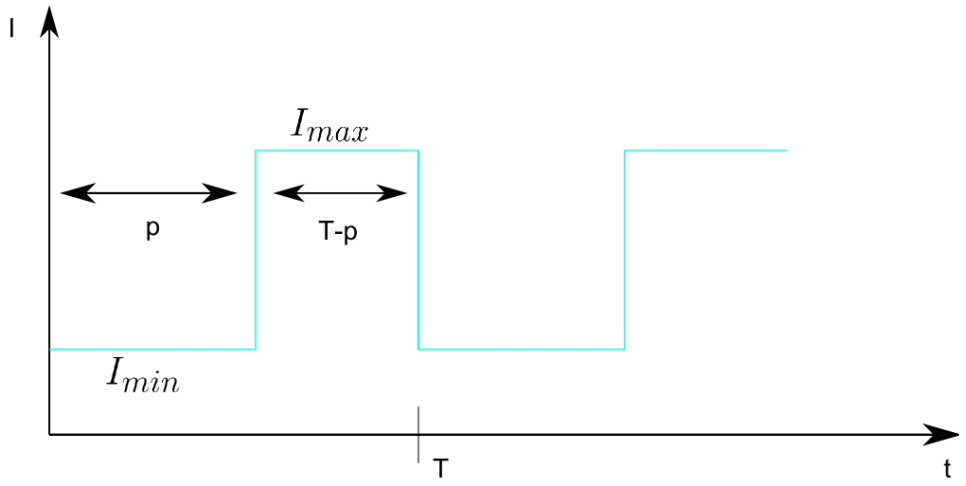

Figure 17: Light signal corresponding to the function defined in eq. 7.2.

is the pth fraction of the complete cycle length, we end up with the following definition for such a light signal:

$$I(t) := \Theta\left[t - \left\lfloor \frac{t}{T} \right\rfloor \cdot T - p\right] \cdot (I_{max} - I_{min}) + I_{min} \tag{7.2}$$

The shape of this signal is presented in fig. 17. Θ is the Heaviside Function and $\lfloor \cdot \rfloor$ the Floor function. Standard deviation an average value of this function can be easily calculated as:

$$\bar{I} = I_{min}/p + I_{max}/(1-p) \tag{7.3}$$

$$\sigma_I = \frac{I_{max} - I_{min}}{\sqrt{p(1-p)}} \tag{7.4}$$

It can be seen that this function allows for the independent adjustment of cycle frequency, average light intensity and standard deviation. A topic for subsequent experimental studies could be to investigate if the maximum light intensity or the standard deviation of the light signal has more physiological impact.

As it has been demonstrated in ch. 6, the Han model responds to such LD cycles in a very plausible manner. According to numerical and analytical investigation it can be said that the average growth

rate decreases with increasing variance and increases with increasing cycle frequency. This follows the idea that the edge cases of zero standard deviation and infinite frequency are physically equivalent to a continuous signal with average intensity.

7.3 How much benefit can there be from mixing?

Even without knowledge about the actual hydrodynamics, the theoretical maximum benefits for growth rate in outdoor algae cultures can be estimated. As in ch. 6, the light intensity inside the volume is considered to follow an exponential decay from surface to bottom (this rough approximation could be improved by more accurate models [62]). Instead of a constant attenuation coefficient, the attenuation should be defined as a linear function of the biomass density as it is proposed by Luo and Al-Dahhan [50]:

$$I = I_0 \exp(-\lambda(X) \cdot z) \tag{7.5}$$

$$\lambda(X) = (k_x \cdot X + k_w) \tag{7.6}$$

Where k_w and k_x arethe attenuation coefficients for water and biomass density, X represents the biomass concentration in the medium. The net growth rate can be computed with the Han model, considering the steady state solution:

$$\mu(I) = \mu_0 \frac{\sigma I}{1 + \sigma\tau I + k_d/k_r \tau\sigma^2 I^2} \tag{7.7}$$

For the estimation of the average growth rate of the culture we consider furthermore the average value for the growth rate of a sufficient number of cells N, which float through the volume while observing the time-dependent light signal $I_i(t)$ for a sufficiently long time span T. N and T will disappear in the final formulas, so their actual value are not important.

$$\bar{\mu} = \frac{1}{N}\sum_{i=1}^{N}\frac{1}{T}\int \mu(I_i(t))dt \tag{7.8}$$

This equation can be simplified and solved for two edge cases: (1) infinitely effective mixing and (2) no mixing. For infinitely strong mixing we assume the light changes for the cells to be rapid. As a consequence, the cells adapt to the average light intensity $\bar{I}$ in the volume while traversing it. For $\bar{I}$ we get:

$$\bar{I}(X) = \frac{1}{L}\int_0^L I(z)dz = \frac{I_0}{\lambda(X)L}(1 - e^{-\lambda(X)}) \tag{7.9}$$

thus we can calculate $\bar{\mu}$ for the complete culture as:

$$\bar{\mu}_{mix} = \frac{1}{N}\sum_{i=1}^{N}\mu(\bar{I})dt = \mu(\bar{I}) \tag{7.10}$$

For the case of no mixing, $I(t)$ is constant for each particle and turns to $I(z)$.

$$\bar{\mu}_{stat} = \frac{1}{N}\sum_{i=1}^{N}\frac{1}{T}\int \mu(I_i(t))dt \tag{7.11}$$

$$= \frac{1}{N}\sum_{i=1}^{N}\mu(I(z_i)) \tag{7.12}$$

Here, the time integration is trivial due to the constant light intensity. Furthermore, the particles are stationary and receive a constant light intensity. Consequently, the sum over N particles can be replaced by an integration over the volume, considering constant density of particles.

$$\begin{aligned}\bar{\mu}_{stat} &= \frac{1}{V}\int_V \mu(I(z))dV && (7.13)\\ &= \frac{1}{L}\int_0^L \mu(I(z))dz && (7.14)\\ &= \frac{1}{L}\int_0^L \mu_0\left(\frac{\sigma I(z)}{1+\sigma\tau I(z)+k_d/k_r\tau\sigma^2 I(z)^2}\right)dz && (7.15)\end{aligned}$$

With substitution, this integral can be solved analytically for $\Delta = \sigma^2\tau^2 - 4\cdot k_d/k_r\tau\sigma^2 > 0$ to:

$$\bar{\mu}_{stat} = \frac{\sigma}{L\lambda\sqrt{\Delta}}\left[\ln\left(\frac{2k_d/k_r\tau\sigma^2\nu+\sigma\tau-\sqrt{\Delta}}{2k_d/k_r\tau\sigma^2\nu+\sigma\tau+\sqrt{\Delta}}\right)\right]_{\nu=I_0}^{\nu=I(L,X)} \quad (7.16)$$

This gives the average growth rate for the static case of no mixing. It should be highlighted that the resulting term is a function of I_0 and X. For the case of $\Delta < 0$, the solution of this integral is analogue to the expression developed in [7]. For all presented examples we assume the same physiological parameters for the Han model as presented in ch. 4. In fig. 18, the PI curve, both estimations for the average growth rate and the theoretical improvement due to mixing is presented. In the presented case, $3\cdot 10^6$ cells/ml were assumed for the biomass density. This relates to a light intensity at the bottom of the volume of about 3%. It can be observed that the maximal values of μ_{mix} and μ_{stat} are heavily shifted towards high light intensities. This is plausible since the particles at the surface shade the lower part of the volume from high light intensities and therefore – on average – mitigate photoinhibition. Moreover, the

potential productivity enhancement due to mixing rate drastically increases with light intensity. The formulas for growth rate are formulated as a direct dependency from biomass density X rather than a light attenuation factor. Based on this, the gross productivities $\hat{P}_{stat}$ and $\hat{P}_{mix}$ can be defined:

$$\hat{P}_{stat}(X, I_0) = \mu_{stat}(\rho, I_0) \cdot X \tag{7.17}$$

$$\hat{P}_{mix}(X, I_0) = \mu_{mix}(\rho, I_0) \cdot X \tag{7.18}$$

$$P_{stat}(X, I_0) = \mu_{stat}(\rho, I_0) \cdot X - R \cdot X \tag{7.19}$$

$$P_{mix}(X, I_0) = \mu_{mix}(\rho, I_0) \cdot X - R \cdot X \tag{7.20}$$

The respiration rate R is assumed as 10 % of the maximum growth rate as proposed by Geider [31]. The net productivities P_{stat} and P_{mix} are defined by substraction of dark respiration $R \cdot X$. In fig. 19, $\hat{P}_{stat}$ and $\hat{P}_{mix}$ are presented as a function of the cell density X. For this figure, 1000 $\mu mol/(sm^2)$ has been chosen as the surface light intensity I_0. It can be observed, that P_{stat} peaks for a relatively low density of about $6 \cdot 10^6$ cells/ml (which refers to $6.8 \cdot 10^{-2}$% of the light intensity at the bottom), while the maximum of P_{mix} lies beyond 10^8 cells/ml (which refers to $7 \cdot 10^{-51}$% of the light intensity at the bottom). The intersections with the linear function describing respiration loss with these productivities indicate the equilibrium cell densities for the different situations. It can be observed, that with increasing cell density, the benefits from mixing are reduced significantely by respiration. This figure illustrates clearly that the benefits of mixing are strictly linked to the cell density and that improvements in productivity can not be expected to be as important for raceway systems with relatively low cell density as for closed

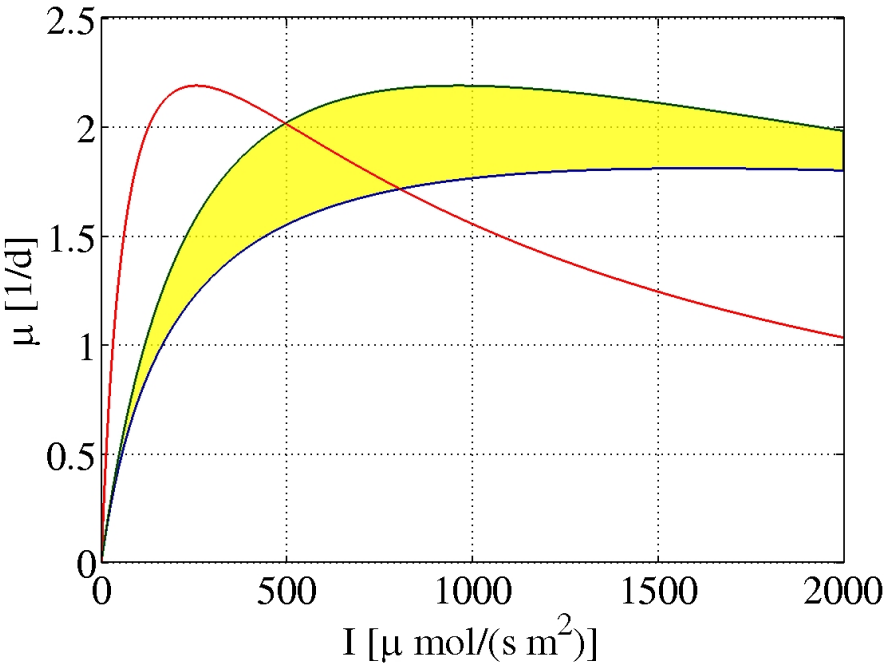

Figure 18: (red curve) PI curve according to the Han Model (green curve) μ_{mix} (blue curve) μ_{stat} (yellow area) Theoretical gain in growth rate due to mixing

PBR systems with high density. Dark respiration imposes a limit on the benefits for cultures with highest densities.

In fig. 20 and 21, the net productivities P_{stat} and P_{mix} are presented as surface plots in dependency of the cell density and the surface light intensity. The solutions for $P = 0$ describe the equilibrium densities for batch operation. In addition, green lines indicate equilibrium densities for different dilution rates for continuous operation (according to $\mu = D + R$). Both expressions show a completely different evolution for increasing light intensity and cell density. P_{stat} yields positive values only for low cell densities. For high cell densities the influence of respiration completely dominates and leads to negative productivities even for very high surface intensities. In contrast, P_{mix} – which yields overall much higher productivities – is positive in most of the domain. The increase of productivity with

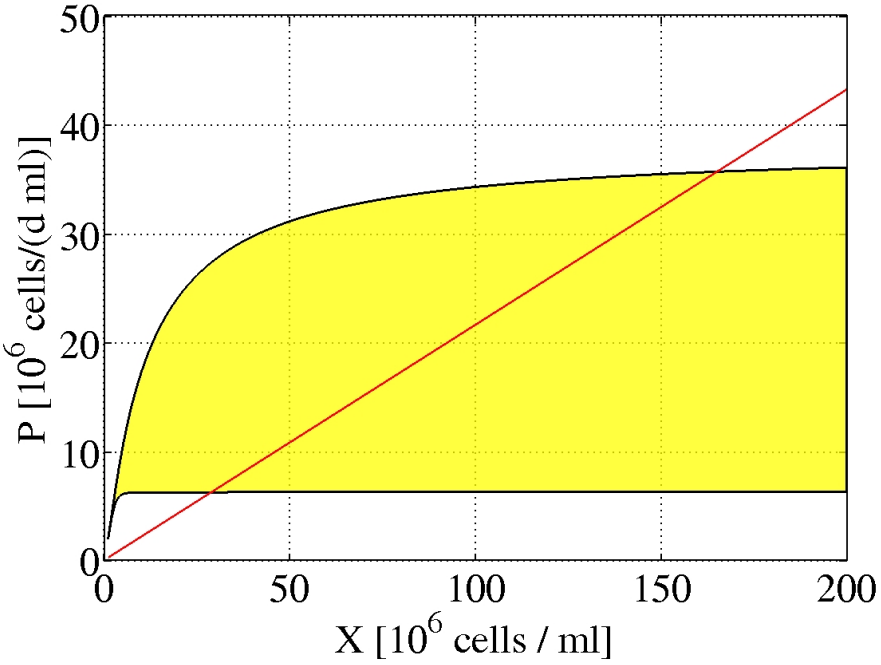

Figure 19: (green curve) P_{mix} (blue curve) P_{stat} (yellow area) Theoretical gain in growth rate due to mixing (red line) losses due to dark respiration

light intensity is very steep for high cell densities. The plot shows that there ought to be a cell density giving a maximum value of P_{mix} for each light intensity. However, P_{mix} refers to the hypothetical situation of *infinite* mixing and therefore only describes an upper limit for the growth rate which can be expected.

From these considerations, two fundamental conclusions can be drawn:

1. For extremely fast mixing, the productivity can be highly improved when opting for high culture densities. Such a dense culture can benefit from high light conditions above $800\mu mol/(sm^2)$.

2. For slow mixing, small culture densities optimize the growth rate. There is no benefit from extreme light conditions.

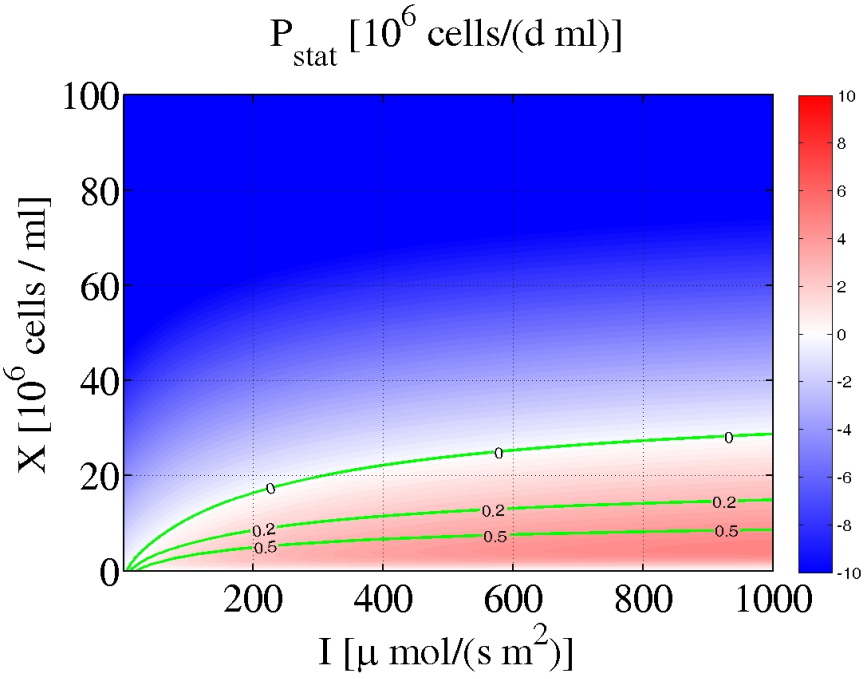

Figure 20: P_{stat} as a function of cell density and surface light intensity. Green lines: stable states for batch and continuous cultivation with different dilution rates

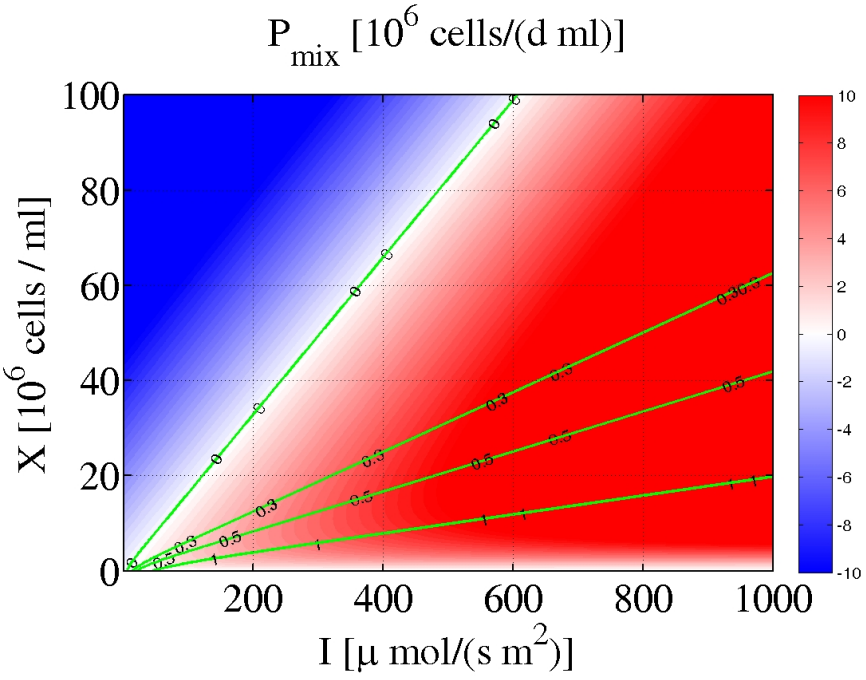

Figure 21: P_{mix} as a function of cell density and surface light intensity, Green lines: stable states for batch and continuous cultivation with different dilution rates

In order to better assess the potential productivity, the foundation is to provide a sound experimental practice for growth rate measurements in various conditions of light. This point is far from evident, and no perfect experimental protocol exists. In the following paragraph, important pitfalls of the objective measurement of photosynthetic responses will be demonstrated.

Using the fit of the data of Neidhardt et al. (cf. fig. 12), we could show that the preacclimation period of the sample can have significant influence on the form of the PI curve measured. In this particular case, this has lead Neidhardt very likely to a misinterpretation of the results. Neidhardt give their measurement protocol in the publication, which allowed for the identification of this effect. Unfortunately, the term PI curve is still frequently used in a way as if it was a static characteristic of a photosynthetic organism, which – if measured appropriately – describes objectively the photosythetic capacity of this organism under the environmental conditions from which this organism has been extracted. While it is true that the PI curve gives important information about the photosynthetic response, our studies show that without precise knowledge about the exact measurement protocol the PI curve is very hard to interpret. When following a protocol as the one of Neidhardt with oxygen measurement and increasing light intensity, three factors with major influence on the outcome can be identified: (1) The utilized light source (2) The exact state of the algae before the measurement (3) The time evolution of light intensity (pattern of light increase).

The light source has influence on the result, because light intensity values say nothing about the spectrum and algae could respond

differently to different spectra at the same light intensity. The Simulation of Neidhardt's data showed a clear dependency of the resulting PI curve from the state of the algae at the beginning of the measurement. In this case, the algae for the HL curve where considerably inhibited before the measurement and therefore showed a different initial slope than for the LL curve. While it is possible to mitigate this effect by prior dark incubation of the sample, it is not easy to suggest a correct length of this dark incubation phase. Depending on species and length of the dark incubation, physiological adjustments can happen and change the result of the experiment. The length of dark incubation therefore has to be seen as an important part of the protocol and needs to be chosen carefully. In addition to these effects, the exact protocol of the measurement itself can have an enormous effect on the shape of the resulting curve. In fig. 22, simulated curves for PI protocols with a different measurement interval are presented. It can be observed, that results vary enormously due to this change in protocol. It can also be observed, that PI curves are always above the steady state solution and that they approximate it with longer measurement intervals. This is plausible since the steady state solution represents the state of the system which is approximated under the reported conditions after a sufficiently long time period. Since for short measurement the culture will suffer less from inhibition, the observed growth rate is higher than the steady state value. If the chosen model accounts also for other dynamic effects – such as photoacclimation – the results could be very different. Therefore it is not possible to conclude from this result: The longer the measurement interval, the more valuable is result. What can be said, is that the longer the measurement interval, the closer the result will be to the steady state solution of the complete model. Unfortunately this

solution gives no information about the current physiological state of the culture (e.g. Acclimation state).

Apart from the measurement interval, the choice of the number of measurement points have a similar effect because it influences the total measurement time. The longer the total measurement protocol, the least the result of the last measurement points will be correlated with the initial state of the algae. According to this, there is no objective criteria to decide what is the 'real' PI curve among the different possible results.

Dynamical effects which change the outcome of PI curves are known for over 30 years now. Nevertheless, due to the high effort which is needed for proper measurements using a single sample for each light intensity [46], 'quick and dirty' single sample measurements are often done – sometimes with poor documentation of the protocol.

7.5 Challenges for long term Lagrangian simulation of open raceways

Hydrodynamic modelling of photobioreactor and raceways which include complex geometry with moving mechanical agitators (paddle wheel or propeller) is known to be a challenging topic. Here we consider a hydrodynamic model run under two conditions making the outputs more delicate. We consider Lagrangian trajectories resulting from the velocity field. The reconstruction of these trajectories requires hypotheses on the velocity field within a volume of the discretization mesh and hypotheses on the reflexion of the particles to the surface. There is a lack of physical models to support these hypotheses. Moreover, a simultaneous computation of thousands

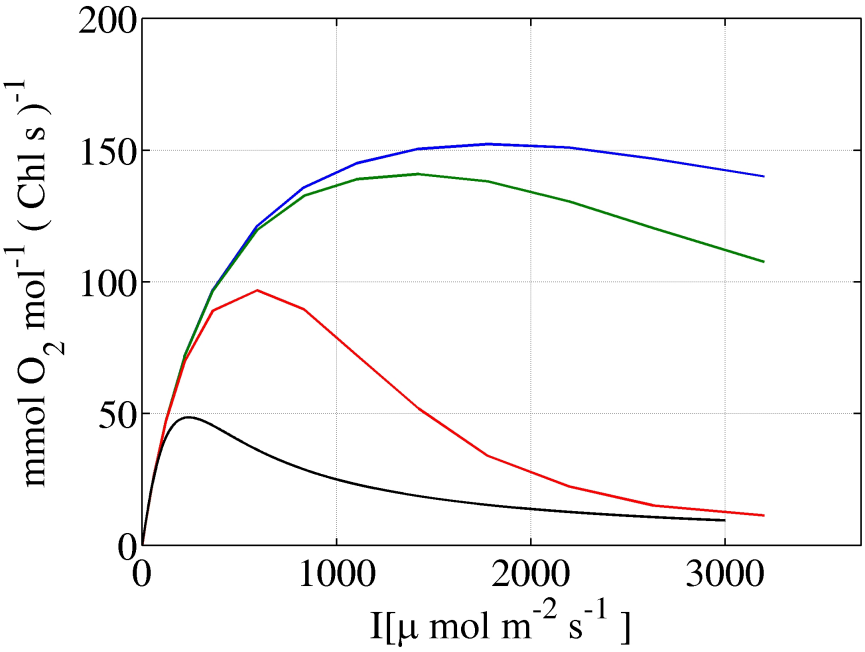

Figure 22: Results from the Han Model for different measurement protocols for the PI curve: (blue) 50s measuring intervals (green) 100s measuring intervals (red) 1000s measuring intervals (black) steady state solution of the Han model

of particles (which is necessary to make statistics on the resulting trajectories) is thus highly demanding both in terms of CPU and memory. To address the productivity question, it is necessary to perform long term simulations:

1. The raceway needs several days in order to reach a stable state when considering all biological processes.
2. There is no implicit averaging over many particles. Each and every trajectory has to be integrated individually using the biological model.

Long term simulations of closed system where the particles explore periodically the same domain is a typical situation leading to error accumulation. The fact that the domain is closed means that an error at some point in time can propagate and accumulate. This

was clearly observed with long term runs of the Freshkiss code for simulating cell trajectories over several days. The particle distribution (even when neglecting any settling property) was eventually not equally distributed. Particle accumulations near the the bottom of the raceway were observed after a sufficiently long period, violating thus the hypothesis of fluid incompressibility. Even if this was observed with Freshkiss, it is very likely that most of the CFD software will present biased results for long term run of Lagrangian trajectories in closed domains (however, since the classical resolution of Navier-Stokes equations are very resource demanding, they are not run for more than hours). Much work remains to be done in this new direction motivated by the specificity of microalgae, and which was probably not studied in any other domain.

Simulation runs with different wheel speeds of the system show that the described artifact is not only a large perturbation but also dependent on the wheel speed and on the length of the simulation time. This makes it impossible to realistically study the effect of the wheel speed. The result obtained would only show the effect of the numerical artifact.

Different strategies can be considered in order to address this issue:

1. Utilize a finer mesh and reduce the time step, in order to reduce the numbers of particles leaving the volume (but it may induce computational costs drastically high).
2. Revisit the discretization scheme for the Lagrangian single cell trajectory reconstruction to guarantee incompressibility after each iteration (the Eulerian system in this approach respects incompressibility)

3. Introduce an artificial correction term which guarantees homogeneity after ith time step.

7.6 Can a small scale raceway give information on the productivity of a large scale raceway?

An important motivation for all the efforts about Experiments with large-scale raceways is the fact that test runs of industrial-scale systems are very expensive. Another reason is that such experiments are strongly dependent on environmental conditions which are influenced by weather and season. This severely limits the comparability of different outdoor studies carried out at different locations or and/or different times.

In order to carry out experiments while mitigating these issues it is imaginable to carry out experiments indoor using small-scale raceway models. This has the advantage, that the environment can be perfectly controlled and that the experimental setup is comparably cheap. Small scale model experiments to test full scale design opportunities is a technique which is often applied in the chemical and technical industry. More often than not, scaling up industrial components can prove to be a very challenging task which has to be treated individually for each different case.

When regarding raceway systems, some issues which have to be addressed immediately become evident. Changing scales of a raceway pond changes will influence a considerable number of processes. Maybe the most important difference is caused by processes which are linked to the ratio of volume to surface: temperature adaption and exchange with the environment, evaporation, light distribution in the volume. Especially the light distribution seems problematic. In

order to trigger realistically certain physiological processes, the same light intensities at the surface as for large scale plants are necessary.

Hydrodynamics itself does not scale linearly. One consequence is that succession of light and dark phases will be much faster in a small raceway, where each cell encounters more frequently the paddle wheel and the raceway turns both inducing depth change. A small raceway will therefore induce more agitation at the cell scale and thus higher productivity, especially at high light. It is not clear if a small raceway where cells meet the (unique) paddle wheel every 20 meters is equivalent to a large raceway with several paddle wheels so that every 20 meters a new paddle wheel is encountered. Indeed, the twisting effect in the raceway turns, due to the difference between the higher interior speed also strongly contribute to vertical cell displacement. As a consequence, the results obtained at small scale must be cautiously considered before possible extrapolations to a large scale.

8

CONCLUSION

Patience is bitter, but its fruit is sweet.

Jean-Jacques Rousseau

In this thesis, the subject of growth prediction in large industry scale raceway system for microalgae cultivation has been approached from an experimental and a modeling perspective. In this context, the important processes influencing the physiological response of the microalgae to short term and long term light variations have been identified and characterized. As a result, we could estimate the contribution of the different mechanisms to growth rate benefits from mixing for low density raceway ponds and a high density closed PBRs. With the presented studies, we could approach the problem of growth rate prediction in raceway ponds from a theoretical, an experimental and a simulation perspective.

The insights from this thesis open up some new interesting scientific questions. At the physiological level, the presented modelling approach highlights how sensitive PI curves can be to the experimental protocol. Model calibration is strongly influenced by the PI response, and thus the way PI curves are generated and interpreted strongly influences the model predictions. Another physiological aspect which should be further investigated is the acclimation strategy of a cell. The model predictions for N- and s-strategy should be validated in various conditions, and especially in varying light.

There are still important questions to address before lab experiments can be realistically scaled up to large scale production systems. One of the issues is the reconstruction of realistic trajectories for microalgae. There is a real challenge in computing long term Lagrangian trajectories, since error accumulates in such closed system. Improvements in numerical computation of hydrodynamics from a Lagrangian perspective should pave the way to more robust trajectory. Experimentally reproducing such signals is not straightforward and there is probably a research axis to determine light profiles which excite the photosynthesis apparatus in a comparable way – leading to efficient system characterization using a procedure of model parameter identification. Once the enormous methodical gap between small scale lab experiments and full scale system is closed, a validation of suitable models with experimental data from outdoor cultures is imaginable. Closing this gap still requires a considerable effort both from an experimental and from a modeling perspective.

BIBLIOGRAPHY

[1] J. M Anderson, Y.-i Park, and W. S Chow. Unifying model for the photoinactivation of Photosystem II in vivo under steady-state photosynthesis. *Photosynthesis Research*, pages 1–13, 1998.

[2] E Audusse and M Bristeau. Approximation of the hydrostatic Navier Stokes system for density stratified flows by a multilayer model: kinetic interpretation and numerical solution. *J of Computational Physics*, 2011.

[3] M Baklouti, F Diaz, C Pinazo, V Faure, and B Quéguiner. Investigation of mechanistic formulations depicting phytoplankton dynamics for models of marine pelagic ecosystems and description of a new model. *Progress in Oceanography*, 71(1):1–33, 2006.

[4] M. J Barbosa, M Janssen, N Ham, J Tramper, and R. H Wijffels. Microalgae cultivation in air-lift reactors: modeling biomass yield and growth rate as a function of mixing frequency. *Biotechnology and bioengineering*, 82(2):170–9, April 2003.

[5] J Beardall, T Burger-Wiersma, M Rijkeboer, A Sukenik, J Lemoalle, Z Dubinsky, and D Fontvielle. Studies on enhanced post-illumination respiration in microalgae. *Journal of Plankton Research*, 16(10):1401–1410, 1994.

[6] O Bernard. *Etude experimentale et theorique de la croissance de dunaliella tertiolecta (chlorophyceae) soumise a une limitation variable*

de nitrate : utilisation de la dynamique transitoire pour la conception et la validation des modeles. PhD thesis, January 1995.

[7] O Bernard. Hurdles and challenges for modelling and control of microalgae for CO2 mitigation and biofuel production. *Journal of Process Control*, 21(10):1378–1389, September 2011.

[8] F Blackman. Optima and limiting factors. *Annals of Botany*, XIX (Lxxiv), 1905.

[9] E. G Bligh and W. J Dyer. A rapid method of total lipid extraction and purification. *Canadian journal of biochemistry and physiology*, 37(8):911–917, 1959.

[10] R Bosma, E. V Zessen, J. H Reith, and J Tramper. Prediction of Volumetric Productivity of an Outdoor Photobioreactor. *Biotechnology*, 97(5):1108–1120, 2007.

[11] G Bougaran, O Bernard, and A Sciandra. Modeling continuous cultures of microalgae colimited by nitrogen and phosphorus. *Journal of theoretical biology*, 2010.

[12] A.-C Boulanger, C Cancès, H Mathis, K Saleh, and N Seguin. OSAMOAL: Optimized Simulations by Adapted MOdels using Asymptotic Limits. *ESAIM: Proceedings*, 38:183–201, January 2013.

[13] V Casulli and R Cheng. Semi-implicit finite difference methods for three-dimensional shallow water flow. *... Journal for numerical methods in fluids*, 1992.

[14] M Cherif and M Loreau. Towards a more biologically realistic use of Droop's equations to model growth under multiple nutrient limitation. *Oikos*, 119(6):897–907, April 2010.

[15] D Chiaramonti, M Prussi, D Casini, M. R Tredici, L Rodolfi, N Bassi, G. C Zittelli, and P Bondioli. Review of energy balance in raceway ponds for microalgae cultivation: Re-thinking a traditional system is possible. *Applied Energy*, 102:101–111, February 2013.

[16] T. a Costache, F. G Acién Fernández, M. M Morales, J. M Fernández-Sevilla, I Stamatin, and E Molina. Comprehensive model of microalgae photosynthesis rate as a function of culture conditions in photobioreactors. *Applied microbiology and biotechnology*, 97(17):7627–37, September 2013.

[17] P Cox, R Betts, C Jones, S Spall, and I Totterdell. Acceleration of global warming due to carbon-cycle feedbacks in a coupled climate model. *Nature*, 408(November):184–187, 2000.

[18] B Demmig-Adams and W. W Adams III. Xanthophyll cycle and light stress in nature: uniform response to excess direct sunlight among higher plant species. *Planta*, 198(3):460–470, 1996.

[19] J Doucha and K Lívanský. Productivity, CO2/O2 exchange and hydraulics in outdoor open high density microalgal (Chlorella sp.) photobioreactors operated in a Middle and Southern European climate. *Journal of Applied Phycology*, 18(6):811–826, November 2006.

[20] M. R Droop. Vitamin B_{12} and marine ecology. {IV}. The kinetics of uptake growth and inhibition in *Monochrysis lutheri*. *J. Mar. Biol. Assoc.*, 48(3):689–733, 1968.

[21] M Droop. In defence of the Cell Quota model of micro-algal growth. *Journal of plankton research*, 2003.

[22] P Eilers and J Peeters. Dynamic behaviour of a model for photosynthesis and photoinhibition. *Ecological Modelling*, 69 (1-2):113–133, September 1993.

[23] P. H. C Eilers and J. C. H Peeters. A model for the relationship between light intensity and the rate of photosynthesis in phytoplankton. *Ecological modelling*, 42(3-4):199–215, 1988.

[24] G. M. . A. S Emilie Le Floc'h. An automatic device for in vivo absorption spectra acquisition and chlorophyll estimation in phytoplankton cultures. *Journal of Applied Phycology*, 14:435–444, 2002.

[25] S Esposito, V Botte, D Iudicone, and M. R D'Alcala'. Numerical analysis of cumulative impact of phytoplankton photoresponses to light variation on carbon assimilation. *Journal of theoretical biology*, 261(3):361–71, December 2009.

[26] P. J Falkowski and J. A Raven. *Aquatic photosynthesis*. Blackwell science, 1997.

[27] P. G Falkowski and J LaRoche. Acclimation to spectral irradiance in algae. *Journal of Phycology*, 27(1):8–14, 1991.

[28] F García, Y Freile-Pelegrín, and D Robledo. Physiological characterization of Dunaliella sp. (Chlorophyta, Volvocales) from Yucatan, Mexico. *Bioresource technology*, 98(7):1359–65, May 2007.

[29] F García-Camacho, A Sánchez-Mirón, E Molina-Grima, F Camacho-Rubio, and J. C Merchuck. A mechanistic model of photosynthesis in microalgae including photoacclimation dynamics. *Journal of theoretical biology*, 304:1–15, July 2012.

[30] R. J Geider, H. L MacIntyre, T. M Kana, R J Geider, H L MacIntyre, and T M Kana. A Dynamic Regulatory Model of Phytoplanktonic Acclimation to Light, Nutrients, and Temperature. *Limnol Oceangr*, 43(4):679, June 1998.

[31] R Geider. Respiration: taxation without representation? *Primary Productivity and Biogeochemical Cycles in the . . .*, 1992.

[32] R Geider, H MacIntyre, and T Kana. Dynamic model of phytoplankton growth and acclimation:responses of the balanced growth rate and the chlorophyll a:carbon ratio to light, nutrient-limitation and temperature. *Marine Ecology Progress Series*, 148: 187–200, 1997.

[33] J. U Grobbelaar. Do light/dark cycles of medium frequency enhance phytoplankton productivity? *Journal of Applied Phycology*, 1(4):333–340, December 1989.

[34] R. R. L Guillard and J. H Ryther. Studies of marine planktonic diatoms. I. Cyclotella nana Hustedt, and Detonula confervacea (cleve) Gran.. *Canadian Journal of Microbiology*, 8(2):229–239, 1962.

[35] J Haldane. Enzymes. 1930.

[36] B. P Han. Photosynthesis-irradiance response at physiological level: A mechanistic model. *J Theor Biol*, 213:121–127, 2001.

[37] P Hartmann, A Nikolaou, A Sciandra, B Chachuat, and O Bernard. Dynamic coupling of photoacclimation and photoinhibition in a model of microalgae growth. *Biotechnol. & Bioeng.*, 2014. – submitted –.

[38] H Havelková-Doušová, O Prášil, and M Behrenfeld. Photoacclimation of Dunaliella tertiolecta (Chlorophyceae) Under Fluctuating Irradiance. *Photosynthetica*, 42(2):273–281, 2004.

[39] O Holub, M. J Seufferheld, C Gohlke, Govindjee, G. J Heiss, and R. M Clegg. Fluorescence lifetime imaging microscopy of Chlamydomonas reinhardtii: non-photochemical quenching mutants and the effect of photosynthetic inhibitors on the slow chlorophyll fluorescence transient. *Journal of microscopy*, 226(Pt 2):90–120, May 2007.

[40] P Horton, M Wentworth, and A Ruban. Control of the light harvesting function of chloroplast membranes: the LHCII-aggregation model for non-photochemical quenching. *Febs Letters*, 2005.

[41] D Iluz, I Alexandrovich, and Z Dubinsky. The enhancement of photosynthesis by fluctuating light. *Artifical Photosynthesis*, 2012.

[42] S. C James and V Boriah. Modeling Algae Growth in an Open-Channel Raceway. *Journal of computational biology : a journal of computational molecular cell biology*, 17(7):895–906, June 2010.

[43] A. D Jassby and T Platt. Mathematical formulation of the relationship between photosynthesis and light for phytoplankton. *Limnology and Oceanography*, 21(4):540–547, 1976.

[44] J. P Jr and J Myers. Growth rate of Chlorella in flashing light. *Plant Physiology*, (8):152–161, 1954.

[45] R Lee. *Phycology*. Cambridge University Press, 2008.

[46] M Lewis and J Smith. A small volume, short-incubation-time method for measure-ment of photosynthesis as a function of incident irradiance. *Marine Ecology-Progress Series*, 13:99–102, 1983.

[47] H. K Lichtenthaler. *Plant Cell Membranes*, volume 148 of *Methods in Enzymology*. Elsevier, 1987.

[48] K Liffman, D. a Paterson, P Liovic, and P Bandopadhayay. Comparing the energy efficiency of different high rate algal raceway pond designs using computational fluid dynamics. *Chemical Engineering Research and Design*, 91(2):221–226, February 2013.

[49] A Longhurst and S Sathyendranath. An estimate of global primary production in the ocean from satellite radiometer data. *Journal of Plankton Research*, 1995.

[50] H.-P Luo and M. H Al-Dahhan. Analyzing and modeling of photobioreactors by combining first principles of physiology and hydrodynamics. *Biotechnology and bioengineering*, 85(4):382–93, February 2004.

[51] G Malara and A Sciandra. A multiparameter phytoplankton culture system driven by microcomputer. *Journal of Applied Phycology*, 3(3):235–241, September 1991.

[52] S Manabe and R Wetherald. On the distribution of climate change resulting from an increase in CO2 content of the atmosphere. *Journal of the Atmospheric ...*, 1980.

[53] Monod. La technique de culture continue. théorie et applications. *Annales de L'intiut Pasteur*, 79:390–410, 1950.

[54] J Monod. *Recherches sur la Croissance des Cultures Bactériennes*. Hermann, Paris, 1942.

[55] J Neidhardt, J. R Benemann, L Zhang, and A Melis. Photosystem-II repair and chloroplast recovery from irradiance stress: relationship between chronic photoinhibition, light-harvesting chlorophyll antenna size and photosynthetic productivity in Dunaliella salina (green algae). *Photosynthesis Research*, pages 175–184, 1998.

[56] M Pahlow and A Oschlies. Optimal allocation backs Droop's cell-quota model. *Marine Ecology Progress Series*, 473(2010):1–5, January 2013.

[57] v Papáček, S Čelikovský, B Rehák, and D Štys. Experimental design for parameter estimation of two time-scale model of photosynthesis and photoinhibition in microalgae. *Mathematics and Computers in Simulation*, 80(6):1302–1309, February 2010.

[58] v Papáček, S Čelikovský, D Stys, and J Ruiz-Leon. Bilinear system as a modelling framework for analysis of microalgal growth. *Kybernetika*, 43(1):1–20, 2007.

[59] I Perner-Nochta and C Posten. Simulations of light intensity variation in photobioreactors. *Journal of Biotechnology*, 131:276–285, 2007.

[60] C Posten. Design principles of photo-bioreactors for cultivation of microalgae. *Engineering in Life Sciences*, 9(3):165–177, June 2009.

[61] J Pruvost, F. L Borgne, and J Legrand. Modelling photobioreactors for mass scale solar production of microalgae. *Citeseer*, 25.

[62] J Pruvost, J Cornet, and J Legrand. Hydrodynamics influence on light conversion in photobioreactors: an energetically consistent analysis. *chemical engineering Science*, 63(14):3679–3694, July 2008.

[63] J Pruvost, L Pottier, and J Legrand. Numerical investigation of hydrodynamic and mixing conditions in a torus photobioreactor. *Chemical Engineering Science*, 61:4476–4489, 2006.

[64] H Qiang and A Richmond. Productivity and photosynthetic efficiency ofSpirulina platensis as affected by light intensity, algal density and rate of mixing in a flat plate photobioreactor. *Journal of Applied Phycology*, 8(2):139–145, March 1996.

[65] R. R Sastre and Z Csögör. Scale-down of microalgae cultivations in tubular photo-bioreactors a conceptual approach. *Journal of Biotechnology*, 2007.

[66] E Sforza, D Simionato, G. M Giacometti, A Bertucco, and T Morosinotto. Adjusted light and dark cycles can optimize photosynthetic efficiency in algae growing in photobioreactors. *PloS one*, 7(6):e38975, January 2012.

[67] B Sialve, N Bernet, and O Bernard. Anaerobic digestion of microalgae as a necessary step to make microalgal biodiesel sustainable. *Biotech. Advances*, 27(4):409–416, 2009.

[68] V Smith. The nitrogen and phosphorus dependence of algal biomass in lakes: an empirical and theoretical analysis. *Limnol. Oceanogr*, 27(6):1101–1112, 1982.

[69] J. H Steele. Environmental control of photosynthesis in the sea. *Limnology and Oceanography*, 7(2):137–150, 1962.

[70] E Tyystjärvi and E. M Aro. The rate constant of photoinhibition, measured in lincomycin-treated leaves, is directly proportional to light intensity. *Proceedings of the National Academy of Sciences of the United States of America*, 93(5):2213–8, March 1996.

[71] C Vejrazka, M Janssen, M Streefland, and R. H Wijffels. Photosynthetic efficiency of Chlamydomonas reinhardtii in flashing light. *Biotechnology and bioengineering*, 108(12):2905–2913, July 2011.

[72] R. H Wijffels and M. J Barbosa. An Outlook on Microalgal Biofuels. *Science*, 329(5993):796–799, August 2010.

[73] X Wu. A model integrating fluid dynamics in photosynthesis and photoinhibition processes. *Chemical Engineering Science*, 56 (11):3527–3538, June 2001.

[74] X Wu and J. C Merchuk. Simulation of algae growth in a bench-scale bubble column reactor. *Biotechnology and bioengineering*, 80 (2):156–68, October 2002.

[75] N Yoshimoto, T Sato, and Y Kondo. Dynamic discrete model of flashing light effect in photosynthesis of microalgae. *Journal of Applied Phycology*, 17(3):207–214, May 2005.

[76] Y Zarmi, G Bel, and C Aflalo. Theoretical Analysis of Culture Growth in Flat-Plate Bioreactors: The Essential Role of Timescales. *Handbook of Microalgal Culture: Applied Phycology and Biotechnology, Second Edition*, 2013.

PUBLICATIONS

In the framework of this Thesis, the following Journal Articles and Proceedings have been written:

Articles:

P Hartmann, Q Bechet, O Bernard, *The effect of photosynthesis time scales on microalgae productivity* , Bioprocess and Biosystems Engineering, 37(1), 2014

submitted:
P Hartmann, A Nikolaou, B Chachuat , Olivier Bernard, *Photoacclimation and Photoinhibition in Microalgae: a modelling approach*

in preparation:
C Combe, P Hartmann, O Bernard, S Rabouille, A Talec, A Sciandra, *Long-term adaptive response to high-frequency light signals in the unicellular photosynthetic eukaryote Dunaliella Salina*

Peer reviewed Conference Proceedings:

P Hartmann, O Bernard, *Investigating photo inhibition processes in a novel Droop-Han modelling approach*, Proceedings of the Watermatex conference (2011)

P Hartmann, Q Bechet, O Bernard, *Interaction between time scales in microalgae based processes* , Control & Automation (MED), 2012 20th Mediterranean Conference on

P Hartmann, A Nikolaou, B Chachuat , Olivier Bernard, *A dynamic Model coupling Photoacclimation and Photoinhibition in Microalgae* , European Control Conference (ECC13) (2013)

P Hartmann, D Demory, C Combe, R Hamouda, A-C Boulanger, M-O Bristeau, J Sainte-Marie, B Sialve, J-P Steyer, S Rabouille, A Sciandra, O, Bernard, *Growth Rate Estimation of algae in Raceway Ponds: A novel Approach* , IFAC World Congress 2014

F Chazalon, S Rabouille, P Hartmann, A Sciandra, O Bernard*A Dynamical Model to study the Response of Microalgae to Pulse Amplitude Modulated Fluorometry* , IFAC World Congress 2014